NEW SECONDARY BATTERIES UTILIZING ELECTRONICALLY CONDUCTIVE POLYMER CATHODES

A FINAL REPORT
for
NASA GRANT NAG 9-173
For the period September 1, 1986 to August 31, 1987

submitted to

NASA Scientific & Technical Information Facility
P.O. Box 8757
Baltimore/Washington International Airport
Maryland 21240

prepared by

Charles R. Martin
Department of Chemistry
Texas A&M University
College Station, Texas 77843

and

Ralph E. White
Department of Chemical Engineering
Texas A&M University
College Station, Texas 77843-3122

August 1987

ABSTRACT

The objectives of this project are to optimize the transport rates in electronically conductive polypyrrole films by controlling the morphology of the film and to assess the utility of these films as cathodes in a lithium/polypyrrole secondary battery. During this research period, a better understanding has been gained of the fundamental electrochemical switching processes within the polypyrrole film. Three publications have been submitted based on the work completed.

TABLE OF CONTENTS

LIST OF FIGURES

I. INTRODUCTION

Polypyrrole is an attractive material for use as a high-energy-density secondary battery because of its potential as an inexpensive, lightweight, and non-corrosive electrode material. Polypyrrole has high conductivity, high specific charge density, and reversible electrochemical redox behavior to switch between conducting and nonconducting states.

This project is a joint project under the direction of Charles R. Martin (Department of Chemistry) and Ralph E. White (Department of Chemical Engineering). This is a joint effort because of the complementary nature of the work done by the co-principal investigators. Martin and his group provide the experimental expertise and White and his group provide data analysis or mathematical modeling expertise.

II. PROGRESS IN MARTIN'S GROUP

The progress made in Martin's group consists of three parts. AC impedance and current pulse relaxation studies of thin polypyrrole films have been conducted to investigated the fundamental electrochemical characteristics of the switching processes. In addition, a lithium/lithium perchlorate/polypyrrole ($Li/LiClO_4/PPy$) secondary battery cell has been designed based on these studies and its assembly is currently in progress.

A. AC IMPEDANCE ANALYSIS

The impedance of thin polypyrrole film (0.27 μm) has been studied at open circuit potentials from -0.4 V to 0.4 V vs. SCE. The purpose of this study is twofold: to show that the diffusion coefficient can be obtained from AC impedance data and to demonstrate that the AC impedance behavior of polypyrrole can be represented by simple equivalent circuits. A detatiled discussion is given in Appendix A.

B. CURRENT PULSE RELAXATION

A new current pulse technique for determining a value for a counter-ion diffusion coefficient in thin films of electronically conductive polymer has been developed. This small amplitude electrochemical experiment is used to circumvent background capacitance problems. Thus, diffusion coefficient information is obtained from the reduced form of the conducting polymer. Under these circumstances, the relatively small capacitive contributions to the electrochemical signal can easily be estimated and compensated. A detatiled discussion of this procedure is given in Appendix B.

C. SECONDARY BATTERY SYSTEM

Polypyrrole, as well as other conducting polymers, has shown promise as a cathode

material for lithium secondary batteries (1-17). Its ability to switch between the oxidized and reduced state and its comparatively high doping level makes it an excellent material for a rechargeable battery. This high doping level combined with the low atomic weight of lithium results in an energy density that compares favorably with other major battery systems. Recent work in this project on the fabrication of a lithium/polypyrrole battery is described next.

1. Experimental Set-Up

A schematic of the $Li/LiClO_4/PPy$ secondary battery cell to be used in this study is shown in Fig. 1. It consists of three parts: a polypyrrole film cathode that has been electrochemically synthesized on a platinum metal surface, a reservoir containing a suitable electrolyte, and a lithium metal anode. The three parts of the cell will be held together with metal clamps.

The cathode (Fig. 2-A.) consists of a polypyrrole film on a platinum disk, attached to a teflon rod inside a glass tube. Teflon tape is used to seal the teflon rod in the glass tube. A platinum wire lead is inserted through the Teflon rod to the back of the platinum disk to make electrical contact to the charging and discharging device.

The reservoir (Fig. 2-B.) is made from glass tubing with ground glass joints at both ends. Glass was chosen as the cell material so that it would be possible to view events inside the cell and position the Luggin capillary by visual inspection. In addition, ground glass joints seal well and are easily taken apart and resealed. Propylene carbonate will initially be used as the solvent and lithium perchlorate as the electrolyte. A silver/silver nitrate electrode (or silver/silver ion electrode, as it is sometimes called) will be used as the reference electrode. The silver/silver chloride reference electrode was ruled out because silver chloride is too soluble in many organic solvents, propylene carbonate being one of them, and the SCE cannot be used because it has an aqueous-

based electrolyte and would be unsuitable for use in the dry box.

The lithium anode is pictured in Fig. 2-C. It consists of a 1.5 mm thick lithium disk on a platinum disk attached to a Teflon rod. A platinum wire lead is attached to the back of the Pt disk through the Teflon rod to the outside of the cell. The anode may passivate if exposed to oxygen and/or moisture, and may need to be scraped to renew the surface. The screw mechanism could then be used to return the anode to its original position in the cell. To prevent passivaton of the lithium anode, all work will be done inside a dry box. Contamination sensors such as $TiCl_4$ for moisture and diethyl zinc for oxygen will be used.

2. Theory

The lithium/polypyrrole system shows much promise as a battery. Its theoretical energy density (307 Wh/kg) compares favorably with other major battery systems (252 Wh/kg for Ni/Cd and 244 Wh/kg for lead-acid). The energy density of a battery, or specific energy as it is sometimes called, is defined (18) as the ratio of the energy obtainable from a cell or battery to its volume (in Watt-hours/liter or Joules/liter) or mass (Wh/kg or Joules/kg). The theoretical energy density of a battery is based only on the active materials that participate in the electrochemical reaction and the potential of the cell. Water, electrolyte, casing, and any other material not involved in the reaction are not included. Free energy values are used to calculate the theoretical energy density from the relationship

$$-\Delta G^\circ = nFE^\circ \qquad [1]$$

where E° is the standard cell potential, n is the number of electrons involved in the half-cell reactions that sum to the overall reaction, and F is Faraday's constant, 96,487 coulombs or 26.8 amp-hours per mole of electrons involved in the half-cell reactions.

Thus, theoretically, one gram-equivalent weight of material releases one faraday of coulombs.

One way to calculate the theoretical energy density of a battery is to assume one gram (or kg) of active mass consists of a material whose collective molecular weight is the sum of the molecular weights of the active mass components. Now assume 1 kg of material and divide by the collective molecular weight, M:

$$\begin{aligned} \frac{\text{1 kg of active material}}{M} &= \#\text{ of moles of total reactant} = x_1 \\ (x_1)(n) &= \#\text{ of moles of electrons} = x_2 \\ (x_2)(F) &= \#\text{ of Ahr} = x_3 \\ (x_3)(E^\circ) &= \#\text{ of Watthr} = x_4 \\ \frac{x_4}{\text{1kg of active material}} &= \text{Energy Density} \end{aligned} \qquad [2]$$

The experimental energy density is lower than the theoretical energy density because in practice one gram-equivalent weight of reactant will not totally react to release a full 26.8 Ahr and because the entire mass of the battery, not just the electrochemically active materials, should be included. The experimental energy density is calculated from the equation

$$\text{Energy density} = \frac{\mathbf{E}}{m} = \frac{1}{m}\int_{t=0}^{t=\infty} IV\,dt \qquad [3]$$

where

$\mathbf{E}$ = energy in watt-hours,

I = current in amps,

V = potential in volts,

t = time of discharge in hours,

and m = mass of the battery in kilograms.

The energy density of a battery can be determined experimentally by discharging the battery. There are several methods that can be used to discharge a battery. Discharging the battery with a constant load through a circuit with a fixed resistor mimics the conditions of actual battery use. Both the potential/time transient and the current/time transient are recorded, and the combined areas under both curves are used to determine the total amount of energy obtained from the battery (Fig. 3). To solve this problem, a numerical method such as the Trapezoid rule can be applied:

$$\mathbf{E} = \int_{t=0}^{t=\infty} IV\,dt = \frac{1}{2}\sum_{t=0}^{n}\left(V_{i+1}I_{i+1} - V_iI_i\right)\left(t_i + t_{i+1}\right) \qquad [4]$$

A review of recent literature (1-17) reveals that the most common method of determining the experimental energy density of a battery is by constant-current charge and discharge of the battery and the use of the relationship (19)

$$\mathbf{E} = \frac{I_{cc}V_{ave}t'}{m} \qquad [5]$$

where

I_{cc} = constant current in amps,

V_{ave} = average value of potential in volts,

and t' = the time beyond which the battery can no longer maintain its rated voltage at a constant current.

Constant current discharges were performed with Ni/Cd, an established battery system, to establish the experimental procedure. The value of V_{ave} was approximately 1.24V-1.25V but t' varied greatly depending on time of charging, rest time between discharges, cycle number, and amount of charging current. A typical constant current discharge curve for the Ni/Cd battery is shown in Fig. 4. This constant current discharge procedure will be used as a basis for comparison in future studies with the Li/$LiClO_4$/PPy battery.

III. PROGRESS IN WHITE'S GROUP

The progress made in White's group consists of developing new mathematical models for a polypyrrole film applications on a rotating disk electrode (RDE) and in a secondary battery cell. Descriptions of the models are presented next.

A. MODEL OF ROTATING DISK ELECTRODE

A mathematical model for a flat (not fibrillar) polypyrrole film on a rotating disk electrode has been developed in an effort to elucidate the kinetic mechanism and charge transfer phenomena within a polypyrrole film. The RDE was chosen because of its well-defined hydrodynamics. The model equations are based on published information that claims that the polypyrrole film is a porous electrode with a high surface-to-volume ratio and a large double layer capacitance, which is proportional to the amount of oxidized polypyrrole film (20-23). The governing equations include migration for a charge species in the electric field, diffusion for charged and noncharged species, electrochemical reaction that occurs within the porous polypyrrloe film, and double layer charging. A mathematical model for predicting potentiostatically controlled cyclic voltammograms for a porous polypyrrole film has been submitted as a technical paper to the *Journal of the Electrochemical society* and is presented in Appendix C.

B. MODEL OF SECONDARY BATTERY CELL

A mathematical model for predicting a charge and a discharge process of a $Li/LiClO_4/PPy$ secondary battery system is presented here as a extension work of RDE study. The objectives of this study are to characterize a $Li/LiClO_4/PPy$ secondary battery and to optimize a charge transfer rates in a polypyrrole film.

The $Li/LiClO_4/PPy$ secondary battery system is shown schematically in Fig. 1 and explained by Martin's group in detailed. The electrolyte in this case consists of 0.2

M $LiClO_4$ in propylene carbonate and is referred to as a binary electrolyte because it is assumed that $LiClO_4$ dissociates in propylene carbonate into charged Li^+ and ClO_4^- ionic species.

During charge and discharge, the reaction occurring at the polypyrrole cathode is

$$PPy^+ClO_4^- + e^- \rightleftharpoons PPy^\circ + ClO_4^- \qquad [6]$$

and the reaction at the lithium anode is

$$Li \rightleftharpoons Li^+ + e^- \qquad [7]$$

so that the overall reaction is

$$PPy^+ClO_4^- + Li \rightleftharpoons PPy^\circ + ClO_4^- + Li^+ \qquad [8]$$

where PPy^+ is the oxidized form of polypyrrole and PPy° is the reduced form of polypyrrole. It is noted that ClO_4^- ion is not oxidized or reduced during the electrochemical reaction. It serves only as a negative counter-ion to preserve electroneutrality in the system.

A section of the cell that is relevant to the development of the model equations is shown schematically in Fig. 5. This section consists of the following boundaries and regions: a platinum current collector/porous polypyrrole cathode interface; a porous polypyrrole cathode of width δ_{PE} (region 1); a porous polypyrrole cathode/reservoir interface; a reservior of width δ_{RE} (region 2); and a reservoir/lithium anode interface.

The dependent variables in the reservoir are: the concentrations of Li^+ (c_+), the concentrations of ClO_4^- (c_-), the superficial current density in the solution phase (i_2), and the potential of the solution phase (Φ_2). In the porous polypyrrole cathode, the dependent variables include the ones in the reservoir, the superficial current density in the solid phase (i_1), and the potential of the solid phase (Φ_1). Values for these

unknowns are obtained by solving the governing equations and boundary conditions as a function of position and time. The assumptions and descriptive equations for the model are presented next.

1. Reservoir

Mass transfer in the reservoir is governed by a differential material balance equation for a dissolved species i:

$$\frac{\partial c_i}{\partial t} = -\nabla \cdot \mathbf{N}_i \qquad [9]$$

The material balance equation depends on the flux of species i, $\mathbf{N}_i$. This flux is due to migration in the electric field and diffusion in the concentration gradient and is expressed as follows:

$$\mathbf{N}_i = -z_i u_i F c_i \nabla \Phi_2 - D_i \nabla c_i \qquad [10]$$

where the ionic mobility, u_i, is described by the Nernst-Einstein equation (24)

$$u_i = \frac{D_i}{RT} \qquad [11]$$

Combining Eq. [9], [10], and [11] yields the governing equation for species i within the reservoir:

$$\frac{\partial c_i}{\partial t} = \frac{z_i D_i F}{RT}\left(c_i \frac{d^2\Phi_2}{dy^2} + \frac{dc_i}{dy}\frac{d\Phi_2}{dy}\right) + D_i\left(\frac{d^2 c_i}{dy^2}\right) \qquad [12]$$

It is assumed that the transport occurs only in the axial direction (i.e., y direction).

The superficial current density is due to the movement of charged species (25)

$$i_2 = F\sum_i z_i \mathbf{N}_i \qquad [13]$$

Substitution of Eq. [10] into [13] yields

$$i_2 = -\kappa\frac{\partial \Phi_2}{\partial y} - F\sum_i z_i D_i \frac{\partial c_i}{\partial y} \qquad [14]$$

where κ is the solution conductivity. The second term on the right in Eq. [14] represents the concentration potential. It must be noted that the concentration potential term will disappear when the ionic diffusion coefficients are all the same. The electroneutrality condition applies in the reservoir region and is given as

$$\sum_{i} z_i c_i = 0 \qquad [15]$$

2. Porous Polypyrrole Cathode

The porous polypyrrole cathode consists of a conductor (PPy^+) and a nonconductor (PPy°) solid phase and a solution phase of binary nonaqueous electrolyte that penetrates the void spaces of the porous matrix. Macroscopic properties are used to describe physically the porous polypyrrole cathode in terms of simple measurable parameters without regard to the actual geometrical details of the pore structure. Two of these properties are the porosity (ϵ) and the MacMullin number ($N_{M,PE}$). The porosity represents the void volume fraction within the volume element occupied by the electrolyte. The MacMullin number is defined as the ratio of the tortuosity to the porosity (26):

$$N_{M,PE} = \tau/\epsilon \qquad [16]$$

The porosity and MacMullin number are assumed to be constant.

Material Balance

To account for the nonhomogeneous structure of the porous matrix, averaging is applied to the local variables within a volume element throughout the porous layer. The differential material balance equation is formulated for a dissolved species i in terms of average quantities as follows (25):

$$\frac{\partial \epsilon c_i}{\partial t} = -\nabla \cdot \mathbf{N}_i + R_i' \qquad [17]$$

where c_i represents the concentration of species i per unit volume of electrolyte within the porous matrix, ϵc_i represents the average concentration per total unit volume including the solid polymer phase and the electrolyte that occupies the space within the matrix, and R_i' is the consumption or production rate of species i due to a psuedo-homogeneous reaction (electrochemical reaction [6]) or double layer charge within the porous polypyrrole electrode and is discussed later.

The flux expression in Eq. [10] can be modified to apply to the porous polypyrrole cathode region. This is accomplished by replacing the diffusion coefficient in Eq. [10] by an effective diffusion coefficient

$$D_{i,e} = \frac{D_i}{N_{M,PE}} \qquad [18]$$

Thus, the flux of species i within the porous region becomes

$$\mathbf{N}_i = -\frac{z_i D_i F}{N_{M,PE} RT} c_i \nabla \Phi_2 - \frac{D_i}{N_{M,PE}} \nabla c_i \qquad [19]$$

Combining the axial component of Eq. [19] with the material balance expression Eq. [17], subject to the assumptions mentioned above, yields the governing equation for species i

$$\frac{\partial \epsilon c_i}{\partial t} = \frac{z_i D_i F}{N_{M,PE} RT} \left(c_i \frac{d^2 \Phi_2}{dy^2} + \frac{dc_i}{dy} \frac{d\Phi_2}{dy} \right) + \frac{D_i}{N_{M,PE}} \left(\frac{d^2 c_i}{dy^2} \right) + R_i' \qquad [20]$$

Charge Balance

As a consequence of the electroneutrality assumption, the charge leaving the solid phase must enter the solution phase. This is expressed as (25)

$$\nabla \cdot i_1 + \nabla \cdot i_2 = 0 \qquad [21]$$

where i_1 is the superficial current density (A/cm^2) in the solid phase, and i_2 is the superficial current density in the solution phase. In the solid phase, the movement of electrons is governed by Ohm's law

$$i_1 = -\sigma_e \frac{\partial \Phi_1}{\partial y} \qquad [22]$$

where σ_e is the effective conductivity of polypyrrole and is proportional to the degree of the oxidation of polypyrrole (Appendix C).

Combining Eq. [19] with [13] gives the superficial current density in the solution phase due to the movement of charged species within the porous polypyrrole cathode region (25)

$$i_2 = -\kappa_e \frac{\partial \Phi_2}{\partial y} - \frac{F}{N_{M,PE}} \sum_i z_i D_i \nabla c_i \qquad [23]$$

where κ_e is the effective solution conductivity.

Transfer Current

The consumption or production rate of species i, R_i', is due to a psuedo-homogeneous reaction (electrochemical reaction [6]) or double layer charge within the porous polypyrrole electrode and is given by (25):

$$R_i' = -\frac{s_i}{n_1 F} j \qquad [24]$$

where j is the transfer current per unit volume (A/cm^3) of the porous polypyrrole cathode region and is related to the current density flowing in the liquid and solid phase as follows:

$$j = -\nabla \cdot i_1 = \nabla \cdot i_2 \qquad [25]$$

The current transferred from the matrix to the solution is involved both in double layer charging and in faradaic electrode reactions (21-23)

$$j = j_F + j_C \qquad [26]$$

where j_F is the faradaic transfer current due to electrochemical reaction [6], and j_C is the capacitive transfer current due to double layer charge.

The faradaic transfer current, j_F, is assumed to be given by the Butler-Volmer equation:

$$j_F = a i_{O1,REF} \left\{ \left(\frac{Q_{F,MAX} - Q_F}{Q_{F,MAX}} \right) \left(\frac{c_-}{c_{-,REF}} \right) \exp\left(\frac{\alpha_{a1} F}{RT} \eta_1 \right) - \left(\frac{Q_F}{Q_{F,MAX}} \right) \exp\left(\frac{-\alpha_{c1} F}{RT} \eta_1 \right) \right\} \quad [27]$$

where a is the electroactive surface area per unit volume, $i_{O1,REF}$ is the exchange current density for reaction [6] at a given reference concentration ($c_{i,REF}$), Q_F is the faradaic charge per unit volume of porous polypyrrole cathode, $Q_{F,MAX}$ is the maximum charge state, and η_1 is the overpotential for reaction [6]. Anodic and cathodic current densities are taken to be positive and negative, respectively. Also, s_i is positive for an anodic reactant and negative for a cathodic reactant. Note also that $\alpha_{a1} + \alpha_{c1} = n_1$.

The overpotential (η_1) is defined by

$$\eta_1 = \Phi_1 - \Phi_2 - U_{1,REF} \quad [28]$$

where $U_{1,REF}$ is the open circuit potential for reaction [6] at a given reference concentration ($c_{i,REF}$). It can be seen that the local faradaic transfer current density depends upon the difference between the potential of the solid phase (Φ_1) and the potential of the solution adjacent to the pore surface (Φ_2). The difference between these two properties is expressed relative to the open-circuit potential ($U_{1,REF}$).

The faradaic charge (Q_F) is related to the faradaic transfer current as follows:

$$\frac{\partial Q_F}{\partial t} = j_F \quad [29]$$

Comparison of Eq. [29] to Eq. [27] shows that the rate of build-up of charge in the polymer film due to a faradaic reaction is related to the maximum amount charge that

can be stored in the film, $Q_{F,MAX}$. Note that according to Eq. [27] when $Q_F = Q_{F,MAX}$ no further oxidation of the film can occur.

The anodic faradaic current passed in the porous polymer film leads to charging of the double layer within the pores of the polypyrrole film. At the interface between the solid and solution, the rate of change of the double layer charge per unit volume of electrode is given by (27-28)

$$j_C = aC\frac{\partial(\Phi_1 - \Phi_2)}{\partial t} \qquad [30]$$

where C is a differential capacitance of double layer per unit area of electrode, and the product aC represents the double layer capacity per unit volume of the porous electrode. The product aC is assumed to be proportional to the amount of PPy^+ in the polypyrrole electrode as follows (21-22):

$$aC = a^* Q_F \qquad [31]$$

where a^* is a proportionality constant which is assumed to be independent of potential. The effect of concentration changes on the potential relationships has been neglected here. The double layer itself is assumed to be in local equilibrium at the appropriate concentration and potential difference $(\Phi_1 - \Phi_2)$.

The capacitive charge per unit volume of the electrode, Q_C, is related to the capacitive transfer current as follows:

$$\frac{\partial Q_C}{\partial t} = j_C \qquad [32]$$

3. Boundary Conditions

To complete the system of equations, the boundary conditions must be specified. The porous polypyrrole cathode is bounded by a platinum current collector on one

face (y=0) and by the reservoir on the other (y=y_{PE}). At the current collector/porous polypyrrole cathode interface, the flux of each species i is equal to zero

$$\mathbf{N}_i = 0 \qquad [33]$$

This equation implies that all the current in the cell leaves the electrolyte and enter the current collector

$$i_1 = i \qquad [34]$$

$$i_2 = 0 \qquad [35]$$

At the porous polypyrrole cathode/reservoir interface, the flux of each species i across the two regions must be continuous

$$\mathbf{N}_{i,y}|_{cathode} = \mathbf{N}_{i,y}|_{reservoir} \qquad [36]$$

This implies that all the current in the cell leaves the solid phase and enter the electrolyte because there is no electroactive solid phase beyond this interface

$$i_1 = 0 \qquad [37]$$

$$i_2 = -i \qquad [38]$$

At the reservoir/lithium anode interface, the rate of consumption or production of a Li^+ by the electrochemical reaction [7] is equal to the net normal flux of Li^+ toward or away from the electrode

$$\frac{s_+ j_A}{n_2 F} = \mathbf{N}_+ \qquad [39]$$

where j_A represents transfer current for reaction [7] at the lithium anode and is given by

$$j_A = i_{O2,REF}\left\{\exp\left(\frac{\alpha_{a2}F}{RT}\eta_2\right) - \exp\left(\frac{-\alpha_{c2}F}{RT}\eta_2\right)\right\} \qquad [40]$$

4. Initial Conditions

The concentration of each species i is given by:

$$c_i = c_{i,REF} \quad [41]$$

For convenience, it is assumed that the cell is initially discharged so that the polypyrrole film is fully reduced and ready to be oxidized. Consequently, the faradaic charge per unit volume in the porous polypyrrole cathode region is initially equal to $Q_{F,MIN}$, a minimal charge state

$$Q_F = Q_{F,MIN} \quad [42]$$

5. Solution Method

In the reservoir, Eq. [12], [14], and [15] represent four governing equations for the determination of the quantities c_+, c_-, Φ_2, and i_2. Φ_1 and i_1 are dummy variables treated as constants and are set arbitrarily to zero. In the porous polypyrrole cathode region, Eq. [15], [20], [21], [22], and [23] represent six governing equations for the determination of the quantities c_+, c_-, Φ_1, Φ_2, i_1, and i_2.

The governing equations and boundary conditions can be written in a one-dimensional finite difference form. The resulting system of equations is solved by using Newman's pentadiagonal block matrix equation solver (29). Implicit stepping can be used for the time derivatives (30). After solving this system of equations, the unknowns (c_+, c_-, Φ_1, Φ_2, i_1, and i_2) are obtained from each node point (I, J) as the funtion of time. The total current density (i) flowing through the cell is equal to the sum of the current density flowing in the solid phase (i_1) and the liquid phase (i_2).

IV. FUTURE STUDY

Future work in this area will be divided between efforts directed at understanding the fundamental mechanism of the switching reaction and those aimed at optimizing the battery cathode performance of conducting polypyrrole films.

A. MARTIN'S GROUP

Future work will be concentrated on experimentation with the $Li/LiClO_4/PPy$ secondary battery cell and collaboration with the model being developed in White's group. Different film thicknesses and fibrillar versions of polypyrrole will be used and comparisons will be made of discharge times, charge/time transients, and current step experiments. Fibrillar versions should yield higher current densities and energy densities.

B. WHITE'S GROUP

It is desired to continue a detailed study of the electrode mechanisms and transport phenomena which affect the performance of the polypyrrole electrode process using previously developed mathematical model for RDE. Unknown kinetic parameters (exchange current density, electroactive area, maximum faradaic charge of polypyrrole, diffusion coefficient, transfer coefficient, etc.) can be estimated from the statistical comparison of model predictions to experimental data which will be prepared by Martin's group.

The mathematical model for predicting the charge and discharge process of the $Li/LiClO_4/PPy$ secondary battery system and estimated kinetic parameters can be used to characterize the battery cell. This task is designed to choose the optimal versions of a fibrillar/microporous morphology of a polypyrrole electrode. The model

can be used to generate performance predictions for a variety of electrode designs, and should lead to optimal morphology of the polypyrrole cathode in the secondary battery cell.

NOTATION

a	specific surface area of the porous polypyrrole cathode, cm^{-1}
a^*	double layer constant, V^{-1}
c_i	concentration of species i, mol/cm^3
$c_{i,REF}$	reference concentration of species i, mol/cm^3
c_+	concentration of Li^+, mol/cm^3
c_-	concentration of ClO_4^-, mol/cm^3
C	differential capacitance of double layer per unit volume, $farad/cm^3$
D_i	diffusion coefficient of species i, cm^2/sec
$D_{i,e}$	effective diffusion coefficient of species i, cm^2/sec
$\mathbf{E}$	energy, W-hr
E°	standard cell potential, V
F	Faraday's constant, 96487 C/mol
i	total current density of the cell, A/cm^2
$i_{Oj,REF}$	exchange current density at reference concentrations for reaction j, A/cm^2
i_1	superficial current density in solid phase, A/cm^2
i_2	superficial current density in solution phase, A/cm^2
I	current, A
I_{cc}	constant current used in battery discharge experiments, A
j	transfer current per unit volume at cathode, A/cm^3
j_A	transfer current per unit volume at anode, A/cm^3
j_C	capacitive transfer current per unit volume at cathode, A/cm^3
j_F	faradaic transfer current per unit volume at cathode, A/cm^3
m	mass of the battery, g
M	molecular weight, g/mol

NOTATION (Continued)

n	number of electrons
n_j	number of electrons transferred in reaction j
$\mathbf{N}_i$	flux vector of species i, mol/cm^2-sec
$\mathbf{N}_{i,y}$	y component of flux vector of species i, mol/cm^2-sec
$N_{M,PE}$	MacMullin number for the porous polypyrrole cathode
Q_C	capacitive charge of double layer per unit volume, C/cm^3
Q_F	faradaic charge of polymer film per unit volume, C/cm^3
$Q_{F,MAX}$	maximum faradaic charge of polymer film per unit volume, C/cm^3
$Q_{F,MIN}$	minimum faradaic charge of polymer film per unit volume, C/cm^3
R	universal gas constant, 8.3143 J/mol-K
R_i'	pseudohomogenous reaction rate of species i, mol/cm^3-sec
s_i	stoichiometric coefficient of species i
t	time, sec
t'	time beyond which battery can no longer maintain its rated voltage at a constant current, sec
T	absolute temperature, K
u_i	mobility of species i, mol-cm^2/J-sec
$U_{j,REF}$	theoretical open-circuit potential for reaction j at reference concentration, V
V	potential, V
V_{ave}	average potential, V
y	perpendicular distance from the platinum current collector surface, cm
y_{PE}	position of a cathode/reservoir interface in y coordinate, cm
y_{RE}	position of a reservoir/anode interface in y coordinate, cm
z_i	proton charge number of species i

NOTATION (Continued)

Greek Symbols

α_{aj}	anodic transfer coefficient for reaction j
α_{cj}	cathodic transfer coefficient for reaction j
δ_{PE}	thickness of polypyrrole film, cm
δ_{RE}	thickness of reservoir, cm
ΔG°	standard Gibb's free energy change, W-hr
ϵ	porosity or void volume fraction
ϵc_i	superficial concentration of species i in a porous cathode, mol/cm^3
η_j	overpotential for reaction j, V
κ	solution conductivity, Ω^{-1}-cm^{-1}
κ_e	effective solution conductivity, Ω^{-1}-cm^{-1}
σ_e	effective solid conductivity, Ω^{-1}-cm^{-1}
τ	tortuosity of porous material
Φ_1	potential in solid phase, V
Φ_2	potential in solution phase, V
Φ_{RE}	potential in the solution at reference electrode, V

REFERENCES

1. A. G. Macdiarmid, L. S. Kang, W. S. Huang, and B. D. Humphrey, *Syntehtic Metals*, **18**, 393 (1987).

2. R. B. Kaner and A. G. Macdiarmid, *Syntehtic Metals*, **14**, 3 (1986).

3. M. Maxfield, S. L. Mu, and A. G. Macdiarmid, *J. Electrochem. Soc.*, **182**, 838 (1985).

4. W. Wangun, P. J. Mammone, and A. G. Macdiarmid, *Syntehtic Metals*, **10**, 235 (1985).

5. J. Caja, R. B. Kaner, and A. G. Macdiarmid, *J. Electrochem. Soc.*, **131**, 2744 (1984).

6. K. Kaneto, M. Maxfield, D. P. Nairns, A. G. MacDiarmid, and A. J. Heeger, *J. Chem. Soc. Faraday Trans.*, **78**, 3417 (1982).

7. P. J. Nigrey, A. G. Macdiarmid, and A. J. Heeger, *Mol. Cryst. liq. Cryst.*, **18**, 309 (1982).

8. P. J. Nigrey, D. MacInnes, Jr., D. P. Nairns, A. G. Macdirmid, and A. J. Heeger, *J. Electrochem. Soc.*, **128**, 1652 (1981).

9. T. Osaka, K. Naoi, H. Sakai, and S. Ogano, *J. Electrochem. Soc.*, **134**, 285 (1987).

10. K. Naoi, A. Ishijima, and T. Osaka, *J. Electroanal. Chem.*, **217**, 203 (1987).

11. P. Passiniemi and J. E. Osterholm, *Syntehtic Metals*, **18**, 637 (1987).

12. L. W. Shacklette, M. Maxfield, S. Gould, J. F. Wolf, T. R. Jow, and R. H. Baughman, *Synthetic Metals*, **18**, 259 (1987).

13. H. Munstedt, G. Kohler, H. Mohwald, D. Naegele, R. Bitthin, G. Ely, and E. Meissner, *Syntehtic Metals*, **18**, 259 (1987).

14. F. Trinidad, J. Alonso-Lopez, and M. Nebot, *J. Applied Electrochemistry*, **17**, 215 (1987).

15. S. Panero, P. Prosperi, B. Klaptse, and B. Scrosati, *Electrochimica Acta*, **31**, 1597 (1986).

16. N. Mermilliod, J. Tanguy, and F. Petiot, *J. Electrochem. Soc.*, **133**, 1073 (1986).

17. T. Yamamoto, M. Zama, and A. Yamamoto, *Chemistry Letters (Chemical Soc. Japan)*, 1985, pp. 563-6.

REFERENCES (Continued)

18. "Handbook of Batteries and Fuel Cells," Ed. by David Linden, McGraw-Hill, 1984, pp. A3-A10.

19. D. Pletcher, "Industrial Electrochemistry", pp. 242-245, Chapman and Hall (1982).

20. A. F. Diaz, J. I. Castillo, J. A. Logan, and W. Lee, *J. Electroanal. Chem.*, **129**, 115 (1981).

21. R. A. Bull, F. F. Fan, and A. J. Bard, *J. Electrochem. Soc.*, **129**, 1009 (1982).

22. S. W. Feldberg, *J. Am. Chem. Soc.*, **106**, 4671 (1984).

23. P. G. Pickup and R. A. Osteryoung, *J. Electroanal. Chem.*, **195**, 271 (1985).

24. J. Newman, "Electrochemical Systems," Prentice-Hall, Englewood Cliffs, NJ (1973).

25. J. Newman and W. Tiedemann, *AIChE J.*, **21**, 25 (1975).

26. W. E. Ryan, R. E. White, and S. L. Kelly, *J. Electrochem. Soc.*, **134**, 2154 (1987).

27. A. M. Johnson and J. Newman, *J. Electrochem. Soc.*, **118**, 510 (1971).

28. P. Delahay, "Double Layer and Electrode Kinetics," Interscience Publisher, Paul Delahay, NY (1965).

29. J. V. Zee, G. Kleine, R. E. White, and J. S. Newman, in "Electrochemical Cell Design," R. E. White, Ed., pp377-389, Plenum Press, NY (1984).

30. B. Carnahan, H. A. Luther, and J. O. Wilkes, "Applied Numerical Methodes," John Wiley & Sons, NY (1969).

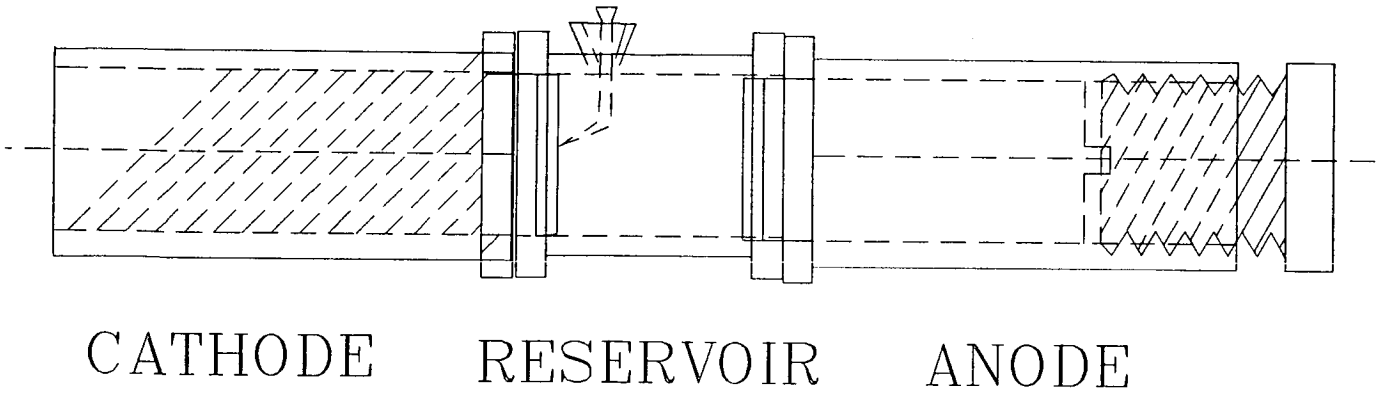

Fig. 1. Schematic of a Li/$LiClO_4$/PPy secondary battery cell

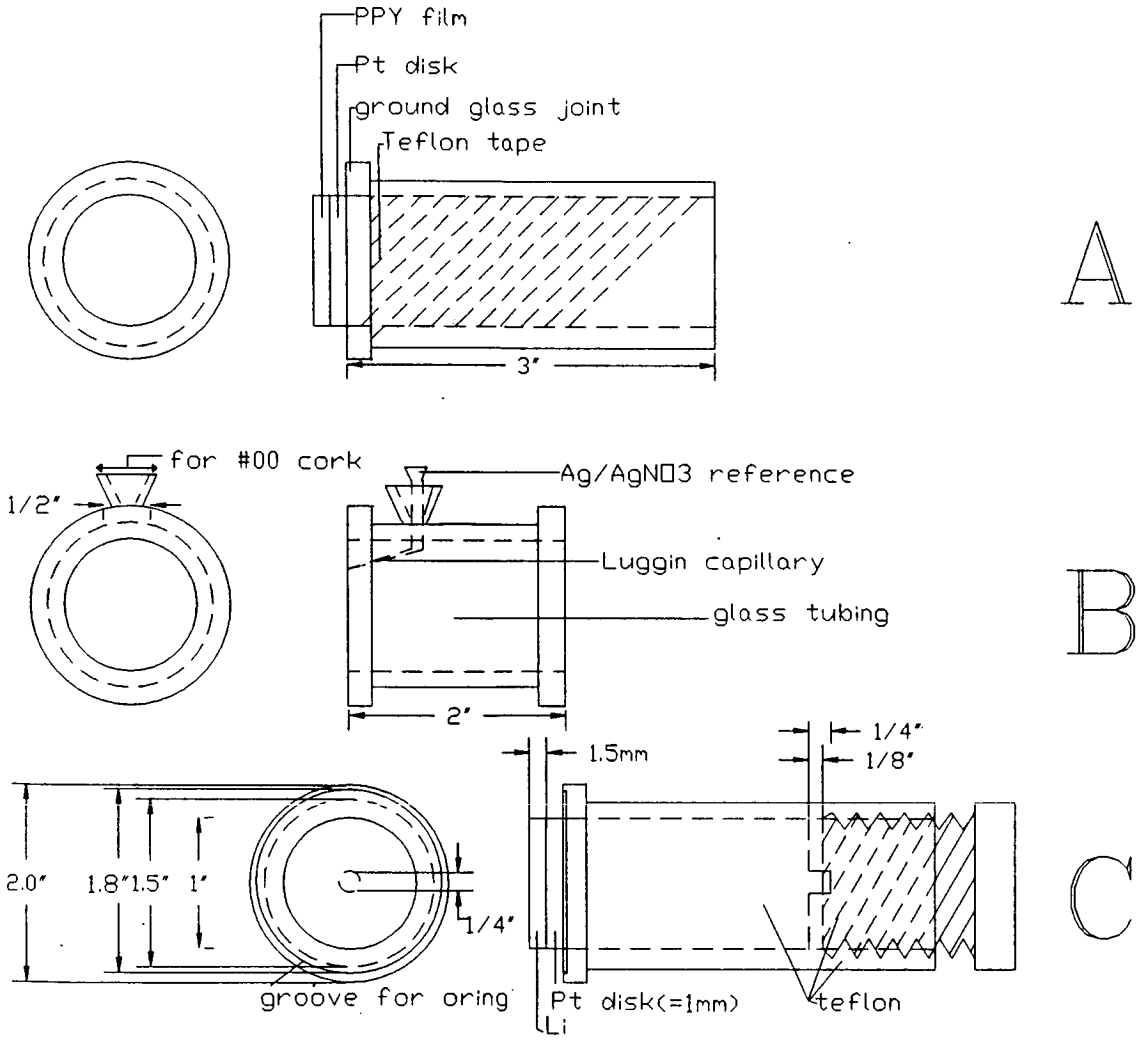

Fig. 2. Detailed schematic of a $Li/LiClO_4/PPy$ battery

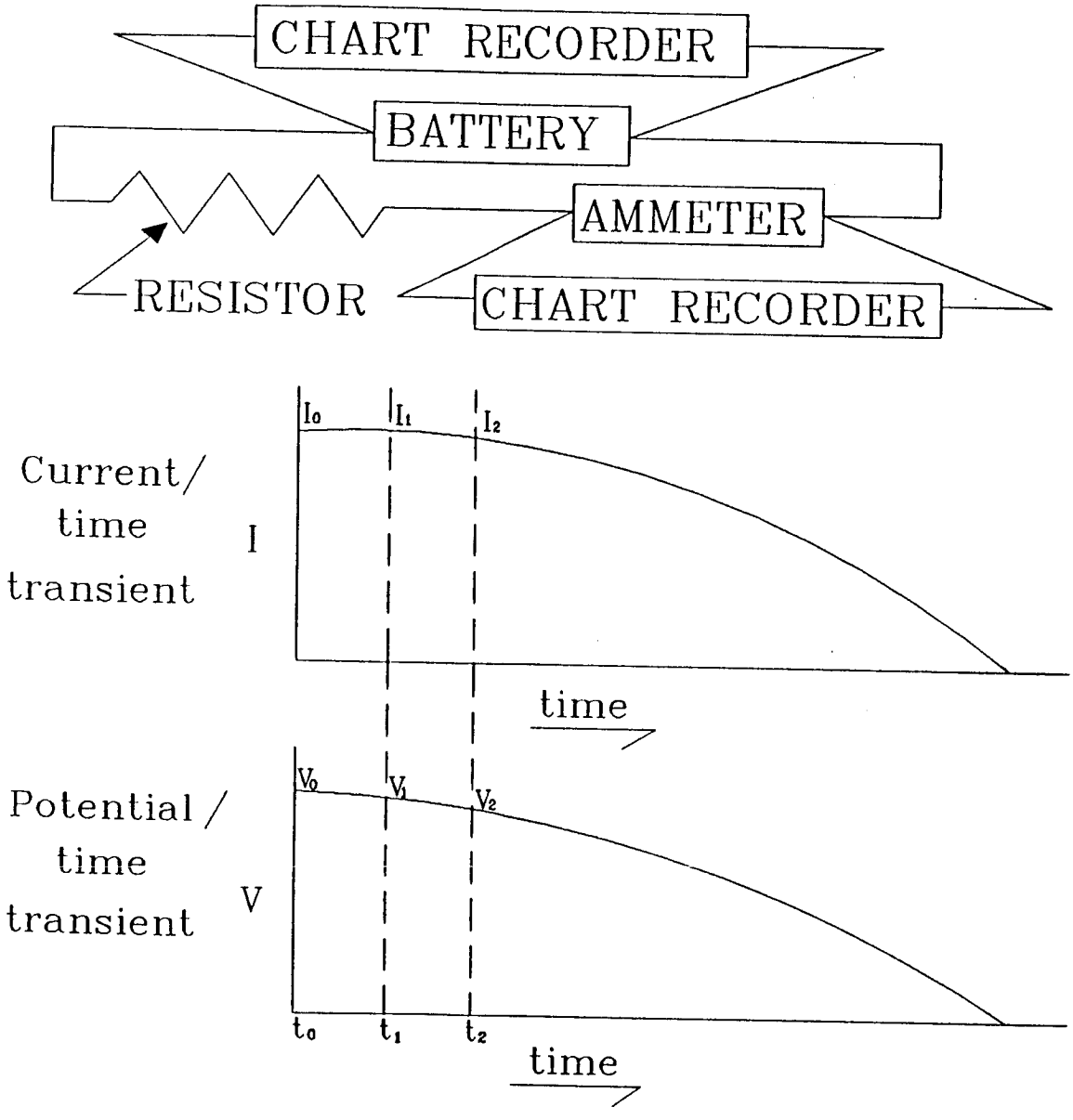

Fig. 3. Constant load battery discharge

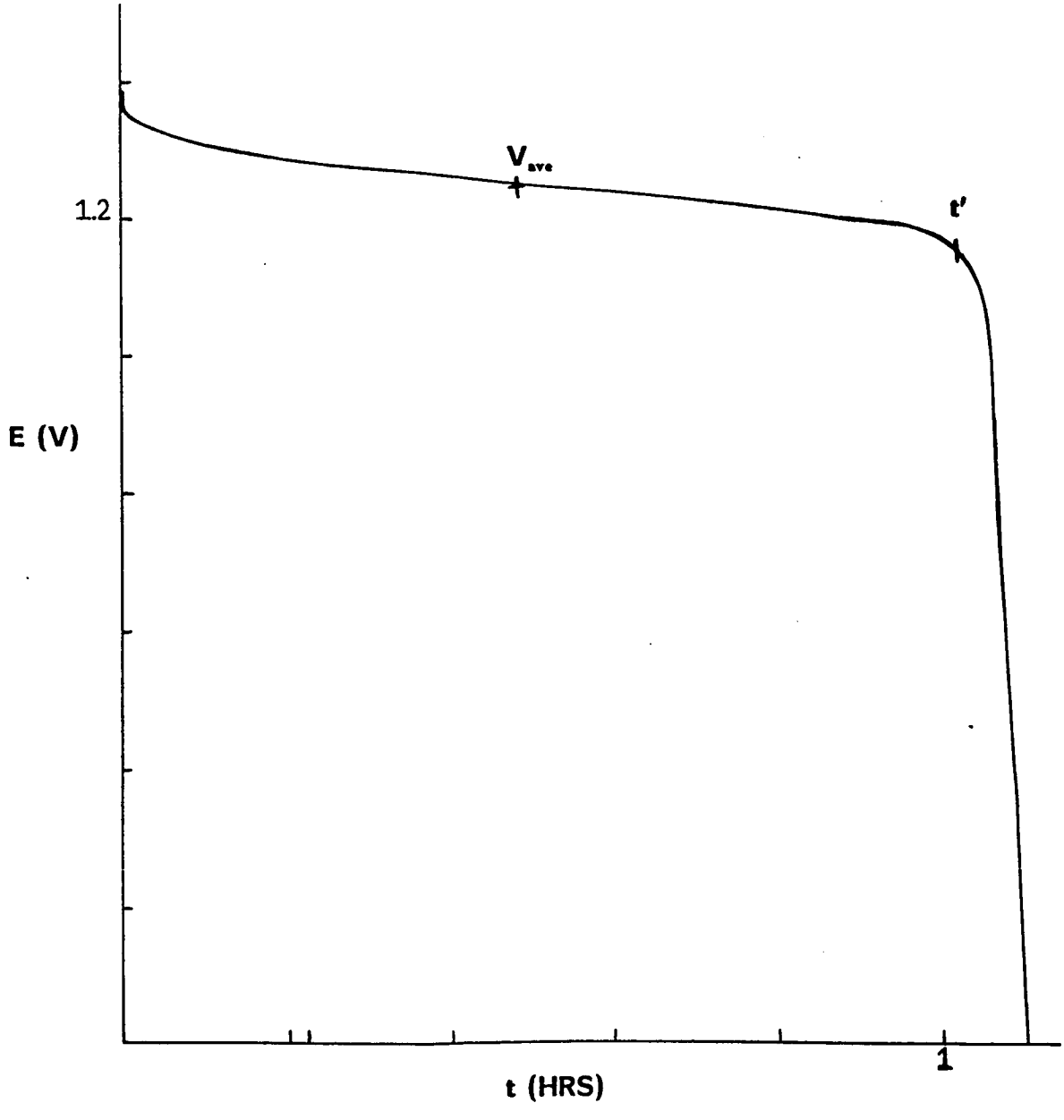

Fig. 4. Typical discharge curve for a Ni/Cd secondary battery

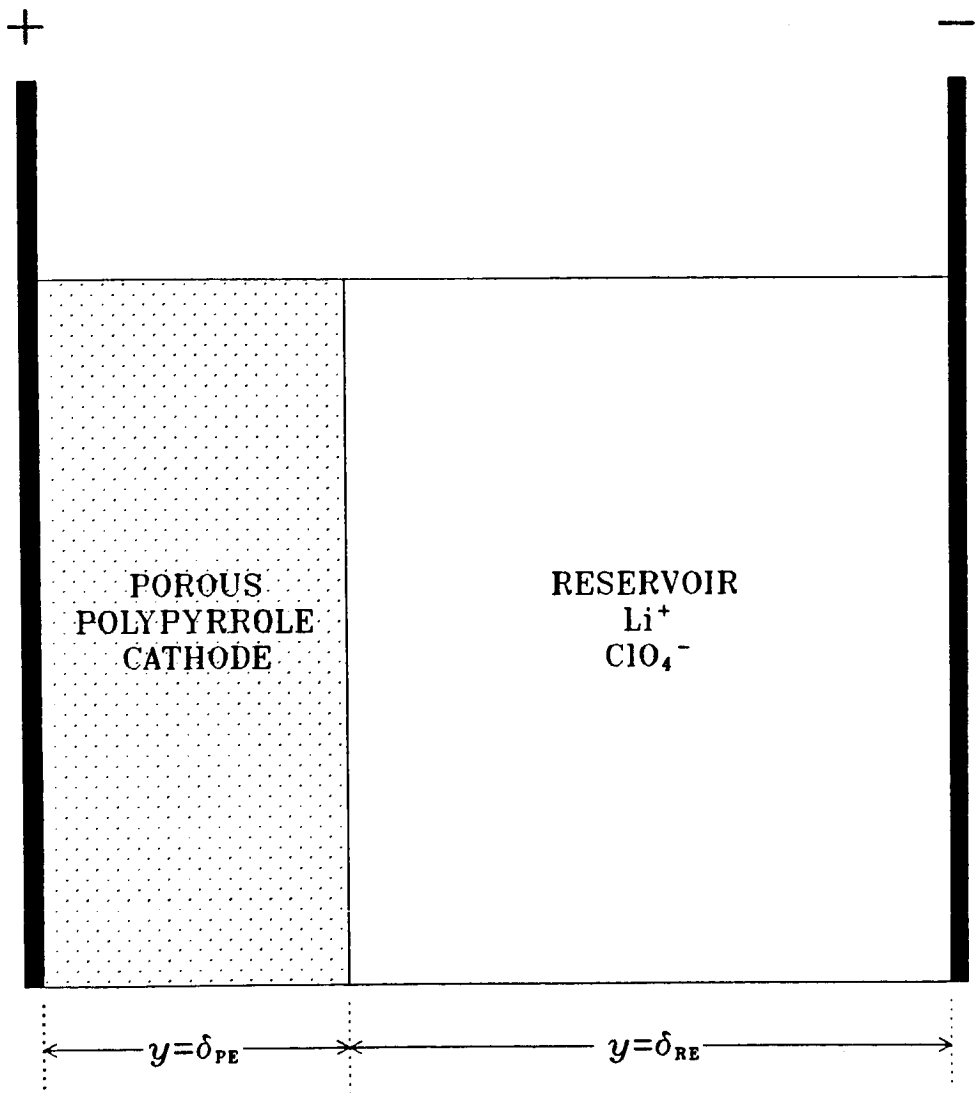

Fig. 5. Schematic of a modeling region

APPENDIX A

P-54

AC IMPEDANCE ANALYSIS OF POLYPYRROLE THIN FILM

AC Impedance Analysis of Polypyrrole Thin Films

Reginald M. Penner** and Charles R. Martin*

Department of Chemistry

Texas A&M University

*Electrochemical Society Active Member, to whom correspondence should be addressed.

**Electrochemical Society Student Member, Present Address:

Department of Chemistry, Stanford University

Stanford, CA 94305

ABSTRACT

The AC impedance spectra of thin (0.27 μm) polypyrrole films have been obtained at open circuit potentials from -0.4 V to 0.4 V vs. SCE. Two limiting cases are discussed for which simplified equivalent circuits are applicable. At very positive potentials, the predominently nonfaradaic AC impedance of polypyrrole is very similar to that observed previously for finite porous metallic films. Modeling of these data with the appropriate equivalent circuit permits effective pore diameter and pore number densities of the oxidized film to be estimated.

At potentials from -0.4 V to -0.3 V, the polypyrrole film is essentially nonelectronically conductive and diffusion of polymer oxidized sites with their associated counterions can be assumed to be linear from the film/substrate electrode interface. The equivalent circuit for the polypyrrole film at these potentials is that previously described for metal oxide, lithium intercalation thin films. Using this model, counterion diffusion coefficents are determined for both semi-infinite and finite diffusion domains. The diffusion coefficient data so obtained is consistant with the existance of a gradient in the morphology of the polypyrrole films in a direction normal to the surface of the electrode.

In addition, the limiting low frequency resistance and capacitance of the polypyrrole thin films is determined and compared to that obtained previously for thicker films of the polymer. The origin of the observed potential dependence of these low frequency circuit components is discussed.

INTRODUCTION

A number of technological applications for electronically conductive polyheterocycles (eg. polypyrrole, polythiophene) have been demonstrated in recent years. These include the application of polyheterocyclic films as potentiostatically controlled ion-gates (1,2), in electrochromic displays (cf.3,4), as battery cathode materials (5-8), and in chemically responsive transistors (9-11). All of these applications rely on the ability of the electronically conductive polymer to "switch" rapidly and reversibly between insulating and conducting redox states. The rate of the polymer redox reaction for electrochemically synthesized conducting polymers has been shown to be inversely related to the thickness of the polymer film (8,10,12) For this reason, the design of polymer-based devices has emphasized the use of extremely thin ($l < 1$ μm) polymer films (8,10,12).

Despite the importance of polyheterocyclic films of submicron thickness, little is currently known about mass transport in these thin films. Previous AC impedance studies of polypyrrole by Burgemayer and Murray (1,2) and more recently by Tanguy et al. (13,14) have employed relatively thick (> 5 μm) polymer films. Such films cannot be quantitatively addressed electrochemically; ie., as-synthesized oxidized polymer cannot be quantitatively reduced (15,16). Consequently, the extraction of mass transport and kinetic information from this data is not straightforward. Bull et al. examined the AC impedance behavior of thin polypyrrole films over a broad frequency band but did not consider mass transport in the analysis of these data (17). Glarum et al. has recently published an analysis of the potential dependant AC impedance behavior of thin electronically conductive polyaniline films (18).

Recently, AC impedance analyses have been applied to the determination of diffusion coefficients in electrochromic WO_3 films (19) and in redox polymer film modified electrodes (20). This work has demonstrated that transport information can be obtained from AC impedance data for any system which exhibits finite, linear diffusion, providing the heterogeneous electron transfer kinetics of the system are suitably fast. AC impedance possesses several advantages for the determination of diffusion coefficients as compared to conventional, large amplitude, electrochemical experiments such as chronocoulometry. In contrast to Cottrell-type experiments in which diffusion coefficient information is obtained while the system is in flux from one redox state to another, the perturbation of the film redox state during an AC impedance experiment is extremely small permitting transport information to be obtained for any discrete ratio [Ox]/[Red]. Consequently, morphological changes in the film structure which can accompany a bulk conversion from one redox state to another are avoided; characteristics of the film associated with a particular redox state can be elucidated. In addition, a wide band of frequencies can be addressed in an AC impedance experiment allowing the characteristic time-scale of an electrochemical process, such as diffusion, to be isolated as the corresponding frequency interval and differentiated from events with other characteristic time-scales. Consequently, both kinetic and mass transport information can obtained from the same experiment.

In this paper, we interpret the AC impedance data obtained for 0.27 μm $\pm$ 0.02 μm films in the context of the limiting behavior which is observed for polypyrrole films at low doping levels and for fully oxidized films. In the former case (Limiting Case I), the polymer film is essentially

nonelectronically conductive. The equivalent circuit appropriate for this system is that described by of Ho et al. (19) and by Franceschetti et al. (21-23). As noted above, diffusion coefficient information has been obtained using this technique for a number of functionally similar systems including WO_3 lithium intercalation films (19,21-23) and Nafion polymer modified electrodes (20,24).

The AC impedance of oxidized polypyrrole (Limiting Case II) has previously been described in terms of a porous electrode model by Bull et al. (16) and by Burgmayer et al. (1,2). However, a more rigorous model has recently been demonstrated for finite, porous electrodes by Keiser et al. (25) and by Candy et al. (26). The latter model permits film parameters such as the equivalent cylindrical pore diameter and pore number density to be calculated from the AC impedance spectra of finite porous films (26). In the present case, the AC impedance observed for oxidized polypyrrole films is interpretted using the analysis of Candy and coworkers (26).

In addition, the limiting low frequency resistance and capacitance of the polypyrrole thin films is determined and compared to that obtained previously for thicker films of the polymer (13,14). The origin of the observed potential dependence of these low frequency circuit components is discussed.

THEORY

Limiting Case I: Lightly Doped Polymer.

As noted above, a number of recent papers describe the interpretation of AC impedance data for transition metal intercalation compounds (19, 21-23) and redox polymer modified electrodes (20,24). In both of these

systems, a redox couple is confined to a thin film, and the diffusion of the electroactive species in each is finite and linear. We have chosen to use the analysis of Ho et al. because it explicitly treats the limiting cases applicable to polypyrrole (19). The authors have made a number of assumptions in the derivation of this model which need to examined here in the context of the application of this theory to electronically conductive polymers. Two of these assumptions are particularly important: 1) diffusion of the intercalating species is linear, and 2) the Warburg impedance is that due to the diffusion of a single species (Li^o) and hence can be characterized by a single diffusion coefficient (19).

In the case of Li_yWO_3 and other electronically conductive transition metal oxide films, it is commonly assumed that intercalation of Li^+ is preceded by charge transfer and ion pair formation, $Li_y^+WO_3^-$ (or Li_yWO_3), at the oxide film/electrolyte interface (19,22). Because intercalation of the Li^+ is commensurate with charge transfer, Li^o is the only mobile species in the film. Diffusion of the intercalated Li^o then occurs linearly from the film/electrolyte interface. A key point regarding the applicability of the data analysis technique employed by Ho et al. to polyheterocyclic films is the extent to which diffusion in the conducting polymer film is linear. At potentials where polypyrrole is a good electronic conductor (E_{oc} > 0.3 V vs. SCE), diffusion cannot be assumed to be linear since the polymer redox reaction can proceed from any conductive surface in the porous film. However, at open circuit potentials from -0.4 V to -0.3 V (100-200 mV negative of $E^{o\prime}$), where the polypyrrole is lightly doped, the data from the present paper as well as previous experimental evidence (27,28) indicates that the conductivity of the polymer is very low. As the bulk electronic

conductivity of the polymer is low, the redox reaction of the polymer can be assumed to proceed only from the Pt substrate/polymer interface. Hence, it is assumed here that diffusion of oxidized polymer sites (and charge compensating anions) is linear from the Pt substrate/polymer interface at potentials < 0.3 V vs. SCE.

The diffusion coefficient for the diffusion of intercalated Li^{o} in a metal oxide matrix is many orders of magnitude smaller than that for the diffusion of Li^{+} in the contacting electrolyte (ca. 10^{-12} vs. 10^{-5} cm^2 sec^{-1} (19)). In contrast to AC impedance analyses of redox couples in solution (29), the diffusion limited current for Li_yWO_3 is always dictated by slow diffusion of Li^{o} and the expression for the Warburg impedance incorporates a single diffusion coefficient (19,23). It is less clear in the case of polypyrrole if the Warburg impedance can be assumed to be dominated by a single diffusing species, eg. diffusion of the anion. The polymer redox reaction for polypyrrole can be written:

$$PPy^{o} + A^{-} \text{-----} > PPy^{+}A^{-} + e^{-}$$

Diffusion of PPy^{+} sites generated by an AC varying potential signal might be limited by the diffusion of the anion, A^{-}, diffusion of the counterion, C^{+}, electron diffusion; (i.e., the rate of electron hopping), or some combination of these. Buttry and coworkers have performed quartz crystal microbalance (QCM) gravimetry on thin polypyrrole and polythiophene films synthesized in acetonitrile (30). These data indicate that bulky tetrabutylammonium cations are excluded from polypyrrole films during oxidation-reduction cycles (30). Under these circumstances, if electron

hopping can be assumed to be facile, diffusion of PPy^+ will be limited by codiffusion of charge compensating BF_4^- anions. Again, a single diffusion coefficient, D_{BF4-}, is adequate to describe the diffusion limited current. The application of the data analysis technique of Ho et al. to nonpermselective polypyrrole films will yield diffusion coefficients which are composite values containing contributions from both anion and cation diffusion (20,29).

AC impedance analysis of polypyrrole, then, can be made to conform to the assumptions made by Ho et al. by insuring that the polymer is not electronically conductive at the potentials at which diffusion coefficient information is obtained, and by employing a tetrabutylammonium cation which is excluded from the polymer film.

The model proposed by Ho et al. assumes the Randles equivalent circuit shown in Figure 1A (31). However, the usual form of the Warburg (diffusional) impedance is modified to compensate for the finite diffusion length of ions in a thin film. The detailed derivation of these expressions is found in reference 19. The explicit form of the finite Warburg impedance is (19):

$$Z_w = R_w - jX_w \tag{1}$$

where:

$$Xw = (\omega C_w)^{-1} = |Z_w| \sin \beta \tag{2}$$

$$Rw = |Z_w| \cos \beta \tag{3}$$

$$|Zw| = |\nu_o / i_o a| \tag{4}$$

where ν_o is the AC potential amplitude, a is the electrode area, and C_w and

Rw are the Warburg capacitance and resistance respectively. The Warburg phase angle, β, is defined as:

$$\beta = \arctan \frac{(\sinh(2kl))+(\sin(2kl))}{(\sinh(2kl))-(\sin(2kl))} \tag{5}$$

with:

$$k = (\omega/2D)^{1/2} \tag{6}$$

where ω is the angular frequency of the applied AC signal and D is the diffusion coefficient of the counterion, BF_4^-. The current amplitude, i_o, is defined as:

$$io = -\frac{zF}{2}\frac{dC_{BF4-}}{dE}\nu_o\,(\omega D)^{1/2}\left(\frac{h2 + s2}{d2}\right)^{1/2} \tag{7}$$

where dC_{BF4-}/dE is the gradient of polymer oxidation state, and hence BF_4^- concentration, with open circuit potential. The expressions for the equivalent series resistance, R_s, and capacitance, C_s, elements of the faradaic impedance (incorporating the finite Warburg elements (Eq. 2,3)) are given by (29):

$$R_s = R_{ct} + R_w = R_{ct} + |\nu_o/i_o a| \cos\beta \tag{8}$$

$$C_s = C_w = (|\nu_o\omega/i_o a| \sin\beta)^{-1} \tag{9}$$

where R_{ct} is the charge transfer resistance; $R_{ct} = RT/zFI_o$. The expressions for the real, Z[re], and imaginary, Z[im], components of the total impedance are obtained by substituting Eq. 8 and Eq. 9 into the expressions for Z[re] and Z[im] in the Randles circuit (29,30):

$$Z[re] = R_u + \frac{R_s}{((C_d/C_s)+1)^2 + (\omega R_s C_d)^2} \tag{10}$$

$$Z[im] = \frac{\omega R_s^2 C_d + C_d/(C_s^2 \omega^1) + (\omega C_s)^{-1}}{((C_d/C_s)+1)^2 + (\omega R_s C_d)^2} \tag{11}$$

Where R_u is the series resistance of the solution and the polymer film.

With these expressions, Nyquist diagrams can be generated for any combination of experimentally adjustable parameters. In practice, two important limiting subcases of Limiting Case I can be differentiated: IA) thick films and/or small diffusion coefficients ($kl \gg 1$), and, IB) thin films and/or large diffusion coefficients ($kl \ll 1$) (19).

Limiting Case IA corresponds to semi-infinite linear diffusion; ie., the maximum excursion of the diffusion layer at steady-state is less than the film thickness. In this case, β becomes 45° and the Nyquist plot (Z[im] vs. Z[re]) is linear with a slope of 1. From this linear region, if dE/dC is known, the diffusion coefficient can be evaluated from the linear dependence of the impedance modulus, |Z|, with $\omega^{-1/2}$ (19):

$$|Z| = |[(dE)/(dC)][FD^{1/2}a]^{-1}w^{-1/2}| \tag{12}$$

In Limiting Case IB, the diffusion layer accesses the entire film volume corresponding to thin-layer electrochemical behavior. The Warburg phase angle, β, is 90^{o} and the Nyquist plot becomes vertical at a resistance of $(R_1+R_{ct}+R_u)$. The value of R_1, and hence the position of this vertical branch, is sensitive to the diffusion coefficient (19):

$$Z[re] = R_1 = \frac{1}{3nFaD}(dE/dC) \qquad (13)$$

The capacitance also becomes frequency independent under these conditions and equal to C_1 (19):

$$Z[im] = \frac{1}{\omega C_1} = |(dE/dC)/nF\omega la| \qquad (14)$$

Eqs. 13 and 14 may be used to calculate D and dC/dE simultaneously from R_1 and C_1 obtained from the low frequency region of the Nyquist plot.

For perfectly homogeneous films, the diffusion coefficients calculated from the semi-infinite frequency regime (Limiting Case IA) ought to agree with those obtained at frequencies corresponding to the finite diffusion case (Limiting Case IB).

Limiting Case II: Oxidized Polymer.

Although the theory for the AC impedance of porous electrodes is well established (32-34), only relatively recently has the AC impedance of thin, porous, metallic films been examined (25,26). The work of Kaiser et al. (25) and Candy et al. (26) has involved finite porous electrodes in contact

with electrolyte solutions containing no redox couple; systems for which the impedance is entirely nonfaradaic. Candy et al. have shown that porous metal layers in which the pores have irregular shapes (as, for example, in Raney-metal surfaces), exhibit impedance behavior similar to that predicted for surfaces consisting of cylindrically shaped pores of a uniform diameter (26). Such poorly defined metal films can be evaluated in terms of the pore radius, pore number density, and pore length of the equivalent cylindrical pore electrode (26).

Feldburg (35) and Burgemayer et al. (2) have calculated that the bulk capacitances of 100-200 C cm^{-3} observed for oxidized polypyrrole films can only be accounted for if the specific capacitance of the polymer, and hence its conductivity, is very similar to that of metals. Oxidized polypyrrole films, then, might be expected to exhibit AC impedance behavior similar to that of porous metal layers. We have applied the recent model proposed by Candy et al. (26) to the analysis of the AC impedance observed for oxidized (E_{oc} > +0.1 V vs. SCE) polypyrrole films in electrolyte solutions containing no electroactive species. The assumptions inherent in this analysis are simply that the conductivity of electrolyte in the pores of the electrode is known and is the same in all pores, and that the specific capacitance of the porous electrode surface, C_{dl}, is known and uniform. In addition, the capacitance of the Pt substrate electrode surface is assumed to be negligibly small relative to that of the porous bulk of the polymer.

The equivalent circuit for a single, electrolyte-filled cylindrical pore is shown in Figure 1B. The cylindrical pore electrode described above contains n such pores connected in parallel (26). This is the equivalent circuit describing an equal number of finite, parallel transmission lines

(25,34). Note that the faradaic branch found in the Randles circuit (containing R_{ct} and Z_w) is absent from this circuit. The real and imaginary components of the impedance for this circuit are given by (25):

$$Z[re] = Ru + (\lambda/l)\frac{\sinh(\lambda/l) - \sin(\lambda/l)}{\cosh(\lambda/l) - \cos(\lambda/l)} \tag{15}$$

$$Z[im] = (\lambda/l)\frac{\sinh(\lambda/l) + \sin(\lambda/l)}{\cosh(\lambda/l) - \cos(\lambda/l)} \tag{16}$$

where l is the equivalent cylindrical pore length, and λ is the penetration depth of the AC signal, given by (26):

$$\lambda = 1/2(r_c\sigma/\omega C_{dl})^{1/2} \tag{17}$$

Where σ is the conductivity of electrolyte in the pores, ω is the angular frequency, r_c is the equivalent cylindrical pore diameter, and C_{dl} is the specific double-layer capacitance. With these equations, Nyquist diagrams can be generated for any desired set of electrode parameters.

Qualitatively, the Nyquist diagrams calculated from this equation are identical in shape to those generated by Eqs. 10 and 11 except for the absence of the charge transfer limited semi-circle. That is, a 45^o linear region is observed at high frequencies ($\lambda \ll 1$), and both the capacitance and resistance reach the limiting values R_l and C_l at low frequencies ($\lambda \gg 1$). However, the origin of the limiting behavior is different in the

present case than in Case I. The penetration depth of the AC signal (Eq. 17) into the pores of the metallic film is a function of σ, C_{dl}, r_c, and ω. As the frequency decreases, l increases and a greater total pore volume with its associated resistance and capacitance are accessed. Thus, as predicted by Eqs. 15 and 16, increases in Z[re] and $(\omega Z[im])^{-1}$ are commensurate with decreasing ω. At some sufficiently low frequency, $\lambda = 1$ and the total volume accessed by the AC signal approximately equals the total available pore volume. At this frequency, Z[re] and $(\omega Z[im])1-$ assume the limiting values R_1 and C_1.

If C_{dl}, σ, and l are known, the equivalent cylindrical parameters r_c and n of the porous film can be calculated from R_1 and C_1 (26):

$$R_1 = \frac{1}{3n\ r_c^2} \tag{18}$$

$$C_1 = 2n\ r_c l C_{dl} \tag{19}$$

The pore length, l, and the volume of electrolyte in the pores of the film, Vp, are related by the expression:

$$l = (3R_1V_p\sigma)^{1/2} \tag{20}$$

As a consequence of this equation, either l or V_p is sufficient when combined with C_{dl}, σ and the experimental values Rl and Cl to calculate r_c and n for a porous film (26).

EXPERIMENTAL

Materials and Equipment

Platinum foil (t = 0.254 mm, Alfa) and extruded Kel-F rod (d = 0.5 in, Afton Plastics Molding) were used to construct Pt disk electrodes as follows. The Kel-F electrode body was first machined to the dimensions shown in Fig. 2. Pt disks (d = 3.3 mm) were then heat-sealed onto the surface of the Kel-F body by melting the Kel-F around the Pt disk with a heat gun and physically pressing the Pt disk into the heat-softened surface with a glass rod. Electrical contact was made to the back of the Pt disk with a copper wire and silver epoxy (Epo-Tek 410E, Epoxy Technology) as shown in Fig. 2. Excess Kel-F was removed from the surface of the Pt/Kel-F electrode by polishing with 400 grit and 600 grit Carbimet (Beuhler) paper until a planar electrode surface was established. This surface was then further polished sequentially with 1.0 μm, 0.3 μm, and 0.05 μm alumina powder (all from Buehler Inc.). After this initial polishing sequence, the electrode surface was polished between experiments with 0.05 μm alumina only.

A large area, Pt gauze counter electrode (25 x 25 mm, AESAR) and a conventional saturated calomel reference electrode (SCE) were employed for all electrochemical experiments.

Tetrabutylammonium tetrafluoroborate electrolyte was prepared from ammonium tetrafluoroborate (97+%, Aldrich) and tetrabutylammoniun bromide (99% Aldrich) and recrystalized from ethyl acetate-pentane. The recrystallized salt was dried envacuo at 100 C for ca. 24 hrs. prior to use. Pyrrole (98%, Aldrich) was distilled in an inert atmosphere and stored over

argon. Acetonitrile (Burdick and Jackson, UV Grade) was used as received. All solutions employed for electrochemical measurements were purged with purified N_2 prior to use.

A EG&G PAR Model 273 potentiostat/galvannostat was employed for film deposition and all electrochemical measurements. Cyclic voltammograms were recorded on a Houston Instruments Model 2000 X-Y recorder. AC impedance measurements were performed in conjunction with a computer controled EG&G Model 5301 Lockin Amplifier and EG&G AC impedance software. At frequencies greater than 5 Hz., the applied sine-wave excitation signal was generated and the current response analyzed by the lockin amplifier-controlled PAR 273. The measured impedances were then transfered to the computer for display and storage. At lower frequencies, the EG&G software removes the lockin amplifier from the circuit and the sine wave excitation signal is computer generated. The current response obtained from any desired number of cycles is measured by the 273, then analyzed by computer via a fast fourier transform (FFT) algorithm. At these lower frequencies, the impedance was determined from the data obtained from 3 cycles. The amplitude of the applied potential sine wave in each case was 10 mV. Calibration of the 5301 is accomplished automatically with internal standards. All impedance measurements were normalized to an electrode area of 1 cm^2.

The conductivity of 0.2 M Bu_4NBF_4, MeCN electrolyte was measured with a Yellow Springs Instruments Model 31 AC conductivity bridge and a conventional YSI parallel plate conductivity cell. The cell constant was determined with KCL solutions. All solutions were equilibrated in a 25 C water bath.

Film Deposition and Electrochemical Measurments

Polypyrrole films were prepared from monomer solutions containing 0.5 M pyrrole, 0.2 M Bu_4NBF_4 in acetonitrile. Polymerization was accomplished galvanostatically in a conventional one-compartment cell at a current density of 1.0 mA cm^{-2}. A polymerization charge of 0.10 C cm^{-2} was found to correspond to an oxidized film thickness of 0.27 $\mu m \pm 0.02$ μm as measured by a Tencor Alfa-Step profilometer. After deposition, the integrity of each polymer film was ascertained by recording a cyclic voltammogram at 20 mV/sec. All electrochemical measurments were conducted in N_2 purged, 0.2 M Bu_4NBF_4, acetonitrile electrolyte.

AC impedance data was obtained by first potentiostating the polymer at the desired potential for 60 seconds, then equilibrating the polymer at open circuit for 120 seconds. The polymer was then potentiostated at the terminal open circuit potential before AC impedance data acquisition was initiated. This procedure resulted in Nyquist diagrams which exhibited no hysteresis with varying potential. This indicates that the impedance data is obtained at each potential on polymer which is in equilibrium with the mean applied potential. The AC impedance was measured for each open circuit potential at 42 frequencies from 0.05 Hz. to 100 KHz.

RESULTS AND DISCUSSION

Figure 3 shows a cyclic voltammogram in 0.2 M Bu_4NBF_4, MeCN electrolyte for a typical 0.27 μm polypyrrole film employed for the AC impedance studies below. The large capacitive currents in the region positive of the polymer redox reaction ($E > +0.1$ V) indicate that the polymer is electronically conductive in its oxidized state. At potentials negative of ca. -0.3 V, the

capacitive currents decrease dramatically since the reduced polymer is an electronic insulator. The unusual, asymmetric shape of this voltammogram has been observed previously for thin polypyrrole films prepared and cycled in Bu_4NBF_4, MeCN electrolyte (36). As mentioned above, such cyclic voltammograms were routinely used to ascertain the quality of the polypyrrole films sythesized prior to performing the AC impedance experiments.

Oxidized polypyrrole

Theoretical Nyquist data for porous metallic films can be calculated for the film parameters r_c and n from Eqs. 15 and 16 provided that σ, C_{dl}, and either l or V_p are known. In the case of porous metal films, values for Vp are conveniently obtained gravimetrically from measurements of the water content of water impregnated films (26). This procedure, however, is impractical for the 0.27 μm polypyrrole films employed in this study since such films are too thin to be removed intact from the substrate electrode surface. For the purposes of estimating the parameters r_c and n, then, V_p was taken to be equal to the total film volume, $V_f = r^2 l$, and l was calculated from Eq. 20. An estimated value for C_{dl} of 20 $\mu F\ cm^2$ was also employed based on the calculations of Feldburg (35). Again, this number which is typical of metal/electrolyte interfaces should be considered to be a limitingly high value. Because r_c is proportional to both C_{dl} and V_p, values for r_c calculated from these estimates of C_{dl} and V_p should be considered maximum values.

Experimental and simulated Nyquist diagrams for polypyrrole at three open circuit potentials in the interval from +0.4 to +0.2 V are shown in

Figure 4. Figure 4A shows a comparison of the experimental data obtained at low frequencies ($f < 5$ Hz.). Note that at all three potentials, Z[re] is nearly frequency independent. As shown in Figure 5, plots of Z[im] (= $1/\omega C_s$) vs. ω^{-1} for this low frequency data are linear ($r > 0.999$) indicating that the capacitance is constant ($C_s = C_l$). Because this potential region is well positive of the polymer electrochemistry ($E^o = -0.2$ V), changes in the formal oxidation state of the polymer over this interval are small, ie. the polymer is essentially 100% oxidized at $E_{oc} > 0.2$ V. The similarity of the three plots shown in Figure 4A, then, corroborates the conclusion that the observed impedence is predominately nonfaradiac. Thus, Case II limiting behavior is observed.

Figures 4B - 4D show the high frequency Nyquist data in greater detail. Simulated plots were generated in each case by fitting to the experimental data using r_c and n as adjustable parameters. The resulting best-fit values for these parameters are listed in Table I. Note that the agreement between the simulated and the experimental data is best at 0.393 V (Fig. 4B). In particular, at this potential the elbow in the Nyquist plot occurs at very similar frequencies; ca. 40 rad sec^{-1} (expt.) vs. 25 rad sec^{-1} (calc.). The values for r_c and n of 4.26 A and 5.43×10^{12} pores cm^{-2} obtained from the simulation at 0.393 V (Table I) are reasonable limiting values in view of what is known about the morphology and mass transport characteristics of polypyrrole films. For example, as mentioned above, the data of Buttry and coworkers indicates that Bu_4N^+ with a crystallographic radius $r_{Bu_4N^+}{}^o = 4.75$ A (39) is excluded from polypyrrole during electrochemical oxidation/reduction cycles whereas ClO_4^- ions ($r_{ClO_4^-}{}^o = 2.5$ A (39)) diffuse into and out of the film (30). In addition, scanning

electron micrographs (SEM) of polypyrrole obtained previously in this lab and by others (cf. 37,38) reveals that polypyrrole has an extremely dense, compact morphology. That individual pores or channels are not resolved by SEM indicates that any such structures must possess dimensions < ca. 50 A.

However, several important discrepancies between the experimental and the simulated data obtained at 0.393 V (Fig. 4B) are evident. Most noticeable are differences in the transistion from the high frequency 45° data to the low frequency limiting region. In contrast to the simulated data, the experimentally observed transition is more gradual; occurring over a band of frequencies from 10 - 60 Hz. Keiser and coworkers have determined that the exact shape of the Nyquist plot for a porous electrode is sensitive to the geometry of the pores (25). Their calculations for a variety of pore geometries predict that positive deviations in the Nyquist data relative to the cylindrical pore case are observed in the transition region for pores which possess a decreasing radius (25); ie., a pore radius less at the electrode end than at the electrolyte end. A similar positive deviation is observed for the data obtained at 0.276 V (Fig. 4C). This deviation may indicate that the mean pore diameter decreases as the polypyrrole film is traversed from the electrolyte/film interface to the electrode. Alternatively, this gradual transition may reflect the non-homogeneity of either r_c or 1.

A second discrepancy relative to the simulated data is observed at frequencies above ca. 10 KHz. where Z[im] becomes negative. Experimental data in this frequency region was irreproducible from film to film. Negative Z[im] values at high frequencies reflect the presence of inductive effects which are not predicted by simple porous electrode theory (25,26).

Consequently, a more complex equivalent circuit may be required to thoroughly describe the electrical behavior of oxidized polypyrrole films.

The Nyquist data obtained at 0.186 V (Fig. 4D) shows evidence of a high frequency semi-circle which is characteristic of charge transfer limitations. The emergence of this feature in the Nyquist plot is expected as the polymer begins to be reduced (19,29). The faradaic component of the current present at this potential may augment the purely nonfaradiac current due to the porous electrode character of the film and contribute to the shift in R_1 which is observed (see intermediate data below). Thus, the equivalent circuit shown in Fig. 2B is not adaquate to describe polypyrrole at this potential and the fit of the simulated to the experimental data in Fig. 4D is poor.

Although no evidence for charge transfer limitations is observed at 0.276 V (Fig. 4C), the fit of this data to the cylindrical porous electrode model is intermediate to that of the 0.393 V data (Fig. 4B) and the 0.186 V data (Fig. 4D). For example, transition to the vertical limiting region occurs at ca. 40 rad sec^{-1} (expt.) vs. 15 rad sec^{-1} (calc). At lower frequencies, the experimental Z[im] data is significantly higher than that predicted from Eqs. 15 and 16.

The fact that the fit between the experimental and simulated data improves as the potential increases from 0.186 V to 0.393 V suggests further improvement might be observed at yet higher open circuit potentials. Unfortunately, irreversible oxidation begins to occur at potentials greater than ca. +0.5 V vs. SCE and reliable AC data in this region cannot be obtained. However, the above data shows that the AC impedance of oxidized polypyrrole can be modeled reasonably well with an extremely simple finite,

porous electrode model which assumes a cylindrical pore geometry. Again, a better fit to the experimental data is possible if a decreasing radius pore geometry is considered. Nyquist diagrams for such films are easily calculated numerically using the procedure of Keiser et al. (25).

Lightly doped polypyrrole

Figure 6 shows experimental and simulated Nyquist diagrams for polypyrrole at open circuit potentials of -0.333V, -0.35V, and -0.361 V. As the cyclic voltammogram in Figure 3 shows, these potentials are at the foot of the polymer oxidation wave. Since these potentials are well negative of $E^{o\prime}$ ($|E^{o\prime} - E_{oc}| > 150$ mV), the concentration of oxidized sites, C_{PPy+} (where $C_{PPy+} = C_{BF4-}$), or the % doping of the polymer ought to be small. As discussed above, the data of previous workers (27,28) and the capacitance data of the present paper indicates that increases in the conductivity of polypyrrole at these E_{oc} values are small, ie. the polymer film is essentially nonconductive. Thus, the AC response of the system ought to conform to Limiting Case I.

Figure 6A shows the experimental low frequency Nyquist plots at these three potentials. Note that Z[re] is nearly frequency independent for $f < 5$ Hz and limiting behavior similar to that observed for oxidized polypyrrole is seen. Plots of Z[im] vs. ω^{-1} at these frequencys are linear ($r > 0.999$) again showing that a constant, limiting low frequency capacitance obtains. Such limiting behavior is accounted for in Limiting Case I by a finite RC transmission line (Fig. 2A) where the nonfaradaic circuit components of the oxidized polymer circuit (Fig. 2B) are replaced by the charge transfer resistance, R_{ct}, the Warburg resistance, R_w, and the Warburg capacitance,

C_W. In addition, the capacitance of the Pt substrate electrode, which was assumed to be negligible in the oxidized polymer case, must be accounted for in Limiting Case I since the total double-layer capacitance of the system is small.

Figures 6B - 6D compare the experimental data obtained at higher frequencies with simulated Nyquist plots. Simulated data calculated from Eqs. 10 and 11 were fit to the experimental data using the diffusion coefficient, $D_{BF_4^-}$, and the gradient of the potential with respect to the concentration, $dE/dC_{BF_4^-}$. The values of these parameters (see Table II) are identical to those calculated from the experimental R1 and C1 using Eqs. 13 and 14. Note that the agreement between the experimental and the simulated data at all three potentials is good. The best-fit diffusion coefficients obtained from the simulation of ca. 1×10^{-9} cm^2 sec^{-1} are approximately an order of magnitude faster than those measured by Genies and coworkers for polypyrrole ($D = 2.3 \times 10^{-10}$ cm^2 sec^{-1} in Et_4NBF_4, MeCN) using chronoamperometry (40). As discussed above, this disparity is not unexpected in view of the very different nature of these two experiments; ie., in the potential step (Cottrell) experiment, diffusion coefficient information is obtained while the film is in flux from one redox state to another (29). However, the diffusion coefficients obtained here are in agreement with those obtained at identical films and potentials by small-amplitude current pulse experiments (41).

Diffusion coefficients can also be calculated from the semi-infinite diffusion region of the Nyquist data. Figure 7A shows the experimental Nyquist plots obtained in this region in greater detail. The slopes calculated from these data (Table II) are in close agreement with the

theoretically predicted slope of unity. Plots of the impedance modulus, $|Z|$, versus $\omega^{-1/2}$ for this frequency domain are shown in Figure 7B. The diffusion coefficient can be calculated from these data by using values for $dE/dC_{BF_4^-}$ obtained from the finite diffusion region (Table II) and Eq. 12. The values for $D_{BF_4^-}$ so obtained (Table II) are smaller at each potential than those calculated from the finite diffusion frequency domain; $(D_{SI}/D_F)_{-0.333} = 0.28$, $(D_{SI}/D_F)_{-0.350} = 0.31$, $(D_{SI}/D_F)_{-0.361} = .28$. Note that D_{SI}/D_F is ca. 0.3 at all three potentials. Rubinstein et al. have observed similar behavior for the AC impedance of the reversible redox couple $Ru(bpy)_3^{3+/2+}$ in Nafion modified electrodes (20). At Nafion modified electrodes, however, diffusion coefficients obtained from the semi-infinite diffusion region are <u>faster</u> by a factor of ca. 3 than those obtained from the finite diffusion limiting region.

The factors which might account for the observed discrepancy between D_{SI} and D_F in the polypyrrole films studied here are identical to those discussed in detail by Rubinstein and coworkers (20). Note that an additional complication in the case of polypyrrole is the estimation of $dE/C_{BF_4^-}$ which cannot be determined by a straightforward coulometric titration without a reliable double-layer capacitance correction. Consequently, the value of $dE/dC_{BF_4^-}$ employed here is that derived from the finite diffusion data. The simultaneous determination of $dE/dC_{BF_4^-}$ and D_{F,BF_4^-} is susceptible to error from film thickness nonuniformity. However, because the thickness of the films used here is known to be 0.27 μm $\pm$ 0.02 μm, film nonuniformity seems an unlikely source of the diffusion coefficient effect.

The possibility exists, however, that the <u>morphology</u> of the polypyrrole

film is nonuniform over the film thickness. Under these circumstances, $D_{SI}/D_F < 1$ would be produced by a film morphology which was dense (transport restrictive) at the electrode/film interface and relatively open at the film/electrolyte interface. It is interesting to note that the existence of such a morphological gradient could also explain the AC impedance data obtained for the oxidized polymer (see explanation above). Furthermore, it is not unlikely that such gradients in the polymer void volume or effective pore diameter might be introduced during electrochemical synthesis of the polymer film. This is particularly true since the polypyrrole polymerization reaction is not diffusion controlled at the current densities employed here (1 mA cm^{-2})(40). Thus, pyrrole monomer is available at the film edge and the polymerization reaction can proceed from the interior surfaces of the film as well as at its exterior (apparent) surface. As a result, the total time available for polymerization at the interior surfaces of the film increases from the film/monomer interface to the electrode. The effective pore diameter of the electrochemically synthesized film, then, increases from the electrode surface to the film edge. It should be noted that although a morphological gradient in the polypyrrole film such as that described above is consistent with the observed AC impedance data, alternative explanations exist. For example, Rubinstein et al. have accounted for the similar effects observed at Nafion-coated electrodes with a model which incorporates two uncoupled parallel diffusion pathways (20).

A second similarity between the present data and that of Rubinstein et al. is the behavior of the experimental data in the transition region (23). As shown in Figs. 4B - 4D, experimental Nyquist plots exhibit a gradual

transition from the semi-infinite (45^{o}) to finite (vertical) diffusion regions of the Nyquist plot whereas a relatively abrupt transition is predicted by Eqs. 10 and 11. This effect is probably best attributed to inhomogeneities in the polymer structure which result in a distribution of diffusion pathways (apparent film thicknesses).

Intermediate oxidation levels.

At potentials from -0.3 V to +0.1 V, significant concentrations of both oxidized and reduced polymer are present in a film which is also a good electronic conductor. Under these circumstances, neither of the equivalent circuits employed above are adequate to describe the AC impedance of the polymer. The faradaic impedance of porous electrodes has been discussed in detail by De Levie (32-34). The proposed models, however, do not consider the finite diffusion case and become complex if the effective pore diameter approaches dimensions of ca. 1 μm (34). In addition, the modeling of polypyrrole at these intermediate potentials is complicated by the need to know the specific double layer capacitance (or the true surface area) of the polymer at each potential. More sophisticated porous electrode models (cf. 42,43) introduce additional adjustable parameters which are difficult to experimentally identify. Finally, it should be noted that the work of Feldburg (35) and others suggests that significant extensions of established porous electrode theory are likely to be neccessary to fully account for the AC impedance behavior of conducting polymers.

Although we have not attempted to identify an equivalent circuit appropriate for the AC data obtained at intermediate potentials, important qualitative data can be obtained in the absence of such a model. Figure 8

shows Nyquist plots for AC impedance data obtained at potentials from +0.1 V to -0.3 V vs. SCE. The low frequency data (Figs. 8A and 8B) show that these data are qualitatively similar to that which was observed at more positive and more negative potentials. Both the capacitance and the resistance assume limiting values, R_l and C_l, at frequencies less that 5 Hz. A plot of R_l and C_l vs. E_{oc} obtained over the entire potential region from +0.4 V to -0.3 V is shown in Figure 9. Note in particular that the capacitance in the region from -0.3 V to -0.4 V is small relative to the maximum C_l values observed at higher potentials; ie., for the fully oxidized polymer. This data supports our assumption (Limiting Case I) that polypyrrole-$BF4^-$ is relatively nonelectronically conducting at these potentials. The value of C_l for the oxidized polymer (3 x 10-2 F cm^{-2} @ E_{oc} = 0.393 V)) corresponds to a bulk capacitance of 350 F cm^{-3}. This number is significantly higher than that observed by Burgemayer et al. (200 F cm^{-3} (2)) and by Diaz et al. (100 F cm^{-3} (36)). Note also that for C_l, a maximum is observed at ca. -0.2 V. These data are similar to that obtained by Tanguy et al. for thick polypyrrole films (13,14). In the vicinity of the switching potential ($E^{o\prime}$) both the faradaic components ($R_{l,f}$ and $C_{l,f}$) and the capacitive components ($R_{l,c}$ and $C_{l,c}$) of R_l and C_l are expected to be significant.

To a first approximation, the limiting low frequency behavior of these components R_l and C_l can be inferred by superimposing the predictions of Limiting Case I (Eqs 13,14) and Limiting Case II (Eqs. 18,19). If the specific double layer capacitance, C_{dl}, of polypyrrole can be assumed to possess an S-shaped dependence with potential (no maximum), Eq. 19 predicts that if r_c and l remain constant, $C_{l,c}$ vs. E_{oc} will have a similar shape. In this case, since the faradaic component, $C_{l,f}$, is a maximum at E_{oc} =

$E^{o\prime}$(24), the superposition of faradaic and capacitive components yields a Cl vs. Eoc relation which has a maximum near Eo', as observed here and previously (13,14). Equation 13 predicts that the faradaic component $R_{l,f}$ ought to be a minimum at $E_{oc} = E^{o\prime}$. Thus, it is difficult to account for the potential dependence of R_l observed here. Since the capacitive component, $R_{l,c}$ is proportional to 1, σ^{-1}, and r_c^{-2} (Eq. 19), relatively dramatic changes in the pore structure (eg. increases in r_c with potential) are probably neccessary to account for the R_l vs. E_{oc} relationship obtained by us and by previous workers (13,14).

Figure 8C,D shows the high frequency Nyquist data obtained at intermediate potentials. Of particular interest is the absence of a well defined semi circle resulting from charge transfer limitations at high frequencies (26,29). The AC impedence data obtained by various workers (2,13) for thick films invariably reveals the presence of such a semi-circle at high frequencies. Unfortunately, quantitative measurement of the heterogeneous rate constant for this system is impossible given the porous electrode nature of the film; ie., the electroactive area of the film is not well defined. However, the present data suggests that the apparent rate constant may decrease considerably with increasing film thickness.

The high frequency resistance, R_h, obtained at Z[im] = 0 is compared to C_l in Figure 10. R_h values are good approximations of the total series resistance of the solution and the polypyrrole film (29). The R_h values observed at positive potentials (R_h = 6.5 ohms $\pm$ 0.2 ohms) can be attributed entirely to the supporting electrolyte resistance; ie., the film resistance of the oxidized polymer is negligible. At potentials negative of -0.2 V, R_h increases rapidly to ca. 20 ohms at -0.6 V. It is interesting to note that

decreases in R_h commensurate with oxidation of the polymer film occur in advance of increases in C_l. Note, for example, that at -0.3 V, the value of R_h is 15% of its value at -0.6 V whereas C_l has only attained ca. 15% of its limiting value. Since the value of C_l is sensitive only to the electronic conductivity of the film whereas that of R_h can reflect either ionic or electronic conductivity, these data suggest that polypyrrole is a good ionic conductor at potentials (near -0.3 V) where it is a relatively poor electronic conductor.

Conclusions

AC impedance data has been presented for thin polypyrrole film-modified electrode surfaces. Although an equivalent circuit which accounts for the observed AC behavior of polypyrrole over a wide range of potentials is likely to be complex, two limiting cases exist for which the equivalent circuits are simplified. At low doping levels (Limiting Case I), the equivalent circuit appropriate for polypyrrole is identical to that used previously to describe the AC impedance of Nafion polymer modified electrodes (20,24) and metal oxide, Li intercalation films (19,21-23). Diffusion coefficients were obtained from the analysis of Ho et al. (19) for both semi-infinite and finite time domains. The approximate ratio of the values $D_{SI}/D_F = 0.3$ at the potentials examined. This observation is consistant with the existence of a morphology gradient normal to the surface of the electrode where the effective pore diameter of the polymer, and therefore the diffusion coefficient $D_{BF_4^-}$, increases in the film with distance from the electrode surface.

The AC impedance data observed for the oxidized polymer (Limiting Case

II) was compared to that predicted for finite, porous metallic films (25,26). The agreement between the experimental and the simulated Nyquist data (calculated from ref. 26) improves with increasing E_{oc}. Using the analysis of Candy and coworkers, film parameters such as the pore radius, pore length, and pore number density can be expressed as their cylindrical pore electrode equivalents (26). The values so obtained for thin polypyrrole films are consistant with what is currently known about mass transport in such films. Better agreement between the simulated and the experimental Nyquist plots ought to be obtained if other pore geometries are considered. In particular, the transition region of the Nyquist data is better accomodated by a model in which the pores possess a decreasing radius from the film edge to the electrode surface. This conclusion is in qualitative agreement with the diffusion coefficient data obtained for the oxidized polymer.

Thus, both mass transport and structural information can be gleaned from AC impedance analysis of polypyrrole films based on these two relatively simple equivalent circuits. In addition, the potential dependence of the low frequency series resistance and capacitance were determined and the origins of the observed dependencies were discussed. Comparisons between the high frequency resistance and the low frequency capacitance indicate that significant ionic conductivity is present for polypyrrole films at very low oxidation levels, prior to the onset of significant electronic conductivity.

Acknowledgments

The authors express appreciation to R.E. White for the use of the AC impedance instrumentation employed in this work.

Credit

This work was suported by the Office of Naval Research, the Robert A. Welch Foundation, the Air Force Office of Scientific Research, and NASA.

References

1. P. Burgmayer and R.W. Murray, *J. Am. Chem. Soc.*, **104**, 6139 (1982).
2. P. Burgmayer and R.W. Murray, *J. Phys, Chem.*, **88**, 2515 (1984).
3. F. Garnier, G. Tourillon, M. Gazard, and J.C. Dubois, *J. Electroanal. Chem.*, **148**, 299 (1983).,
4. M. Gazard, in "Handbook of Conducting Polymers, Volume 1," Marcel Dekker, Inc., New York, 1986, p. 673.
5. J.H. Kaufman, T.-C. Chung, A.J. Heeger, and F. Wudl, *J. Electrochem. Soc.*, **131**, 2092 (1984).
6. N. Mermilliod, J. Tanguy, and F. Petiot, *J. Electrochem. Soc.*, **133**, 1073 (1986).
7. P. Button, J. Mastragostino, S. Panero and G. Scrosati, *Electrochimica ACTA*, **31**, 783 (1986).
8. F. Trinidad, J. Alonso-Lopez, and M. Nebot, *J. App. Electrochem.*, **17**, 215 (1987).
9. S. Chao and M.S. Wrighton, *J. Am. Chem. Soc.*, **109**, 2197 (1987).
10. E.P. Lofton, J.W. Thackeray, and M.S. Wrighton, *J. Phys. Chem.*, **90**, 6080 (1986), and references therein.
11. M. Josowicz and J. Janata, Anal. Chem., **58**, 514 (1986).
12. T. Osaka, K. Naoi, S. Ogano, and S. Nakamura, *Chem. Lett.*, 1687 (1986).
13. J. Tanguy, N. Mermilliod, and M. Hoclet, *J. Electrochem. Soc.*, **134**, 795 (1987).
14. J. Tanguy, N. Mermilliod, and M. Hoclet, *Syth. Met.*, **18**, 7 (1987).
15. A.F. Diaz, J.I. Castillo, J.A. Logan, and W.-Y. Lee, *J. Electroanal. Chem.*, **129**, 115 (1981).

16. G.B. Street, T.C. Clarke, M. Krounbi, K. Kanazawa, V. Lee, P. Pfluger, J.C. Scott, and G. Wieser, *Mol. Cryst. Liq. Cryst.*, **83**, 253 (1982).

17. R.A. Bull, F-R. F. Fan, and A.J. Bard, *J. Electrochem. Soc.*, **129**, 1009 (1982).

18. S.H. Glarum and J.H. Marshall, *J. Electrochem. Soc.*, **134**, 142 (1987).

19. C. Ho, I.D. Raistrick, and R.A. Huggins, *J. Electrochem. Soc.*, **127**, 343 (1980).

20. I. Rubinstein, J. Rishpon, and S. Gottesfeld, *J. Electrochem. Soc.*, **133**, 729 (1986).

21. D.R. Franceschetti and J.R. MacDonald, *J. Electrochem. Soc.*, **101**, 307 (1979).

22. D.R. Franceschetti and J.R. MacDonald, *J. Electrochem. Soc.*, **129**, 1754 (1982).

23. D.R. Franseschetti, *J. Electroanal. Chem.*, **178**, 1 (1984).

24. C. Gabrielli, O. Haas, and H. Takenouti, *J. App. Electrochem.*, **17**, 18 (1987).

25. H. Keiser, K.D. Beccu, and M.A. Gutjahr, *Electrochimica ACTA*, **21**, 539 (1976).

26. J-P. Candy, P. Fouilloux, M. Keddam and K. Takenouti, *Electrochimica ACTA*, **26**, 1029 (1981).

27. B.J. Feldman, P Burgemayer, and R.W. Murray, *J. Am. Chem. Soc.*, **107**, 872 (1985).

28. G.R. Kittlesen, H.S. White, and M.S. Wrighton, *J. Am. Chem. Soc.*, **106**, 7389 (1984).

29. A.J. Bard and L.R. Faulkner, "Electrochemical Methods: Theory and Applications," John Wiley & Sons, New York, 1980, p. 350.

30. D.A. Buttry, personnal communication, June, 1987.

31. J.E.B. Randles, *Disc. Faraday Soc.*, 1, 11 (1947).

32. R. De Levie, *Electrochimica ACTA*, **8**, 751 (1963).

33. R. De Levie, *Electrochimica ACTA*, **9**, 1231 (1964).

34. R. De Levie, in "Advances in Electrochemistry and Electrochemical Engineering," Chapt. 6, John Wiley & Sons, New York, 1967.

35. S.W. Feldburg, *J. Am. Chem. Soc.*, **106**, 4671 (1984).

36. A.F. Diaz, J.I. Castillo, J.A. Logan, and W.Y. Lee, *J. Electroanal. Chem.*, **129**, 115 (1981).

37. A.F. Diaz, W-Y. Lee, A. Logan, D.C. Green, *J. Electroanal. Chem.*, **108**, 377 (1980).

38. A.F. Diaz, *Chemical Scripta*, **17**, 145 (1981).

39. B. Kratochvil and H.L. Yeager, "Topics in Current Chemistry," Vol. 27, Springer Verlag, New York, 1972, p. 45.

40. E.M. Genies, G. Bidan, and A.F. Diaz, *J. Electroanal. Chem.*, **149**, 101 (1983).

41. R.M. Penner, L.S. Van Dyke, C.R. Martin, manuscript in preparation.

42. M. Tomkiewicz, *J. Electrochem. Soc.*, **126**, 2221 (1978).

43. M. Hepal and M. Tomkiewicz, *J. Electrochem. Soc.*, **131**, 1288 (1984).

Table I. Summary of Film Parameters Calculated From AC Impedance Data For Oxidized Polypyrrole.

E_{oc} (V vs. SCE)	equivalent cylindrical pore radius[a] (cm)	pore number density[a] (cm^{-2})	pore length[b] (cm)
0.393	4.26×10^{-8}	5.43×10^{12}	8.72×10^{-4}
0.276	2.63×10^{-8}	1.23×10^{13}	1.01×10^{-3}
0.186	1.96×10^{-8}	1.90×10^{13}	1.17×10^{-3}

[a]Values for r_c and n were determined by fitting Nyquist plots calculated from Eqs. 15 and 16 to the experiment data. The values of C_l used for these calculations were obtained from the slope of $Z[im] = (\omega C_s)^{-1}$ vs. ω^{-1} at $f < 5$ Hz. R_l was determined from Z[re] at ca. f = 1 Hz. and corrected for R_u.

[b]Calculated from Eq. 20 assuming the pore volume V_p = the total film volume, V_f.

Table II. Summary of Transport Data Calculated For Semi-Infinite (SI) and Finite (F) Frequency Regimes For Lightly Doped Polypyrrole.

E_{oc} (V vs. SCE)	D_F[a] ($cm^2\ sec^{-1}$)	dE/dC[a] ($V\ cm^3\ mol^{-1}$)	$d\|Z\|/d(\omega^{-1/2})$[b] (ohms rad^{-1} sec)	D_{SI}[c] (cm2 sec-1)
-0.333	1.40×10^{-9}	593	1.36	3.87×10^{-10}
-0.350	3.31×10^{-9}	1140	1.02	1.03×10^{-9}
-0.361	3.38×10^{-9}	1300	1.20	9.36×10^{-10}

[a]Obtained by fitting Nyquist data calculated from Eqs. 10 and 11 to the experiment Nyquist data at each potential. The best fit values D_F and dE/dC so obtained approximate those obtained from R_1 and C_1 and Eqs. 13 and 14.

[b]Obtained from the slope of the 45° linear region of the Nyquist plots shown in Fig. 7A.

[c]Calculated from $d|Z|/d(\omega^{-1/2})$ using Eq. 12.

Figure Captions

Figure 1 - A. Randel's equivalent circuit with a finite Warburg element, $Z_{w,F}$. (19), B. Finite RC transmission line circuit equivalent to that of a finite pore with a uniform radius (ex. a cylindrical pore).

Figure 2 - Schematic diagram of the platinum disk electrode employed in this work. a. 7mm glass tube, b. copper wire, c. Kel-F electrode body; diameter = ca. 10 mm, d. silver epoxy contact, e. Pt disk; diameter = 3.3 mm.

Figure 3 - Cyclic voltammogram for a typical 0.27 μm polypyrrole film in 0.2 M Bu_4NBF_4, MeCN electrolyte at 20 mV sec^{-1}.

Figure 4 - A. Nyquist diagram comparing the low frequency ($f < 0.25$ Hz.) AC impedance data obtained at three potentials for an oxidized polypyrrole film. ○ - 0.393 V, ● - 0.286 V, △ - 0.186 V. Frequencies in Hz. are as shown.

B-D. Nyquist diagrams comparing experimental and simulated AC impedance data for an oxidized polypyrrole film. Frequencies (Hz.) for simulated data (solid line) are indexed on the right of each plot. Frequencies for the experimental data (open circles) are indexed at the left of each plot.

A. 0.393 V, B. 0.286 V, C. 0.186 V.

Simulated data calculated from Eqs. 15 and 16.

Figure 5 - Typical plot of Z[im] vs. ω^{-1} for data obtained at low frequencies. These data at f < 5 Hz. and 0.393 V.

Figure 6 - A. Nyquist diagrams comparing the low frequency AC impedance behavior at three potentials for a lightly doped polypyrrole film. ○ - -0.333 V, △ - -0.350 V, ● - -0.361 V.

B-D. Comparisons of experimental and simulated Nyquist diagrams. Frequencies (Hz.) for simulated data (solid line) are indexed on the right of each plot. Experimental data (open circles) are indexed at the left of each plot. A. -0.333 V, B. -0.350 V, C. -0.361 V.

Figure 7 - A. Comparison of the 45° semi-infinite region of the Nyquist data obtained for a lightly doped polypyrrole film. The slopes calculated for these plots are listed in Table II.

○ - -0.333 V, ● - -0.350 V, △ - -0.361 V.

B. Plots of |Z| vs. $\omega^{-1/2}$ for the linear regions of the plots shown in Fig. 7A.

□ - -0.333 V, △ - -0.350 V, ○ - -0.361 V.

Figure 8 - A,B. Comparison of experimental Nyquist data obtained at low frequencies for potentials from +0.1 V to -0.3 V. Frequencies in Hz. as shown.

A. ○ - 0.093 V, ● - 0.001 V, △ - -0.091 V, ▲ - -0.140 V.

B. ○ - -0.211 V, ● - -0.255 V △ - -0.299 V.

Figure 8 - C.D. Comparison of higher frequency experimental Nyquist data obtained at the same potentials. Identity of plots same as for Fig. 8 A,B. Frequencies in Hz. as shown.

Figure 9 - Low frequency resistance, R_l, and capacitance, C_l, vs. E_{oc}. R_l measured at 0.25 Hz., C_l obtained from plots of Z[im] vs. ω^{-1}.

Figure 10 - High frequency resistance, R_h, and low frequency capacitance, C_l, vs. Eoc. R_h = Z[re] at Z[im] = 0.

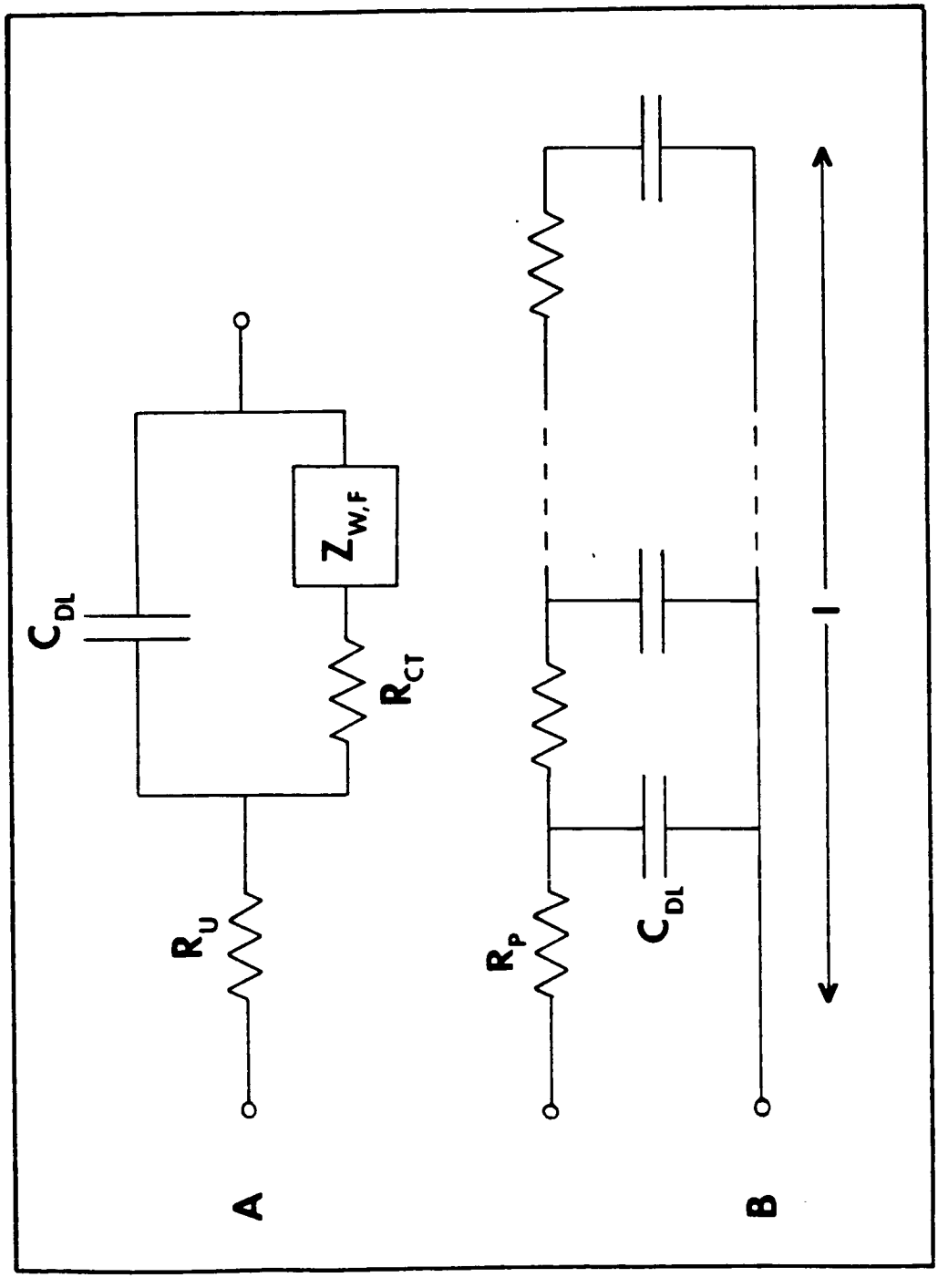

FIGURE 1

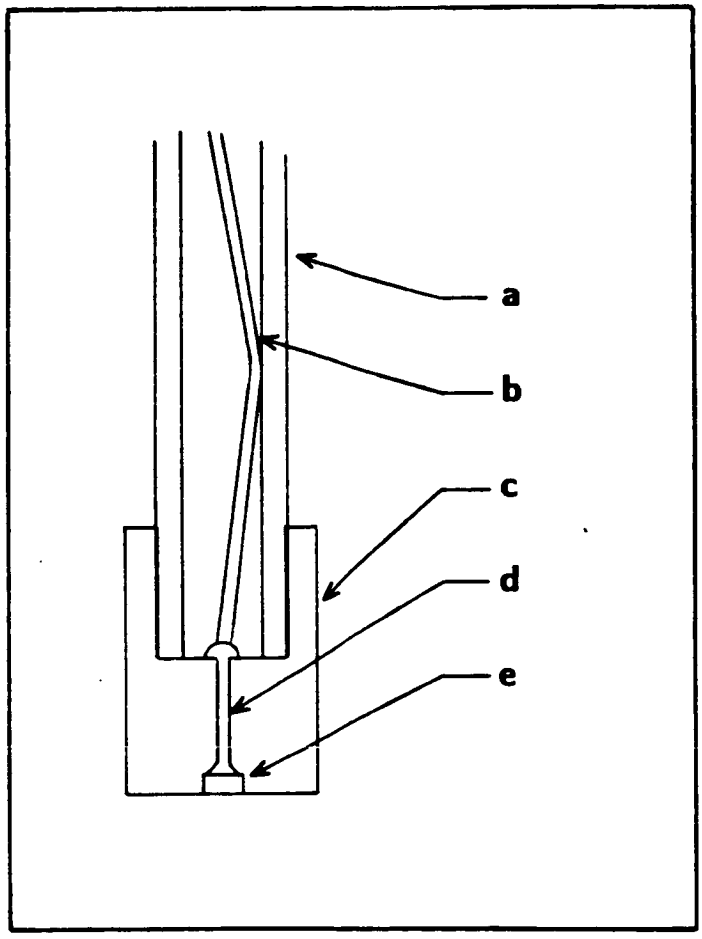

Figure 2

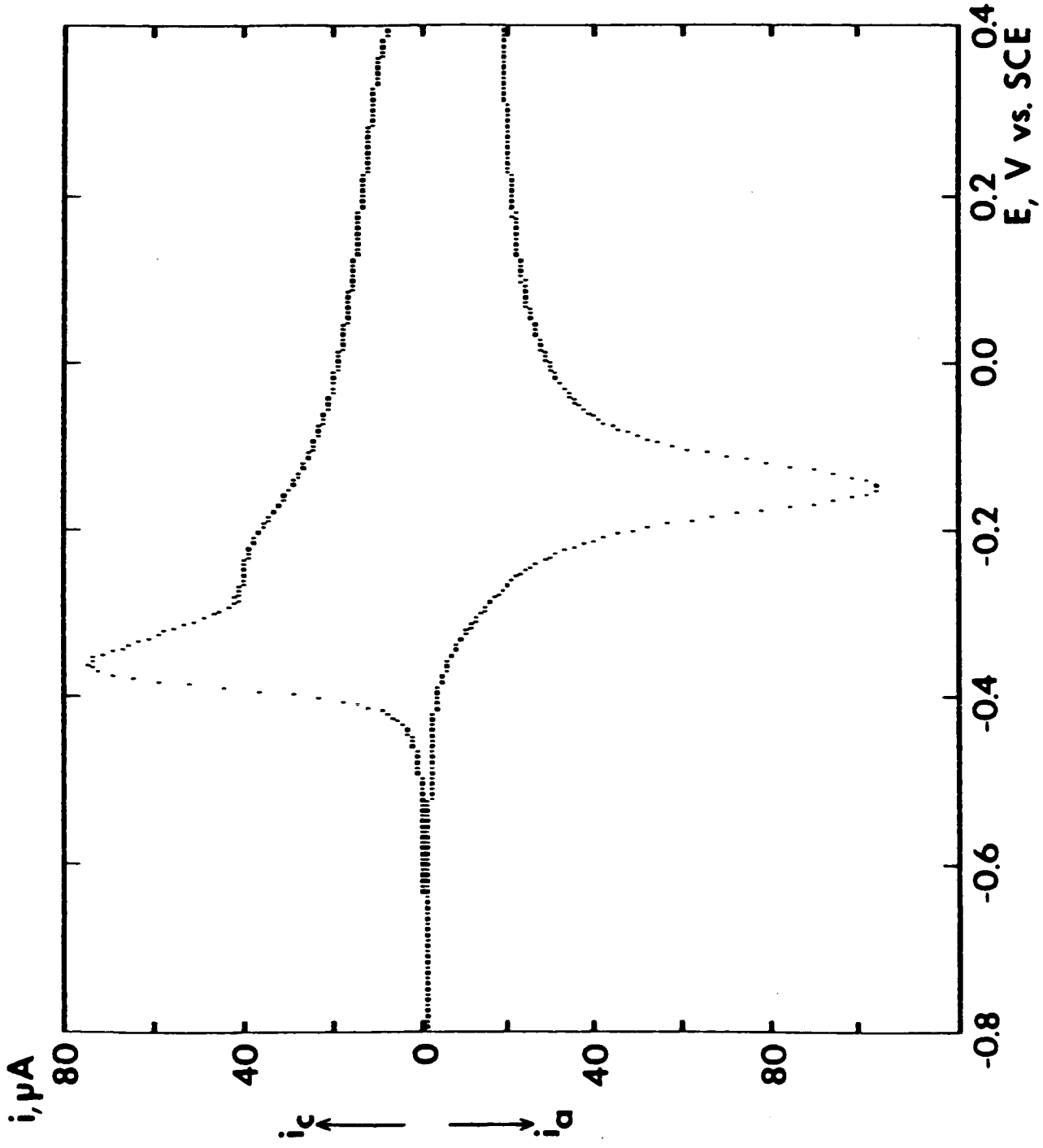

Figure 3

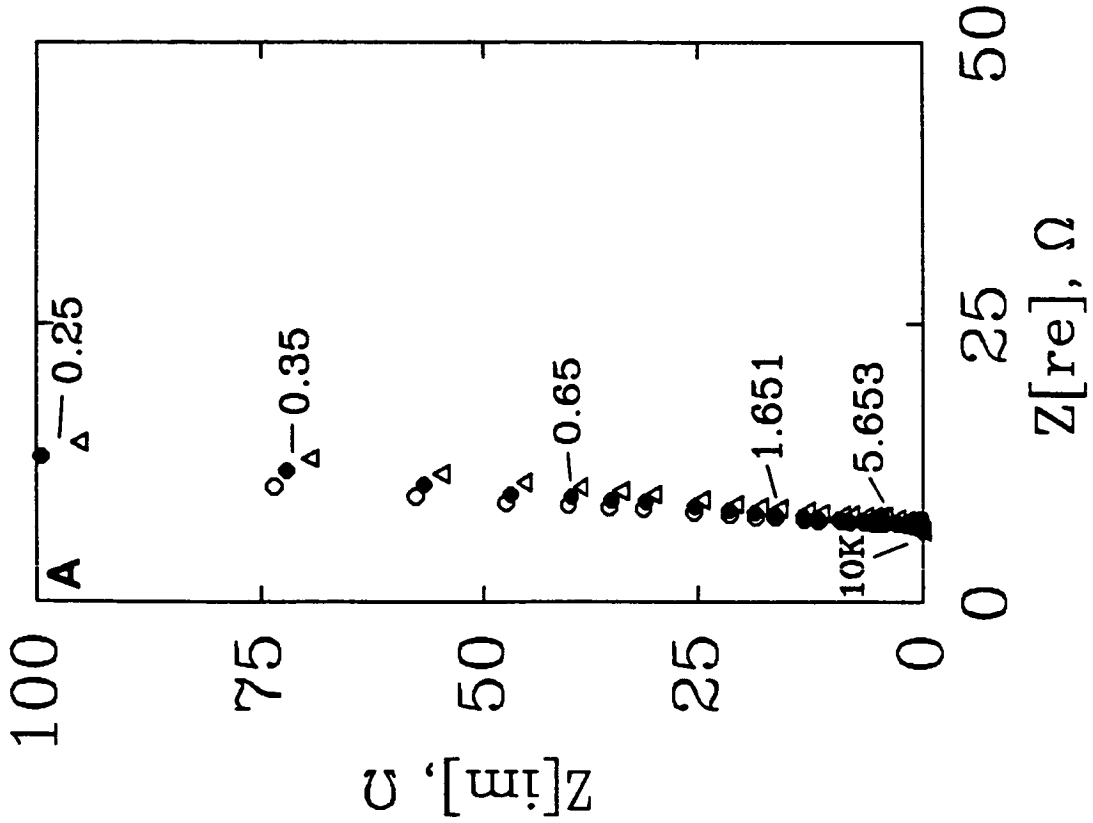

Figure 4-A

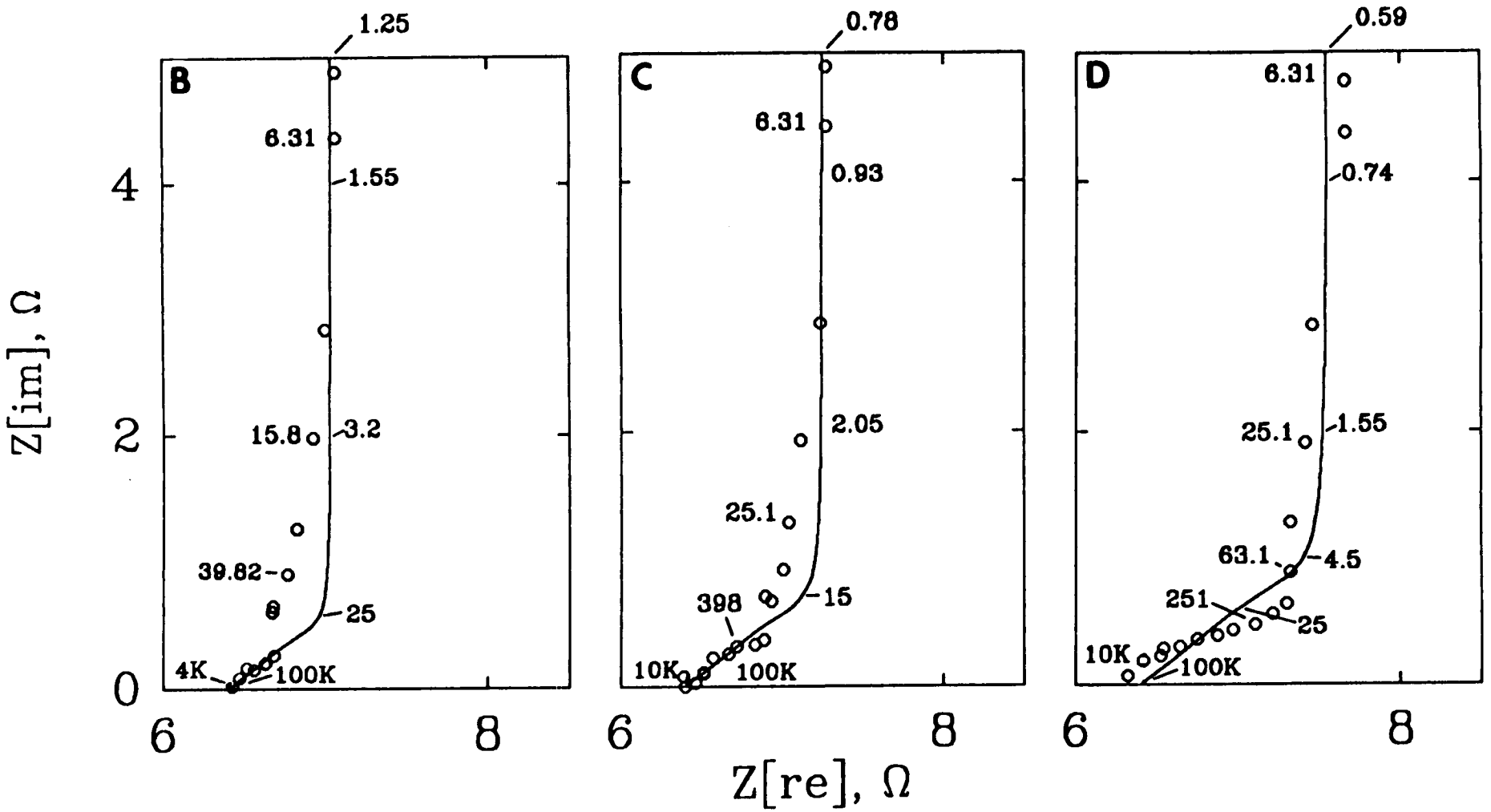
B
C
D
1.25
6.31
1.55
3.2
15.8
39.82
25
4K
100K
0.78
6.31
0.93
2.05
25.1
398
15
10K
100K
0.59
6.31
0.74
25.1
1.55
63.1
4.5
251
25
10K
100K
Z[im], Ω
Z[re], Ω
0
2
4
6
8

Figure 4-B,C,& D

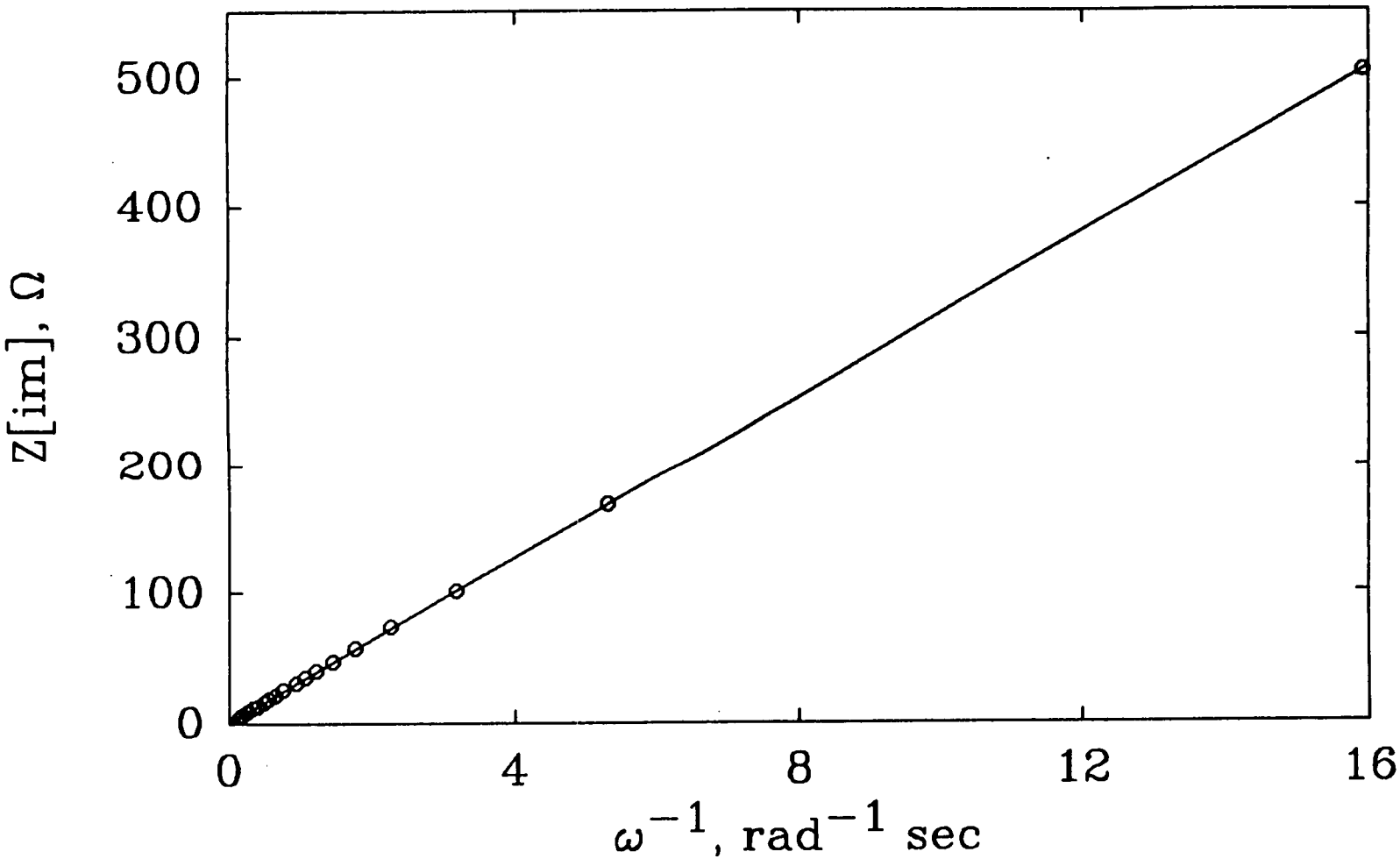

Figure 5

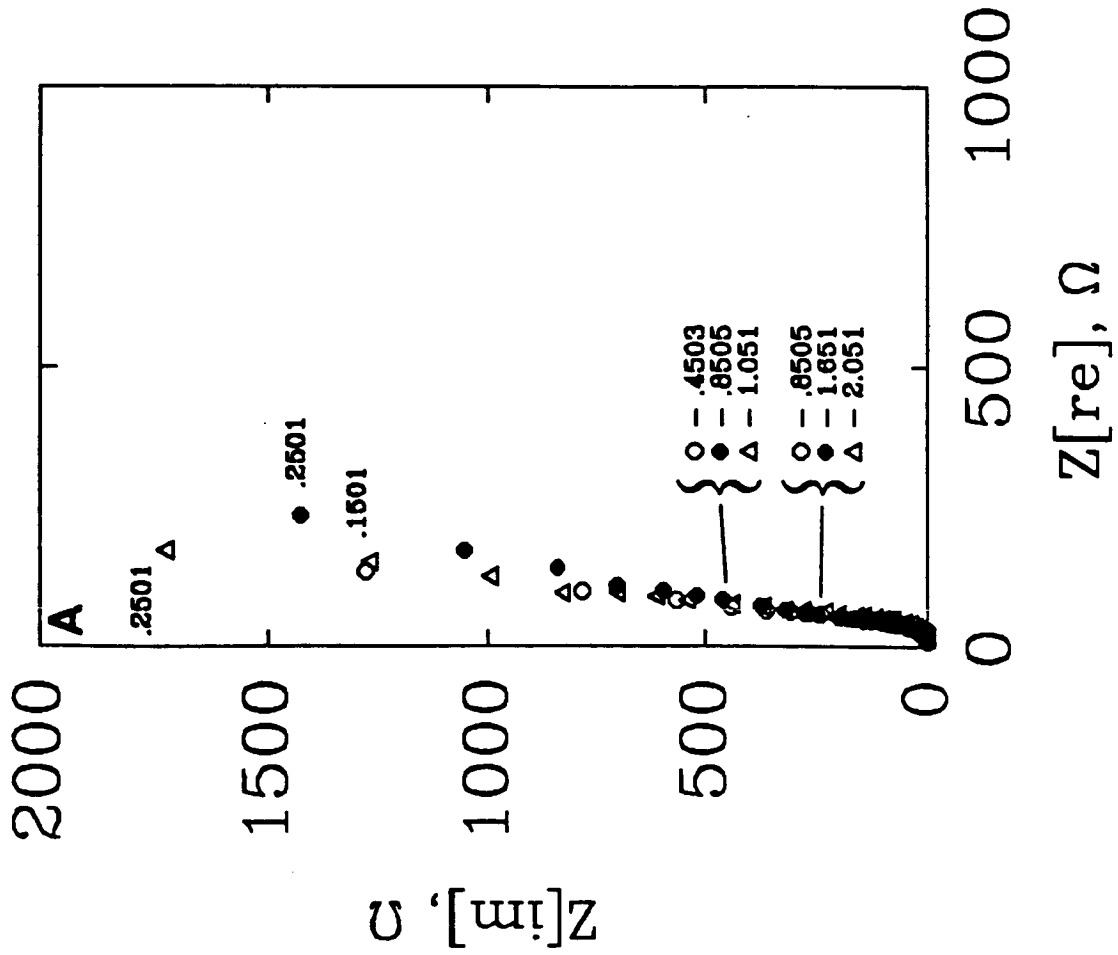
A
.2501
.2501
.1501
.4503
.8505
1.051
.8505
1.851
2.051
2000
1500
1000
500
0
0
500
1000
Z[im], Ω
Z[re], Ω

Figure 6-A

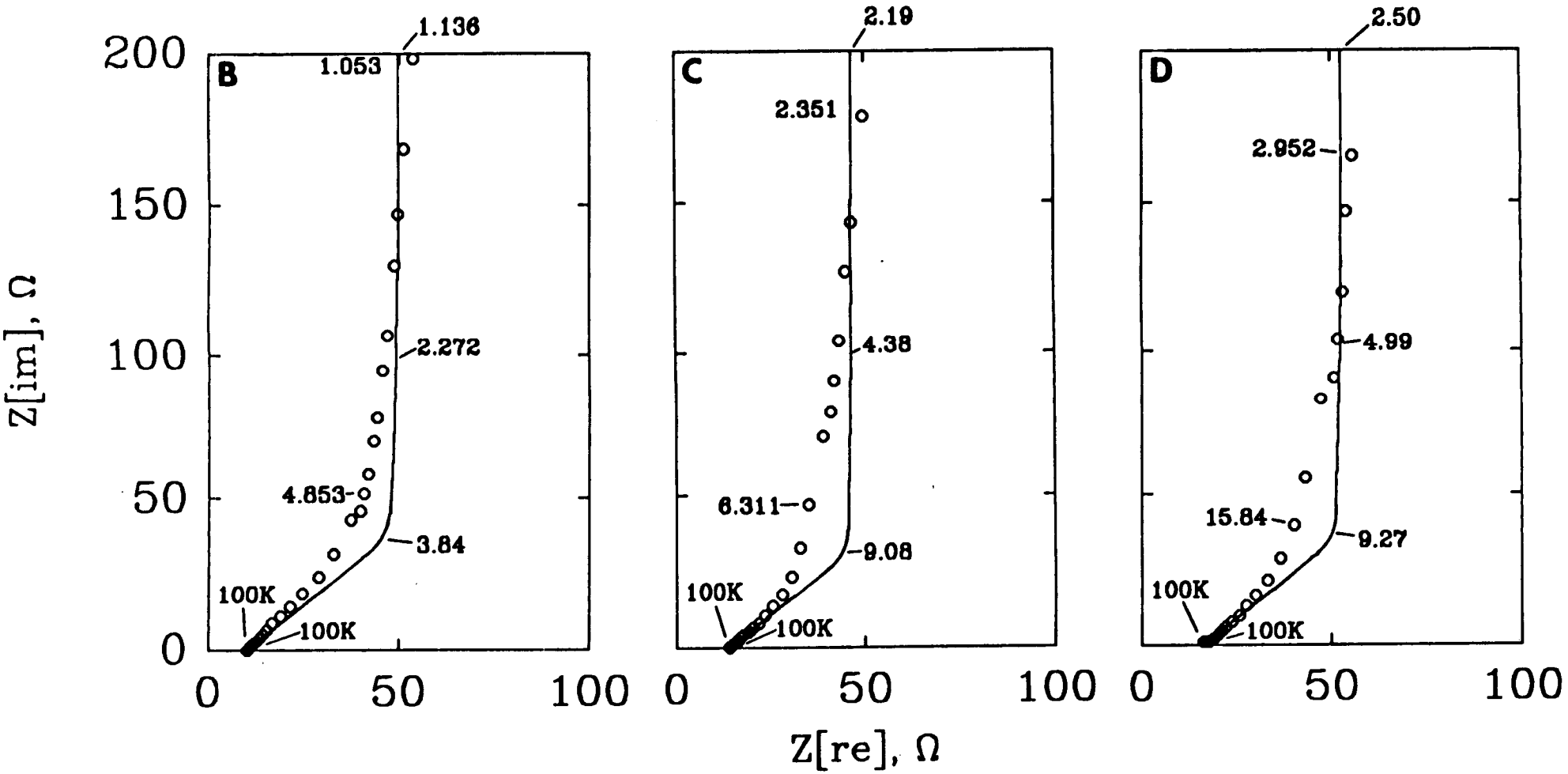
B
C
D
1.136
1.053
2.272
4.853
3.84
100K
100K
2.19
2.351
4.38
6.311
9.08
100K
100K
2.50
2.952
4.99
15.84
9.27
100K
100K
200
150
100
50
0
0
50
100
Z[im], Ω
Z[re], Ω

Figure 6-B,C,& D

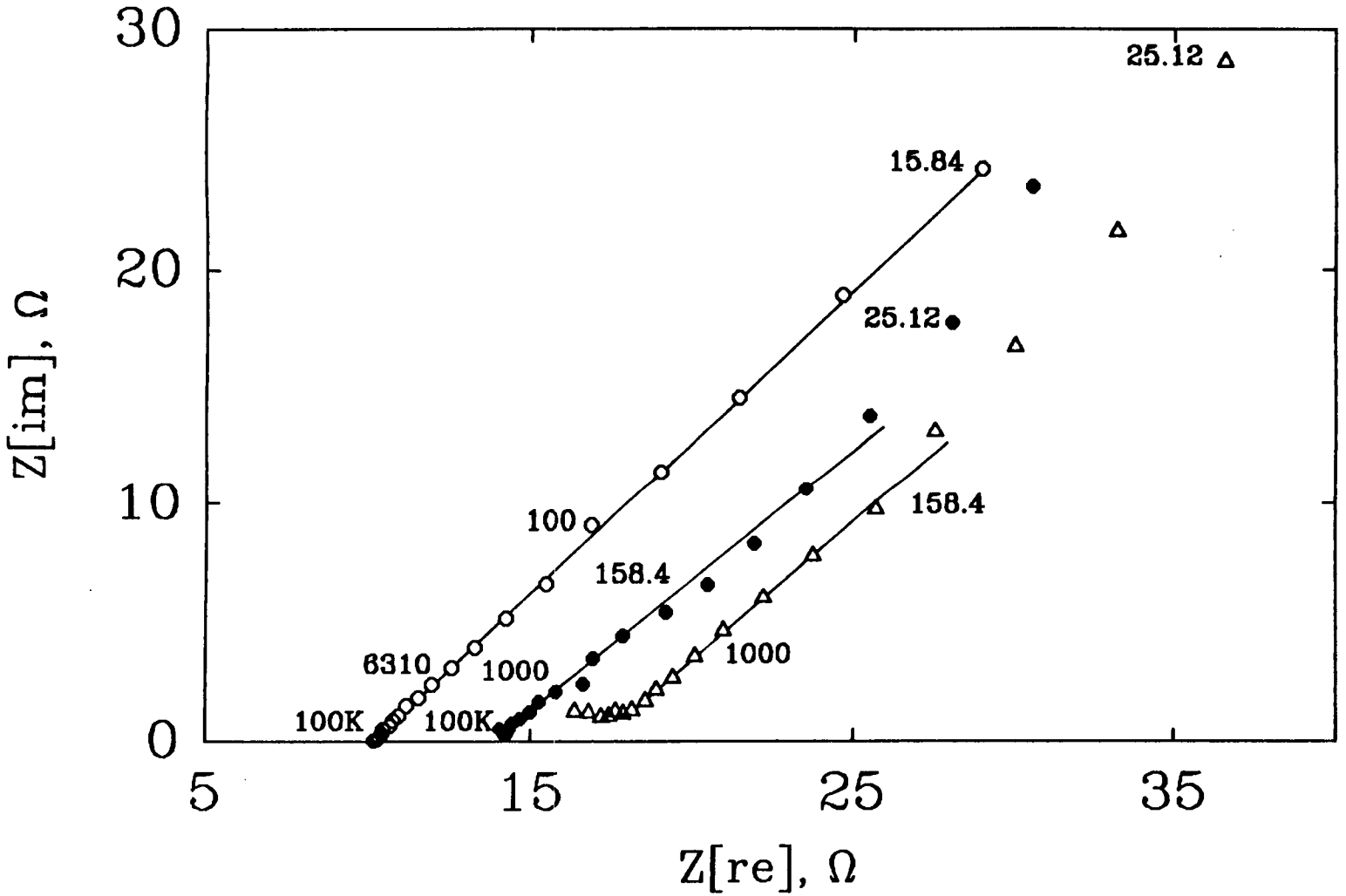
30
20
10
0
5
15
25
35
Z[im], Ω
Z[re], Ω
25.12
15.84
25.12
100
158.4
158.4
6310
1000
1000
100K
100K

Figure 7-A

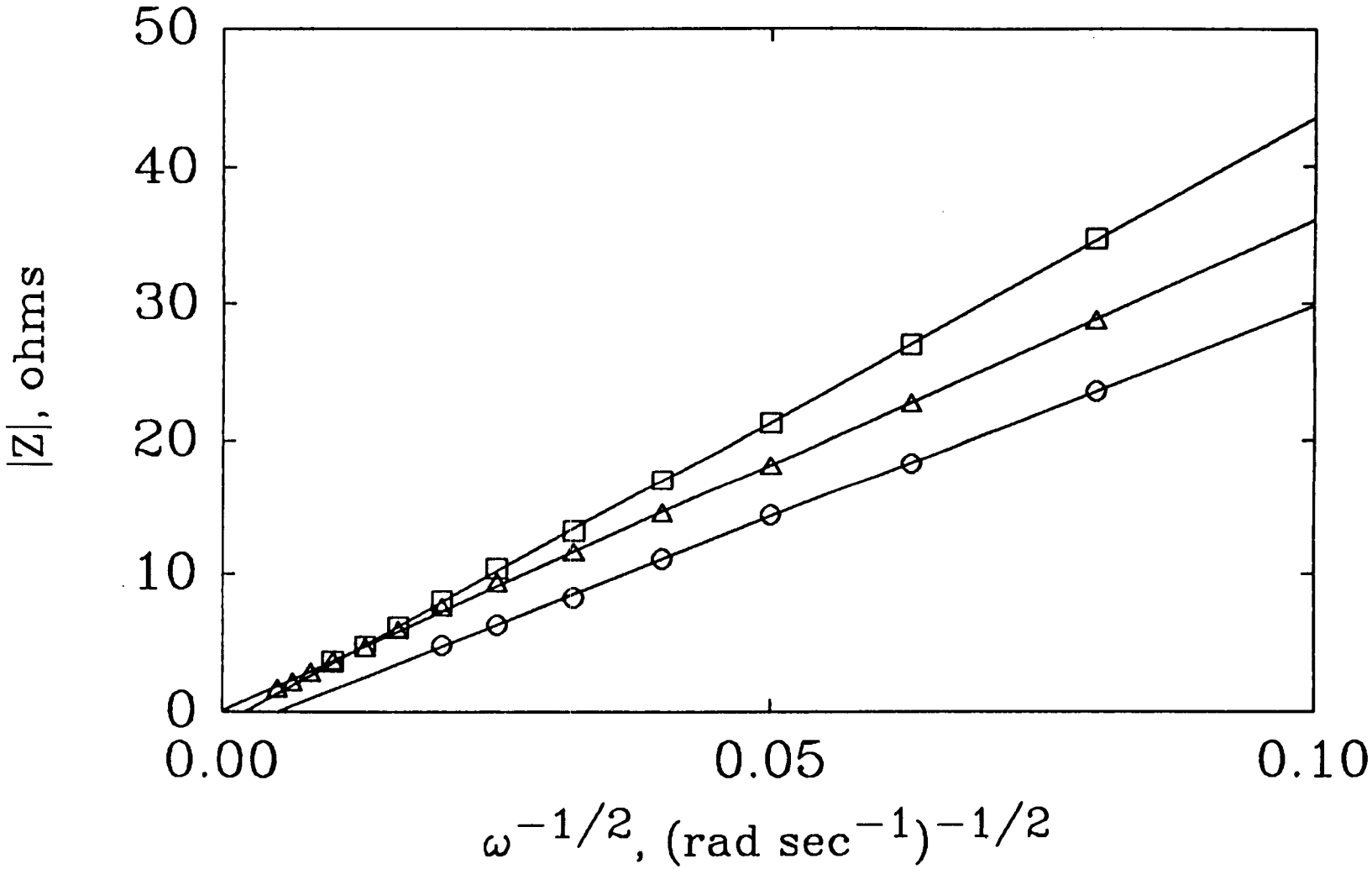

Figure 7-B

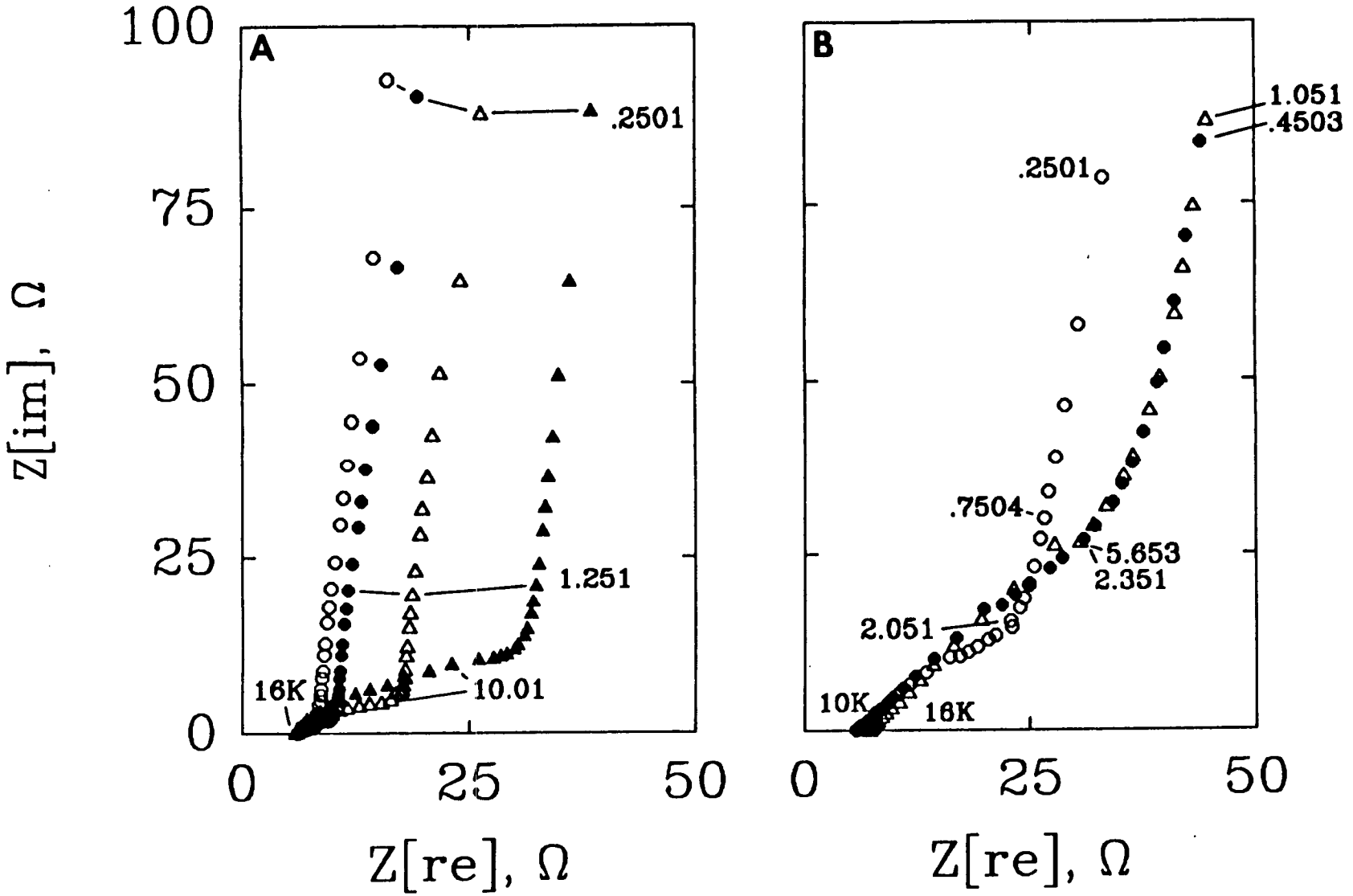
A
B
100
75
50
25
0
Z[im], Ω
.2501
1.251
10.01
16K
0
25
50
Z[re], Ω
1.051
.4503
.2501
.7504
5.653
2.351
2.051
10K
16K
0
25
50
Z[re], Ω

Figure 8-A,B

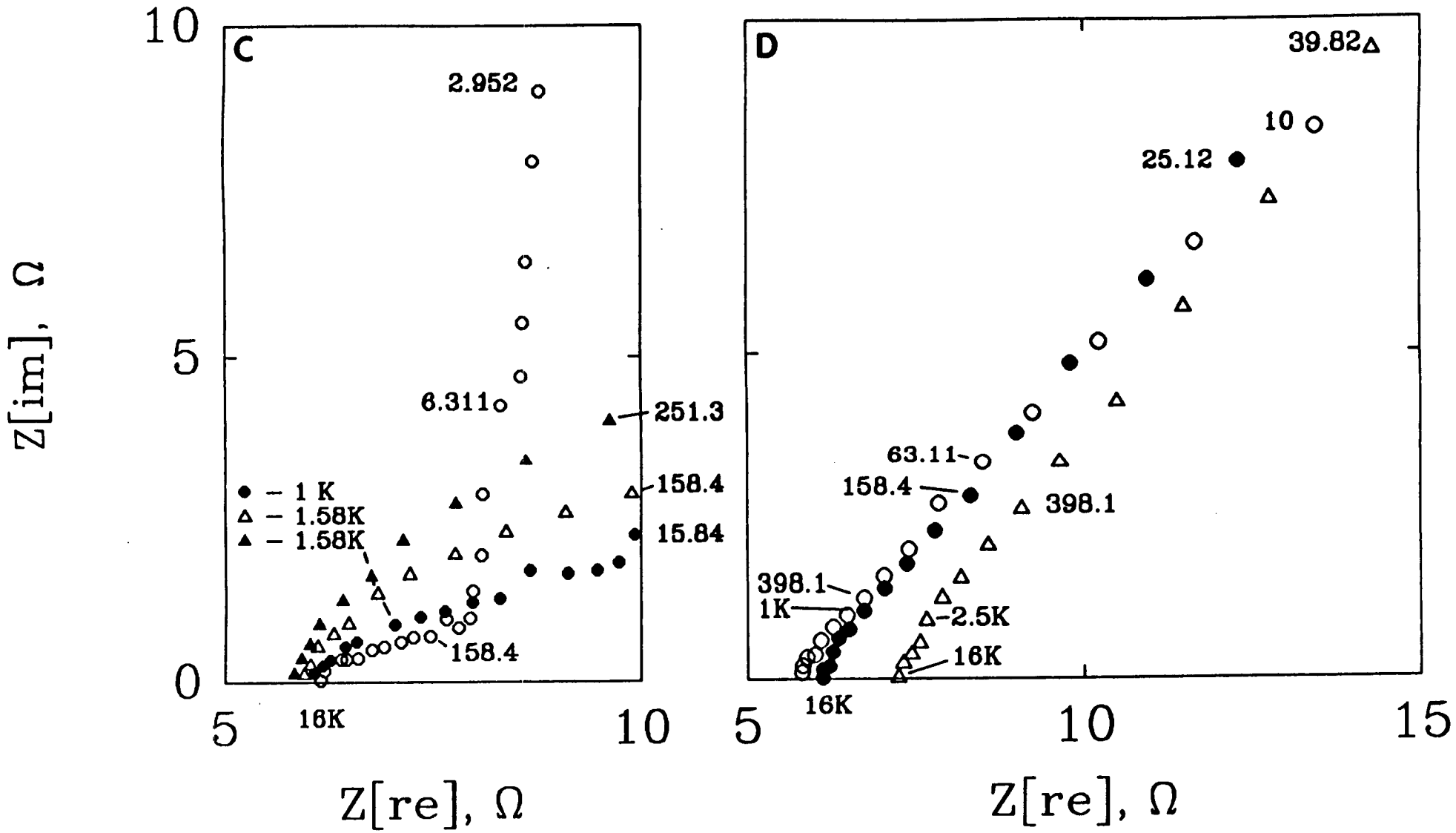
C
D
10
5
0
5
10
15
Z[im], Ω
Z[re], Ω
Z[re], Ω
2.952
6.311
251.3
158.4
15.84
158.4
16K
● – 1 K
△ – 1.58K
▲ – 1.58K
39.82△
10
25.12
63.11
158.4
398.1
398.1
1K
2.5K
16K
16K

Figure 8-C,D

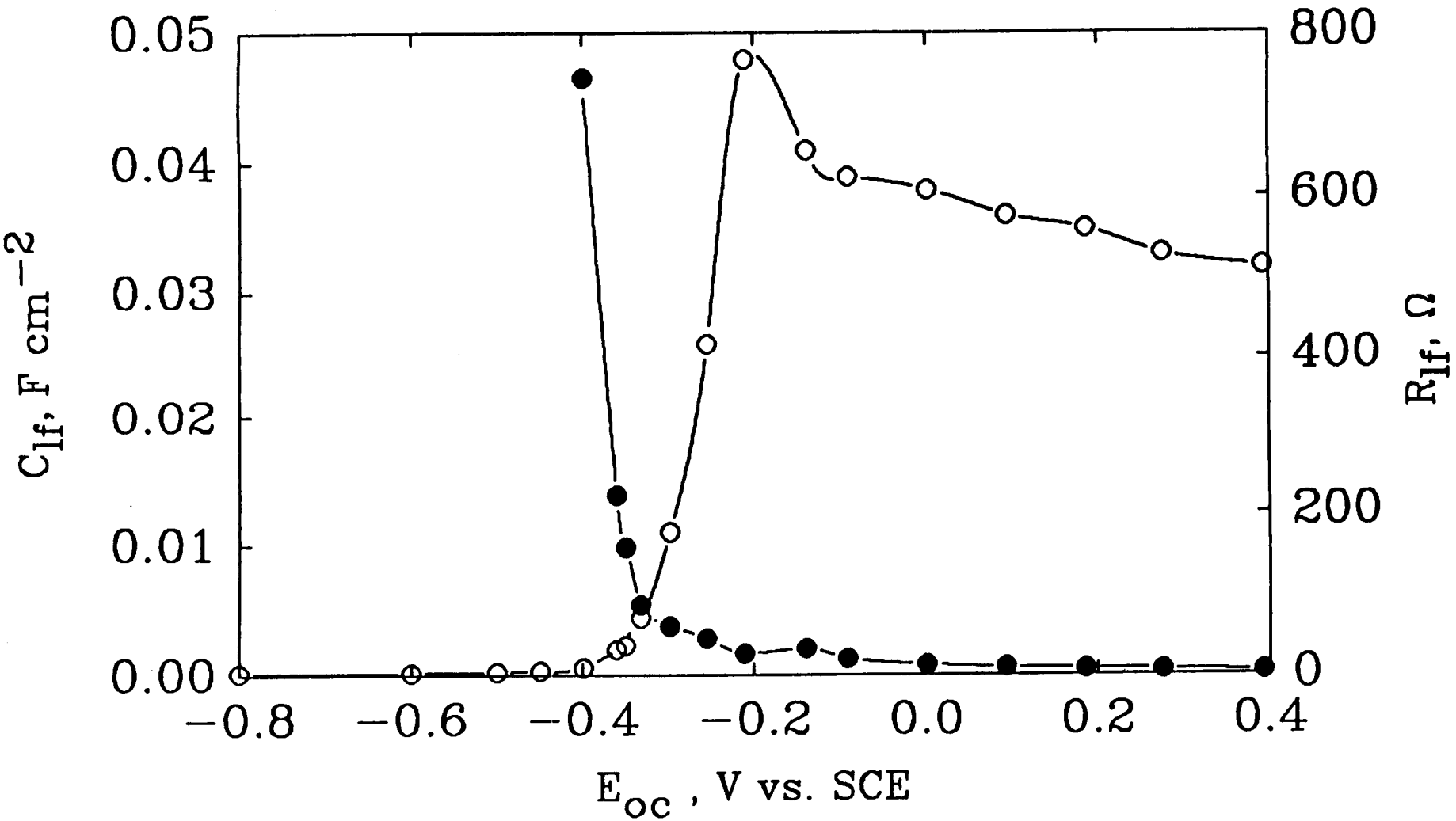
0.05
0.04
0.03
0.02
0.01
0.00
800
600
400
200
0
−0.8
−0.6
−0.4
−0.2
0.0
0.2
0.4
C_{lf}, F cm^{-2}
R_{lf}, Ω
E_{oc} , V vs. SCE

Figure 9

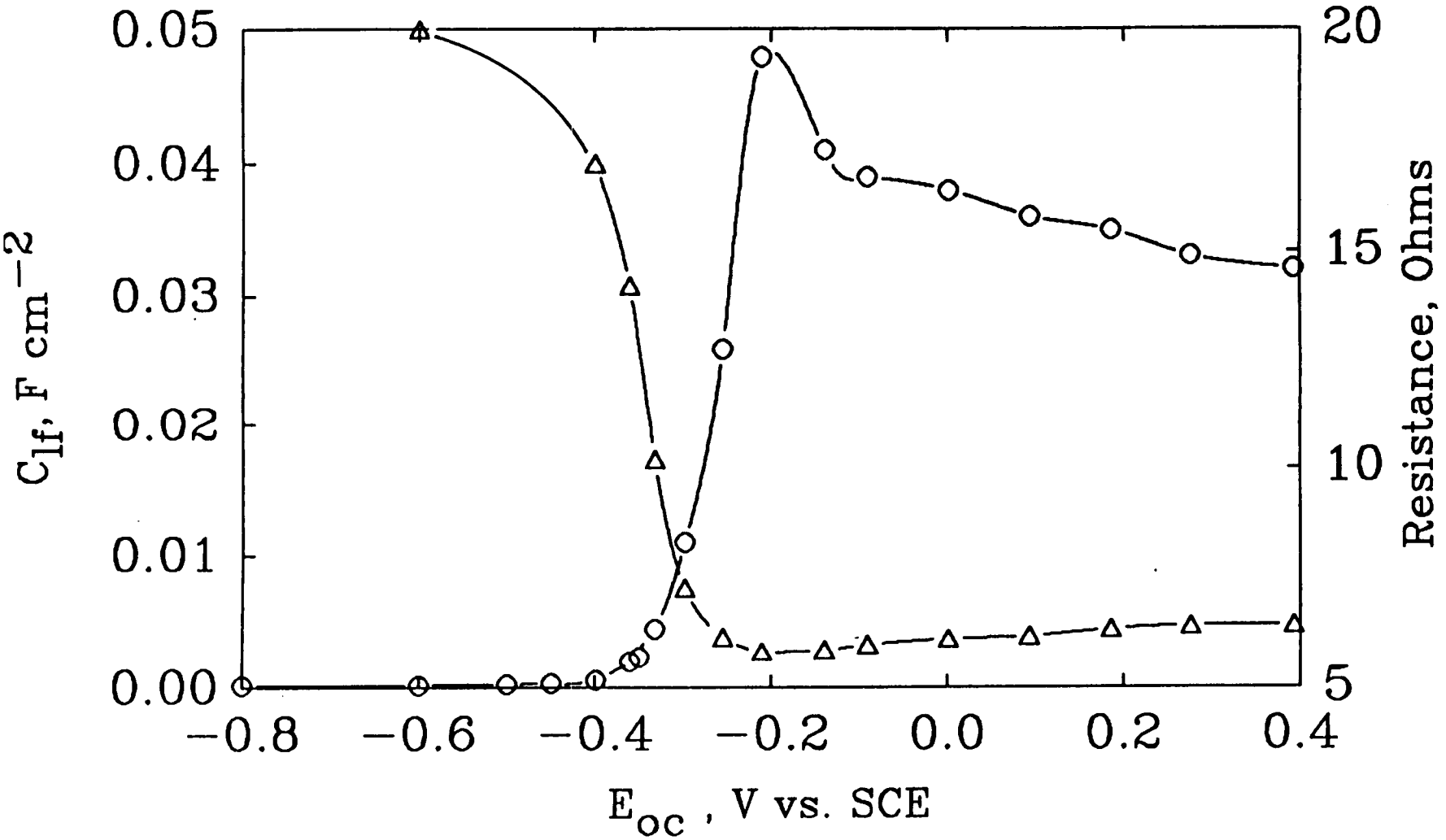
0.05
0.04
0.03
0.02
0.01
0.00
C_{lf}, F cm^{-2}
20
15
10
5
Resistance, Ohms
−0.8
−0.6
−0.4
−0.2
0.0
0.2
0.4
E_{oc} , V vs. SCE

Figure 10

APPENDIX B

DETERMINATION OF DIFFUSION COEFFICIENTS IN POLYPYRROLE THIN FILMS USING A CURRENT PULSE RELAXATION METHOD

Determination of Diffusion Coefficients in Polypyrrole Thin Films Using a Current Pulse Relaxation Method

Reginald M. Penner**[1], Leon S. Van Dyke**, and Charles R. Martin*

Department of Chemistry

Texas A&M University

*Electrochemical Society Active member, to whom correspondance should be addressed.

**Electrochemical Society Student member.

[1]Present Address: Department of Chemistry, Stanford University, Stanford, CA 94305

Introduction

Diffusion coefficients for mobile species in electronically conductive polyheterocycles have been reported by several groups (1-5). In each case, a large amplitude electrochemical experiment such as potential step chronocoulometry (6) ~~has been~~ employed. Techniques like these based on the Cottrell Equation have been used previously to measure apparent diffusion coefficients in nonelectronically conductive redox polymer films (cf. 7-10). Unfortunately, an inherent problem with the application of large amplitude electrochemical methods to electronically conductive polymers is that of background correction. Feldburg (11) has shown that the charge associated with switching a conducting polymer between conducting and insulating redox states (as required by any large amplitude experiment) has a large capacitive component which is inseparable from the faradaic charge. That is, there is no simple method for correcting the experimentally observed signal (usually Q(t) or i(t)) for capacitive contributions. In the absense of a capacitance correction, the Cottrell Equation cannot yield accurate diffusion coefficient information (6). Moreover, this same problem exists for other large amplitude experiments such as cyclic voltammetry, differential pulse voltammetry, and chronopotentiometry.

A small amplitude electrochemical experiment, however, can circumvent the background correction problem since diffusion coefficient information can be gleened from an experiment in which the conducting polymer remains in the reduced (nonconducting) state. Under these circumstances, the relatively small capacitive contributions to the electrochemical signal can easily be estimated and compensated. Such a small amplitude current pulse experiment has been developed by Steele and coworkers (12) and by Worrell

and coworkers (13-16) to measure diffusion coefficients for intercalated species in alkali metal intercalation compounds. Using a more rigorous mathematical treatment of this experiment, we have developed a modification of the current pulse method suitable for thin, redox film-modified electrode systems. In addition to solving problems associated with background correction, the current pulse - E_{oc} relaxation method presented here has a number of other advantages for the determination of diffusion coefficients in thin films.

Here we describe this new method and its application to the determination of diffusion coefficients in electrochemically synthesized polypyrrole thin films. Diffusion coefficients for such films in Et_4NBF_4, MeCN are determined for a series of submicron film thicknesses. In addition, we report measurments of the double-layer capacitance, C_{dl}, and the resistance, R_u, of polypyrrole thin films as a function of potential obtained with the galvanostatic pulse method. Measurments of the electrolyte concentration in reduced polypyrrole films are also presented to aid in the interpretation of these data.

Theory

Previous current pulse - E_{oc} relaxation experiments - As noted above, a small amplitude, current pulse experiment was first used by Steele and coworkers (12) and by Worrell and coworkers (13-16) to measure diffusion coefficients for alkali metal atoms in layers of the intercalation compounds TaS_2, TiS_2 and TiO_2. The application of this technique to diffusion coefficient determinations in alkali metal intercalation compounds is now well established (17,18). In a typical experiment, a current pulse of some

duration, τ, and amplitude, i_p, is used to inject the diffusing species (usually Li^o or Na^o) at the electrolyte/film (electrode)interface. At the termination of the current pulse, the working electrode is returned to open circuit and its potential, E_{oc}, is monitored as a function of time. The perturbation in the concentration of the electroactive species at the electrode surface results in a displacement of E_{oc} as predicted by the Nernst equation (6):

$$E_{oc} = E^o_{ox/red} + (RT/nF)\ \ln([ox]_{x=0}/[red]_{x=0}) \qquad [1]$$

ie. E_{oc} is determined by the ratio [ox]/[red] at the electrode surface. At the termination of the current pulse ($t = \tau$), the electrochemically generated diffusion layer has a narrow distance distribution and the maximum potential excursion, $\Delta E_{oc} = |E_{oc,initial} - E_{oc,t}|$, is observed. At successively longer times, t, after the termination of the current pulse, the concentration of diffusing species at the electrode surface, $C_{diff,x=0}$, and ΔE_{oc} decrease as the diffusion layer relaxes into the bulk of the film. Since the rate at which the film reequilibrates is dependent on the diffusion coefficient, D_{diff}, of the intercalated species, D_{diff} can be determined from the experimentally observed rate at which ΔE_{oc} relaxes to $E_{oc,initial}$. In all systems studied to date, the rate of E_{oc} relaxation is linear with $t^{-1/2}$, and D_{diff} is extracted from the slope of this plot (12-16).

In the application of the current pulse - E_{oc} relaxation technique to alkali metal intercalation compounds, several assumptions are made which simplify the mathematical treatment of the experiment. These assumptions

are as follows: i) diffusion of the intercalated species is semi-infinite linear from the film/electrolyte interface. This assumption imposes an experimental constraint on the maximum duration of the experiment (6):

$$t_{max} < l^2/2D \qquad [2]$$

where l = film thickness, and t_{max} = time at which diffusion layer reaches film/electrolyte interface (maximum total experiment duration), ii) the equilibrium concentration of the injected species is not significantly perturbed by the quantity of diffusing species introduced by the current pulse, and, iii) the initial distribution of diffusing species existing at the termination of the current pulse is infinitely narrow, ie the diffusing species is initially dispersed in a plane at x=0 (19). If these assumptions are valid, the time dependence of ΔE_{oc} is given by (13,14,19):

$$\Delta E_{oc} = \frac{mi_p t}{FA(\ Dt)^{1/2}} \qquad [3]$$

where t is the time after the termination of the current pulse, and m is the slope of the linear E_{oc} vs. C_{diff} relation.

Assumption (i) limits the time window available for obtaining linear E_{oc} vs. $t^{-1/2}$ behavior consistant with Eq. 3 for any film thickness. Diffusion coefficients of 1 x 10^{-8} cm^2 sec^{-1} (Li_yTaS_2 (13)) and layer thicknesses, l = 50 μm, which are typical parameters for alkali metal intercalation compounds, correspond to t_{max} values (Eq. 2) of ca. 1000 sec. Experimentally, linear E_{oc} vs. $t^{-1/2}$ behavior is routinely observed for t < ca. 100 sec (12-15).

Although the diffusion coefficients measured for polypyrrole films are similar, much thinner films are required ($l < 1$ μm). The corresponding t_{max} value for such films is ca. 0.5 sec or less. Figure 1 shows the ΔE_{oc} vs. $t^{-1/2}$ plots obtained at several pulse current amplitudes for a typical 0.54 μm polypyrrole film. Note that as expected, ΔE_{oc} is not linear with $t^{-1/2}$ indicating that the simple, limiting behavior described by Eq. 3 is not observed for this system.

Calculation of $C_{diff,x=0}$ vs. time transients - Application of the current pulse - E_{oc} relaxation experiment to the measurement of diffusion coefficients in thin ($l < 1.0$ μm) films requires that an expression for ΔE_{oc} vs. t be derived which is free of the constraints imposed by assumptions (i) - (iv) above. We have accomplished this by calculating ΔE_{oc} vs. time transients with an expression which describes finite diffusion from a known initial distribution of diffusing species (that generated by the current pulse). The $C_{diff,x=0}$ vs. time transients generated from this more rigorous expression are converted to E_{oc} vs. time transients using calibration curve as described below. Since a simple $t^{-1/2}$ dependance is not observed for the resulting transients, diffusion coefficients are obtained by fitting the simulated E_{oc} vs. time transients to experimentally obtained transients.

Generation of simulated $C_{diff,x=0}$ vs. time transients for the current pulse experiment involves two discrete calculations. First, the initial concentration-distance profile of diffusing species must be calculated from the experimental current pulse parameters. This initial distribution is then used to calculate $C_{diff,x=0}$ for times after the termination of the

current pulse.

The equation describing linear diffusion for any initial distribution of diffusing species, f(x)', and finite geometry is given by (19):

$$C(x,t) = \frac{1}{l}\int_0^l f(x')dx' + \frac{2}{l}\sum_{n=1}^{\infty}\exp\left(\frac{-Dn^2\pi^2 t}{l^2}\right)\cos\left(\frac{n\pi x}{l}\right)\int_0^l f(x')\cos\left(\frac{n\pi x'}{l}\right)dx' \quad [4]$$

where x is the distance from the planar source (electrode), C(x,t) is the concentration of diffusing species at any x and $t > \tau$, t is the time after the termination of the current pulse, and l is the film thickness. $C_{diff,x=0}$ is obtained by solving Eq. 4 for x=0 the appropriate initial distribution of diffusing species. The expression which we have employed for f(x)' is that for a continuous planar source of diffusing species in semi-infinite geometry (20):

$$C(x',t) = \frac{i}{nF}\sqrt{\frac{t}{\pi D}}\exp\left(\frac{x^2}{4Dt}\right) - \frac{ix}{2nFD}erfc\left(\frac{x}{2\sqrt{Dt}}\right) \quad [5]$$

where τ is the current pulse duration, C(x',τ) is the concentration - distance profile (initial distribution) at $t = \tau$, and i is the current pulse amplitude. Note that Eq. 5 treats the semi-infinite case. Consequently, an experimental constraint is imposed on the maximum pulse duration, τ_{max}, which is the same as that given by Eq. 2 above. This constraint is much less serious that that associated with Eq. 3 since the current pulse duration is easily confined to acceptible values. For example, if D and l are taken to be 1 x 10^{-8} cm^2 sec^{-1} and 0.5 μm, respectively, the maximum allowable pulse duration (Eq. 2) is ca. 100 msec. With this provision, substitution of Eq. 5 into Eq. 4 yields an exact expression for $C_{diff,x=0}$

for any desired combination of experimental parameters.

Eqs. 4 & 5 assume that the diffusion coefficient of the thin film is uniform. $C_{diff,x=0}$ vs. time transients were also calculated which consider linear variations (increases) of the D_{diff} with increasing distance from the planar source. This was accomplished by assigning a diffusion coefficient, Dx, consistant with the desired gradient to every distance increment $x + \Delta x$ for which the numerical integration was performed. The initial distribution was then calculated using Eq. 5 exactly as before. The resulting initial distribution accounts rigorously for the existance of the diffusion coefficient gradient. The C_{diff} vs. x relation so obtained is then substituted into Eq. 4 where each time increment, $t + \Delta t$, was assigned an effective diffusion coefficient, $D_{eff,t}$. The value of Deff,t at each time increment $t + \Delta t$ was the average of the diffusion coefficient at the electrode surface, D_{min}, and D_x at a distance equal to the excursion of the diffusion layer, $D_{x,diff}$. Thus, the $D_{eff,t}$ value operative for some time interval $t + \Delta t$ is given by the equation:

$$D_{eff,t} = (2D_{min} + ((2Dt)^{1/2})D_{grad}))/\ 2$$
$$= (2D_{min} + D_{x,diff})/2 \qquad [6]$$

where $(2Dt)^{1/2}$ is the approximate diffusion layer thickness, D_{min} is the minimum diffusion coefficient at $x = 0$, and D_{grad} is the gradient of the diffusion coefficient with distance, x, from the planar source. This modification to Eq. 5 assumes that at each time interval $t + \Delta t$, $D_{eff,t}$ is uniform over the entire diffusion layer thickness.

Experimental

Materials and equipment - Platinum disk electrodes (r = 1.15 mm) were constructed and pretreated as described previously (21). Tin oxide coated glass OTE's (area = 15 cm^2) were used to prepare large area polypyrrole films suitable for conductivity measurements. These electrodes were cleaned in concentrated H_2SO_4 prior to use. Tetraethylammonium tetrafluoroborate (99%, Aldrich) was recrystallized from methanol and dried envacuo at 100 C for ca. 24 hrs. prior to use. Pyrrole (99%, Aldrich) was distilled under an inert atmosphere immediately prior to use. Acetonitrile (UV grade, Burdick & Jackson) was used as recieved. All solutions employed for electrochemical measurements were purged with purified N_2 prior to use.

The glass cells employed for all electrochemical measurements were of a conventional one compartment design. A large area, Pt gauze counter electrode (25 x 25 mm, AESAR) and a conventional saturated calomel reference electrode (SCE) were used for all electrochemical experiments.

Conductivity measurements were accomplished with a Yellow Springs Instruments Model 31 AC conductivity bridge and a YSI Model 3402 cell (cell constant = 0.1 ohm cm^{-1}).

Film deposition - Polypyrrole films were deposited from monomer solutions containing 0.5 M pyrrole in 0.2 M Et_4NBF_4, acetonitrile. Polymer deposition was accomplished galvanostatically using a EG&G Princeton Applied Research Model 273 potentiostat/galvanostat. A polymerization current density of 1.0 mA cm^{-2} was used for all films. Reproducible steady state potentials of 0.84 V $\pm$ 0.01 V vs. SCE were observed during film deposition at this current density.

C-2

Polypyrrole films were prepared with the above procedure in a series of film thicknesses from 0.1 μm to ca. 1.6 μm. The film thickness was measured for dried, oxidized films using a Tencor Alpha Step profilometer. As shown in Figure 2, the relationship between polymerization charge and film thickness is linear for polypyrrole films over this interval. The slope of the plot in Figure 2 is 37.8 mC · 0.1 μm^{-1}; substantially greater than the 24 mC · 0.1 μm^{-1} observed previously for polypyrrole-BF_4^- films prepared by Diaz et al (22). This calibration curve was used to prepare polypyrrole films of known thicknesses as described above. After film deposition, polypyrrole modified electrodes were transfered to monomer free, 0.2 M Et_4NBF_4, MeCN electrolyte and a cyclic voltammogram was recorded to ascertain the film quality. All subsequent electrochemical measurements were performed in this electrolyte.

Current step R_u and C_{dl} measurements - 0.27 μm thick polypyrrole films were used for the measurement of R_u and C_{dl}. R_u and C_{dl} information were obtained at open circuit potentials from -0.6 V to 0.4 V vs. SCE using the galvanostatic pulse method as described previously for polyacetylene films (23). In the present case, a train of four current pulses were generated with an IBM PC XT computer and applied with the PAR Model 273 potentiostat/galvannostat. Current pulses had durations of 1 msec and magnitudes of 290 $\mu A\ cm^{-2}$, 585 $\mu A\ cm^{-2}$, 875 $\mu A\ cm^{-2}$, and 1.17 $mA\ cm^{-2}$. Adjacent current pulses were separated by open circuit intervals of ca. 50 msec. The rise-time observed for the PAR Model 273 was < 2 μsec. Potential transients at $t \leq 100$ μsec were recorded with a Nicollet Model 2090 digital storage oscilloscope.

Prior to the application of the current pulse train, polypyrrole films were potentiostated at the desired potential for 120 sec, then allowed to equilibrate at open circuit until no potential drift was observed. The resulting R_u and C_{dl} data obtained at a series of potentials exhibited no significant hysteresis with varying potential. This indicates that the pretreatment procedure employed resulted in films which were essentially equilibrilibrated at the terminal open circuit potential. At each potential, the values of R_u and C_{dl} were obtained from plots of iR and dE/dt vs. i_p, respectively, as described below.

Film electrolyte concentration mesurements - 0.5 μm polypyrrole films were deposited on 15 cm^2 SnO_2 - glass electrodes as above. Freshly deposited films were then transfered to 0.2 M Et_4NBF_4, MECN electrolyte and reduced potentiostatically at -0.8 V for 10 minutes. During this time, the films changed from the characteristic black color of oxidized films to the characteristic yellow color of reduced polypyrrole. Three different procedures were then used to effect the extraction of the reduced films. "Unrinsed" films were transfered from the electrolyte solution directly to 100 ml pure MeCN in an electrolytic beaker where they were extracted for 20 h. "Dip-rinsed" films were removed from the electrolyte solution and quickly dipped into pure MeCN before extracting as above. "Long-rinsed" films were treated as per the dip-rinse procedure above except that film-covered electrodes were stirred in the MeCN rinse for ca. 10 sec prior to removal and extraction.

After the 20 h extraction period, the conductivity of the leaching solution was measured. A water bath was used to maintain a constant

temperature of 30 C for all conductivity measurments. The concentration of Et_4NBF_4 was determined from the conductivites observed for the leaching solutions by using a calibration curve constructed with Et_4NBF_4, MeCN solutions of known concentrations. The concentration of supporting electrolyte in the films was determined from the amount of measured electrolyte using a film volume of 7.5×10^{-4} cm^3.

Preparation of E_{OC} vs. [ppy^+] calibration curves - Determination of diffusion coefficients with the current pulse method necessitates converting the concentration of diffusing species at the electrode surface, $C_{diff,x=0}$, to E_{OC} values so that calculated and experimental data can be compared. In the case of electronically conductive polymers, the relationship between polymer oxidized sites, ppy^+, (or holes, h^+) and E_{OC} is required. In the present case, this relationship was established empirically using a procedure similar to the Electrochemical Voltage Spectroscopy (EVS) employed by Kaufman and coworkers to determine the % doping vs. E_{OC} relationship for polyacetylene (24-26).

The procedure used here was as follows. Freshly prepared 0.27 μm polypyrrole films were reduced potentiostatically at 1.0 V vs. SCE until currents decayed to ca. 100 nA cm^{-2}. Such films were assumed to be quantitatively reduced. A small quantity of anodic charge was then injected with a constant current pulse of 500 nA x 1 sec after which the working electrode was returned to open circuit. After allowing the electrode to equilibrate at open circuit for 20 sec., the terminal open circuit potential was recorded, a second charge injection performed, and the cycle repeated. This charge injection-equilibration cycle was repeated until the desired

terminal E_{oc} was acheived. In this way the $Q_{injected}$ vs. E_{oc} relationship can be determined for the potential interval of interest. The current modulation program for the collection of these data was controlled by the IBM PC XT using PAR Headstart electrochemical software and executed by the PAR MOdel 273. Excellent film to film reproducibility of the $Q_{injected}$ vs. E_{oc} calibration curves was obtained using this procedure. As discussed in detail below, the "raw" calibration data so obtained must be compensated for the effects of capacitance before the injected charge can be related to oxidized polymer equivalents.

Current pulse diffusion coefficient determinations - Current pulse induced E_{oc} transients were obtained by first reducing freshly synthesized, oxidized films at a potential of -0.8 V vs. SCE. Films were assumed to be quantitatively reduced at this potential when the observed current density decreased to ca. 500 nA cm^{-2}. The film was then potentiostated at an initial potential, $E_{initial}$ = -0.4 V. After allowing the current to decay again to < 500 nA cm-2, the working electrode was switched to open circuit and a 50 msec anodic current pulse of the desired amplitude (100 - 400 μA cm^{-2}) was applied. Current pulses were generated with a Princeton Applied Research Model 175 programmer and applied with a PAR Model 173 potentiostat/galvanostat. The resulting potential transients were recorded with the Nicollet Model 2090 oscilloscope. Note that after equilibration of the film at -0.4 V, virtually no drift in potential was observed upon switching to open circuit. Subsequent current pulse experiments at other current densities were performed by rereducing the film at -0.8 V and then reequilibrating at -0.4 V as before.

Calculation of simulated Eoc vs. time transients - Programs for generating simulated ΔE_{oc} vs. time transients were written in PASCAL (Turbo Pascal, Borland) and executed on a Compaq Portable II computer. Simulated and experimental data were compared using LOTUS 123 (Lotus Development) graphics. Curve fitting of the simulated transients to the experimental data was accomplished manually.

Results and Discussion

Cyclic voltammetry of polypyrrole films - A typical cyclic voltammogram at 20 mV sec^{-1} for a 0.27 μm polypyrrole film in 0.2 M Et_4NBF_4, MeCN is shown in Figure 3. Cyclic voltammograms for thicker films such as those used for diffusion coefficient measurements were qualitatively similar. As noted above, cyclic voltammograms were routinely used to ascertain the uniformity of freshly synthesized films prior to performing other electrochemical measurements.

C_{dl} and R_u determinations - Our primary purpose for conducting the galvannostatic pulse experiments was to obtain the C_{dl} vs. E_{oc} data required to correct $Q_{injected}$ vs. E_{oc} calibration curves for capacitive charge contributions. Thus, C_{dl} vs. E_{oc} data for potentials $E_{oc} < -0.3$ V were required. However, current pulse experiments were conducted over the entire potential interval from -0.6 V to 0.4 V so that the C_{dl} and R_u data so obtained could be compared with that previously obtained from the AC impedance analyses of polypyrrole thin films (21).

The galvannostatic pulse method has previously been used to obtained R_u

and C_{dl} information for electronically conductive polyacetylene films by Will (23). At very short times (t < 100 μsec) after the application of the current step, the potential response is approximated by that for a series RC circuit (6,23):

$$E = i_p(R_u + t/C_{dl}) \qquad [6]$$

Where R^u is the total series resistance of the circuit and C_{dl} is the double layer capacitance. The displacement of the potential immediatly after the application of the current pulse (t < 5 msec) is equal to ipRu (6). A linear increase of the potential with time is observed at longer times (5 msec < t < 100 msec) since this current is primarily that associated with the charging of the electrical double-layer (6).

Typical E vs. t transients for a 0.27 μm polypyrrole film are shown in Figure 4a. The line indicated for each plot is the linear regression fit of the data in the interval 20 μsec < t < 100 μsec. dE/dt values obtained from the slopes of these lines were plotted vs. the current pulse amplitude (Fig. 4b) and Cdl was calculated from the slope using the Eq. 6 (6,23). Values for the total uncompensated resistance of the system, R_u, were obtained from plots of iR_u (measured at 20 μsec) vs. i_{step} (Fig. 4b)(6).

Figure 5 shows the resulting C_{dl} and R_u values obtained from current pulse measurments at open circuit potentials from -0.6 to +0.4 V. The resistance of ca. 6 ohms observed for the oxidized conducting film is approximately that expected from the electrolyte resistance alone (21). Thus, resistance in excess of this value can be attributed to the polypyrrole film. C_{dl} values obtained at potentials E_{oc} < -0.4 V of 20 - 30

$\mu F\ cm^{-2}$ are similar to those observed for bare platinum electrodes in this electrolyte. Thus, at potentials were polypyrrole is not electronically conductive, the capacitance is approximately that derived from the charging of the platinum substrate surface only. At potentials $E_{oc} > -0.2$ V, C_{dl} reaches a maximum of ca. $2.5 \times 10^{-4}\ F\ cm^{-2}$ of geometric electrode area. This corresponds to a capacitance per unit volume of ca. $9\ F\ cm^{-3}$. This value is approximately an order of magnitude smaller than that obtained from cyclic voltammetry (27) and AC impedance measurements (21,28). This disparity is probably due to a nonuniform a current density distribution for the porous, electronically conductive film. At the short times accessed in this experiment, the current density is likely to be supported preferentially by double-layer charging of the exterior surfaces of the film. Consequently, the C_{dl} values observed for oxidized polymer with the current pulse method may approximate the capacitance of film/electrolyte interface. If this is the case, the C_{dl} value for the oxidized polymer obtained here tranlates to a roughness factor, R, (actual surface area/geometric surface area) of ca. 10 assuming the specific capacitance of the polymer is similar to that of platinum, $20\ \mu F\ cm^{-2}$. This R value seems reasonable considering the rough surface topology of electrochemically synthesized polypyrrole films.

Reduced, nonelectronically conductive films should not exhibit this effect, and C_{dl} values obtained at potentials, Eoc < -0.3 V ought to accurately reflect the total C_{dl} of the system. We have used these data to correct the $Q_{injected}$ vs. E_{oc} calibration data for capacitive contributions as discussed below. Note that accurate C_{dl} values are not obtained at potentials from -0.3 - -0.4 V by either cyclic voltammetry or AC impedance

since the currents measured by both methods at these potentials contain a significant faradaic component (21,29).

The variation of C_{dl} and R_u with potential shown in Figure 5 parallels the C_{dl} and R_u vs. E_{oc} data obtained previously from the AC impedance analyses of thin polypyrrole films (21). As the potential of the film is increased from -0.6 V, a sharp decrease in R_u is observed at potentials from -0.5 V to -0.3 V; at potentials negative of the transition in C_{dl}. Decreases in R_u at these potentials may reflect increases in either the ionic or the electronic conductivity of the electrochemical circuit (polymer film + electrolyte). However, C_{dl} scales with the electronic conductivity of the polymer film only. Thus, decreases in R_u in the absence of commensurate increases in C_{dl}, as observed for the polypyrrole/BF_4^- films here, must be the result of decreases in the ionic conductivity of the film. The data shown in Figure 5 suggests that at potentials of ca. -0.4 V, polypyrrole films possess high ionic conductivity but are relatively nonelectronically conductive. The origin of this effect is discussed below.

Measurement of the electrolyte concentration in ppy^O films - We have estimated the concentration of free electrolyte in reduced polypyrrole (ppy^O) films by extracting electrochemically reduced films in pure acetonitrile and measuring the conductivity of the leaching solution as described above. This information is important to the interpretation of the transport data obtained using the current pulse - E_{oc} relaxation technique described below. In addition, these data provide insight to the mechanism responsible for the transition in R_u at very negative potentials.

Film electrolyte concentrations as measured for 0.5 μm polypyrrole

films using unrinsed, dip-rinsed, and long-rinsed extraction techniques are listed in Table I. The precision of the data obtained for unrinsed films was low due to the fact that variable quantities of electrolyte adhered to the electrode as it was withdrawn from the electrolyte solution. This excess electrolyte was transfered to the leaching solution resulting in conductivity values and film electrolyte concentrations which we believe are anomolously high.

Good precision was obtained by dip-rinsing the polypyrrole films prior to extraction, as described above. The film electrolyte concentration of 5.4 M ± 0.5 M obtained using this procedure is surprisingly high considering the resistivity observed for such films. Note that reduced films were potentiostated at -0.8 V prior to dip-rinsing and extraction. This potential is well negative of the increase in R_u observed at -0.3 V - -0.5 V (Figure 5). These data suggest that the mobility of the electrolyte in the polymer at potentials E_{oc} < -0.3 V is limited, possibly due to a transport-restrictive morphology assumed by the polymer at these potentials. In this case, the increase in R_u shown in Figure 5 could be effected by morphological changes in the polymer which increase the film electrolyte mobility.

As shown in Table I, long-rinsed films (duration ca. 10 sec) yielded smaller film electrolyte concentrations. Some extraction of electrolyte from the film during the pre-rinse is inevitable with this procedure. Consequently, the electrolyte concentrations estimated with the long-rinse procedure are undoubtedly too low. However, the concentration values observed for long-rinsed films of ca. 2.85 M seem to suggest that removal of excess electrolyte is accomplished reliably with the faster, dip-rinse

procedure.

Preparation of [ppy$^+$] vs. E_{oc} calibration curves - The procedure for calculating E_{oc} relaxation transients necessitates converting the $C_{diff,x=0}$ values obtained from Eqs. 4 & 5 to E_{oc} values so that calculated and experimental data can be compared. This can be accomplished for a conventional redox couple simply by using the Nernst equation (Eq. 1). However, electronically conductive polymers may not conform strictly to the Nernst equation. Our approach has been to construct an empirical calibration curve by experimentally relating C_{ppy+} to E_{oc}. A similar procedure has been used to relate C_{Li} or C_{Na} to E_{oc} in alkali metal intercalation compound films (12-16).

The preparation of raw $Q_{injected}$ vs. E_{oc} calibration curves (or coulometric titration curves (29)) is discussed in detail above. One such curve for the potential interval from -0.3 V to -0.4 V is shown in Figure 6a. Note that current pulse - Eoc relaxation experiments were confined to this potential interval. $Q_{injected}$ values cannot be directly converted to chemical equivalents without first correcting for capacitive contributions. We have used C_{dl} values obtained from the current pulse experiments to subtract capacitive charge contributions from $Q_{injected}$. The resulting charge values corrected for capacitance, Q_{corr}, are plotted with $Q_{injected}$ in Figure 6a. Qcorr values were then converted to concentrations of oxidized polymer sites, C_{ppy}^+, assuming n = 1 eq mole^{-1}. A typical corrected calibration curve and the 4th order polynomial least squares fit to these data are shown in Figure 6b. Note that C_{ppy+} is calculated for a film thickness of 0.27 μm. The equation for the polynomial best fit was

subsequently used to convert calculated C_{ppy+} values to E_{oc} values for comparison to experimentally obtained data.

Interpretation of diffusion coefficients for polypyrrole - The open circuit potential observed for a polypyrrole film is determined by the concentration of oxidized sites in the polymer. Thus, if ideal Nernstian behavior were observed for polypyrrole, the appropriate Nernst equation is analogous to Eq. 1:

$$E_{oc} = E^{o}_{ppy+/ppyo} + (RT/nF)\ \ln(C_{ppy+,x=0}/C_{ppyo,x=0}) \qquad [8]$$

ie. E_{oc} is determined by the concentration of oxidized polymer sites, $C_{ppy^+,x=0}$ (or holes, h^+) at the electrode surface. In the strictest sense, diffusion coefficients measured using the current pulse - E_{oc} relaxation technique are values for the diffusion of these electrochemically generated holes, h^+. However, it is commonly assumed that diffusion of these positively charged species is limited by that of electrostatically bound anions, in this case BF_4^-. Given the unexpectedly large concentrations of free electrolyte in reduced polypyrrole films reported above, the possibility also exists that anions and cations are relatively immobile species, and that the apparent diffusion coefficient is limited by the rate of electron-hopping between essentially stationary anionic sites. Alternatively, the measured diffusion coefficient may reflect contributions from both cation and anion diffusion. We are currently measuring diffusion coefficients for a large number of electrolytes in order to ascertain the relative importance of factors such as cation size and anion size in an

attempt to understand diffusion in these polymers more completely. In the present work, we have refered to all measured diffusion coefficient values as $D_{Et_4NBF_4}$ consistant with the previously established convention (1-5). However, it should be noted that the factors controlling the diffusion of electrochemically generated h^+ in the polyheterocycles have not as yet been elucidated.

Behavior of simulated E_{oc} vs. time transients - Simulated ΔE_{oc} vs. time transients were calculated using conventional numerical methods from Eqs. 4 & 5. The rate of the E_{oc} decay following the termination of the current pulse depends primarily on the film thickness, 1, and the diffusion coefficient, D_{diff} as shown in Eq. 5. Figure 7 shows simulated E_{oc} vs. time transients for a series of four diffusion coefficient values and experimental parameters similar to those encountered in the present study. These data show that for 1 = 0.5 μm, substantial differences in the E_{oc} relaxation rate exist for diffusion coefficients which differ by as little as 20%. Note that these E_{oc} relaxation transients occur on a convenient experimental time scale of ca. 1 sec.

The effect of film thickness on simulated ΔE_{oc} vs. time transients is shown in Figure 8. Both the rate of the E_{oc} relaxation and the value of the final equilibrium potential are noticably affected by changes in the film thickness of 20%. As shown in Eq. 5, the approximately exponential Eoc relaxtion rate is proportional to exp (1^{-2}). Thus, errors present in the measurement of the film thickness radically affect the accuracy of the diffusion coefficients calculated with this technique.

Simulated ΔE_{oc} vs. time transients can also be generated for films in

which the diffusion coefficient is nonuniform using the procedure outlined above. Such transients were calculated assuming a linear gradient of the diffusion coefficient, D_{grad}, with film thickness for comparison with the experimental ΔE_{OC} vs. time transients obtained for 0.73 mm and 0.95 mm films (see discussion below). The effect of D_{grad} on simulated ΔE_{OC} vs. time transients is shown in Figure 9. Note that the diffusion coefficient, D_{min}, at x=0 for each of the transients A-D was 1 x 10^{-9} cm^2 sec^{-1}. The rate of the observed E_{OC} relaxation rate increases with D_{grad} as expected. However, in constrast to the behavior shown in Figure 7, the maximum excursion in E_{OC} observed at short times is similar for all of the transients Fig. 9A - 9D.

Experimental Eoc vs. time transients for polypyrrole thin films - Diffusion coefficients were measured for polypyrrole films with thicknesses of 0.35 μm, 0.54 μm, 0.73 μm, and 0.95 μm. Polypyrrole films with thicknesses greater than ca. 1 μm cannot be quantitatively addressed electrochemically, ie. the as-synthesized oxidized films cannot be quantitively reduced (27,30). For this reason, films with thicknesses greater than 1 μm were not employed in this study.

Current pulse experiments were performed from an initial potential of -0.4 V vs. SCE. The maximum potential excursions observed for these experiments were approximately 50 mV. Thus, all current pulse - Eoc relaxation experiments were confined to potentials from -0.4 V to -0.35 V vs. SCE. Because this potential interval is well negative of the polymer E^o of -0.2 V, the polypyrrole film remained in its reduced, nonconducting redox state throughout the experiment. The fact that polypyrrole films at these potentials are essentially nonelectronically conductive is supported

by the capacitance data of the present paper (Figure 5) and by previous experimental evidence (21,31,32).

ΔE_{oc} vs. time transients were obtained for all films with current pulse amplitudes of 100, 200, 300, and 400 $\mu A\ cm^{-2}$, anodic. The quantity of charge injected during the current pulse, $Q_{injected}$, was corrected for capacitance. The capacitive component of $Q_{injected}$ was estimated from the C_{dl} data obtained from the current pulse experiments discussed above based on the maximum potential excursion observed during the application of the current pulse.

Simulated E_{oc} vs. time transients were fit to experimental transients for 0.35 μm and 0.54 μm polypyrrole films assuming the diffusion coefficient in these films was uniform. Excellent agreement between simulated and experimental transients was obtained at current pulse amplitudes of from 100 - 400 $\mu A\ cm^{-2}$ for films of either thicknesses. Typical simulated and experimental transients are shown in Figure 10 for a 0.5 μm film. The best fit diffusion coefficients obtained from these data are listed in Table II. Note that the variation in diffusion coefficient values observed over the range of current densities employed here was typically less than 10%. It is worth noting that the experimental parameters employed for these measurements are incompatible with the assumptions listed above for Eq. 3. For example, the overall redox state of the polypyrrole film is substantially altered for ip = 300 $\mu A\ cm^{-2}$ and 400 $\mu A\ cm^{-2}$ as evidenced by the terminal ΔE_{oc} values observed for equilibrated films. In addition, the excursion of the diffusion layer as calculated from Eq. 2 excedes the film thickness for both 0.35 μm and 0.54 mm film thicknesses ($t_{max} < 0.5$ sec) indicating that diffusion is effectively finite. Thus, the nonlinearity of

experimental ΔE_{oc} vs. $t^{-1/2}$ plots such as that shown in Fig. 1 is not surprising. However, these effects are taken fully into account by Eq. 4 & 5 as evidenced by the excellent fit obtained between experiment transients and those calculated from these equations.

It is important to note that the diffusion layer thickness at the termination of the current pulse does not equal the film thickness for pulse durations of 50 msec. For example, the 0.35 μm films prepared in this study which exhibited the fastest diffusion coefficients, t_{max} values calculated from Eq. 2 and the $D_{Et_4NBF_4}$ values listed in Table II are greater than 75 msec. Thus, diffusion during generation of the initial distribution is effectively semi-infinite and the experimental constraint imposed by Eq. 5 is satisfied.

The diffusion coefficient values measured for 0.35 μm and 0.54 μm thick films (Table II) are higher than the those for polypyrrole-BF_4^- thin films measured by Diaz and coworkers with chronoamperometry (34). We have previously reported $D_{Et_4NBF_4}$ values for polypyyrole films in Bu_4NBF_4, MeCN electrolyte using AC impedance methods. The values so obtained of ca. 1 x 10^{-9} cm^2 sec^{-1} are also significantly slower than observed here. Although it is tempting to attribute this latter disparity to the higher mobility of the Et_4N^+ cation as compared to Bu_4N^+, as noted above we are currently measuring $D_{Et_4NBF_4}$ values for a large number of electrolytes using both AC impedance and current pulse - E_{oc} relaxation methods in order to ascertain the origin of this effect. The difference in the diffusion coefficients obtained for the 0.35 μm film and the 0.54 μm film are reproducible. The origin of this effect is discussed in detail below.

Adaquate agreement between experimental and simulated E_{oc} vs. time

transients was obtained again assuming a uniform diffusion coefficient for films with thicknesses of 0.73 μm. However, experimentally observed ΔE_{oc} values at short times are greater by as much as 1 - 2 mV than the ΔE_{oc} values predicted by the best fit simulated data. In effect, a good fit of the simulated to the experimental data cannot be obtained for both the short time ΔE_{oc} data ($t < 0.1$ sec) and the data obtained at longer times. This is shown in Figure 11a where an experimental ΔE_{oc} vs. time transient for a typical 0.73 mm film (i_p = 100 μA) is compared with simulated transients. Three simulated transients were calculated; the diffusion coefficient corresponding to curve A was that neccessary to achieve the ΔE_{oc} excursion observed at times $t < 0.1$ sec, curve B was calculated using a $D_{Et_4NBF_4}$ value appropriate for the long time data, $t > 0.1$ sec. These diffusion coefficients values are listed in Table II. Note that $D_{Et_4NBF_4}$, curve A is approximately a factor of two faster than $D_{Et_4NBF_4}$, curve B. These data suggest that the diffusion coefficient may vary (increase) with increasing distance from the substrate electrode in the polypyrrole film. In order to test the effect that such a gradient would have on the resulting ΔE_{oc} vs. time relaxation transients, simulated transients were calculated assuming a linear gradient of $D_{Et_4NBF_4}$ with film thickness. The calculation of such transients is described in the theory section above. Figure 11a, curve C shows the best fit to the experimental data obtained with this model. The diffusion coefficient at the electrode/film interface for curve C was 4.2×10^{-9} cm^2 sec^{-1} and that at the film electrolyte interface was 8×10^{-8} cm^2 sec^{-1}. Note that ΔE_{oc} at times, $t < 0.1$ sec is fit well with this model, and the fit to data for $t > 0.1$ sec is slightly worse than that obtained with a uniform $D_{Et_4NBF_4} = 7 \times 10^{-9}$ cm^2 sec^{-1}, (curve B).

Experimental ΔE_{oc} vs. time curves for the 0.95 μm thick polypyrrole films were analyzed using exactly the same procedure as that employed for the 0.73 μm films above. A typical ΔE_{oc} vs. time transient for such a film (ip = 100 μA) is shown in Figure 11b. Again, curves A and B represent the best fits of simulated data for uniform $D_{Et_4NBF_4}$ values to the short time and the long time regions of the experimental transient, respectively. For this thicker polypyrrole film, the disparity between either curve A or B and the experimental data is more pronounced than for the 0.73 μm films. The diffusion coefficients corresponding to these curves (Table II) differ by a fact of 2. Figure 11b shows that the uniform diffusion coefficient model is clearly inadequete to describe the experimental ΔE_{oc} vs. time transients. Figure 11b, curve C represents the best fit obtained considering a linear gradient of diffusion coefficients in the film. The initial, short time regions of the experimental data are very well accomodated, although the ΔE_{oc} decay at times $t > 0.2$ sec procedes at a slower rate than predicted by this model. Again, the D_{min} value corresponding to curve C is similar to that used to obtain curve A.

To summerize the data presented for 0.73 μm and 0.95 μm polypyrrole films, the existance of a linear diffusion coefficient gradient does not account perfectly for the observed ΔE_{oc} - time transients. However, significantly better agreement is obtained particularly for the short time data than is possible by assuming uniform diffusion coefficient values for these films. Consequently, it seems likely that some dependence of $D_{Et_4NBF_4}$ exists on the film thickness in these relatively thick films. As a result, $D_{Et_4NBF_4}$ values increase with film thickness from the electrode/film interface to the film edge. The origin of this effect, and that responsible

for the variation of $D_{Et_4NBF_4}$ observed over the entire thickness interval from 0.35 μm - 0.95 μm is discussed below.

The increases in $D_{Et_4NBF_4}$ with film thickness observed here suggests that a gradient in the morphology of polypyrrole may exist in these thin films. This conclusion is supported by the fact that a diffusion coefficient gradient can be invoked to improve the aggreement between simulated and experimental ΔE_{oc} - time transients obtained for thick (0.73 μm and 0.95 μm) films. We have previously observed inconsistancies in the AC impedance specta of polypyrrole thin films which also suggest the presence of such a morphology gradient (21). As noted in this previous paper, the electrochemical synthesis of polypyrrole may facilitate the introduction of such morphology "density" gradients since the polymerization reaction does not occur at diffusion control (34). As a result, the polymerization reaction can procede at interior surfaces of the polymer film as well as at the film edge. The greatest accumulation of electrochemically deposited polymer then occurs near the electrode surface where the longest total duration is available for polymerization. The effective pore diameter (and hence $D_{Et_4NBF_4}$) of the resulting film increases with distance from the substrate electrode.

Conclusion

In the most general sense, we present here a small amplitude, DC electrochemical method for measuring diffusion coefficients in redox polymer thin films. The advantages of the current pulse - E_{oc} relaxation method as compared to conventional large amplitude electrochemical techniques (eg. chronocoulometry) are as follows: i) the current amplitude, i_p, can be

adjusted to very small values limited only by instrumental constraints, ie. potential sensitivity. Consequently, E_{oc} excursions can easily be confined to $\Delta E_{oc} < 10$ mV. Thus, diffusion coefficient information can be obtained for any discrete ratio [ox]/[red] and characteristics of the system associated with a particular redox state can be elucidated, ii) diffusion coefficient information is obtained from an open circuit region of the experiment. The adverse effects of migration and iR drop, which can be particularly serious for film-modified electrodes, are minimized as a result, iii) the model for calculating ΔE_{oc} - time transient presented here considers the finite diffusion case. Unlike electrochemical techniques based on the Cottrell equation, it is unneccessary to achieve semi-infinite diffusion in order to obtain reliable diffusion coefficient information, and, iv) the numerical approach to calculating ΔE_{oc} - time transients facilitates modifications which take into consideration effects such as the diffusion coefficient - thickness gradient discussed *vida supra*.

It should be noted that the application of the current pulse - Eoc relaxation technique to redox polymer films will be simplified in many case since the construction of an empirial calibration curve will not be nessessary for systems which can be assumed to exhibit Nernstian behavior.

The AC impedance analysis of redox films previously reported by Ho et al (29) and Rubinstein et al (33) can evince similar advantages due to the small amplitude of the applied potential sine-wave. Since diffusion coefficient information for the AC impedance experiment is obtained at steady-state, this experiment ought to be considered complimentary to the DC current pulse - E_{oc} relaxation experiment.

We have reported diffusion coefficients for polypyrrole thin films at a

series of submicron film thicknesses. These data point to the existence of a diffusion coefficient gradient with distance from the electrode surface in the polypyrrole film. Such a gradient might be due to structural changes in the film such that the polymer morpholgy is dense (transport restrictive) at the electrode/film interface and relatively open at the film/electrolyte interface. Since the electrochemical syntheses of other electronically conducting polyheterocycles (eg. polythiophene) are similar to that for polypyrrole, this observation may prove to be a general one.

In addition, the current pulse measurments of C_{dl} and R_u vs. potential presented here corroborate data previously obtained by AC impedence analyses of polypyrrole thin films (21). The magnitude of the C_{dl} values measured for the oxidized polymer suggests that the current pulse technique yields C_{dl} values for the polymer/electrolyte interface only, ie. the capacitance of the film edge. Measurements of the electrolyte concentration in reduced polypyrrole films reveal that quantitatively reduced films contain unexpectedly large concentrations of free electrolyte. This information has important implications for the interpetation of the observed dependencies of C_{dl} and R_u on potential.

Credit

This work was suported by the Office of Naval Research, the Robert A. Welch Foundation, the Air Force Office of Scientific Research, and NASA.

References

1. E.M. Genies, G. Bidan, and A.F. Diaz, *J. Electroanal. Chem.*, **149**, 101 (1983).
2. P. Marque, J. Roncali, and F. Garnier, *J. Electroanal. Chem.*, **218**, 107 (1987).
3. G. Nagasubramanian, S. Di Stefano, and J. Moacanin, *J. Phys. Chem.*, **90**, 4447 (1986).
4. C. Chiba, T. Ohsaka, and N. Oyama, *J. Electroanal. Chem.*, **217**, 239 (1987).
5. N.S. Sundaresan, S. Basak, M. Ponerantz, and J.R. Reynolds, *J.C.S. Chem. Commun.*, In Press.
6. A.J. Bard and L.R. Faulkner, "Electrochemical Methods: Theory and Applications," John Wiley & Sons, New York, 1980, Chpts. 3,4.
7. P. Daum, J.R. Lenhard, D. Rolison, and R.W. Murray, *J. Am. Chem. Soc.*, **102**, 4649 (1980).
8. C.R. Martin and K.A. Dollard, *J. Electroanal. Chem.*, **159**, 127 (1983).
9. F.C. Anson, J.M. Saveant, and K. Shigehara, *J. Am. Chem. Soc.*, **105**, 1096 (1983).
10. D.A. Buttry and F.C. Anson, *J. Am. Chem. Soc.*, **105**, 685 (1983).
11. S.W. Feldburg, *J. Am. Chem. Soc.*, **106**, 4671 (1984).
12. D.A. Winn, J.M. Shemilt, and B.C.H. Steele, *Mat. Res. Bull.*, **11**, 559 (1976).
13. S. Basu and W.L. Worrell, in "Fast Ion Transport in Solids", P. Vashishta, J.N. Mundy, G,K. Shenoy, Editors, p. 149, Elsevier North Holland, Inc., Amsterdam (1979).

14. S. Basu and W.L. Worrell, "Proceedings of the Symposium on Electrode Materials and Process for Energy Conversion and Storage", J.D.E. McIntyre, S. Srinivasan and F.G. Will, Editors, p. 861, The Electrochemical Society, Princeton, NJ (1977).

15. A.S. Nagelburg and W.L. Worrell, ibid., p. 861 (1977).

16. A.S. Nagelburg and W.L. Worrell, p. 948, The Electrochemical Society Extended Abstracts, Vol 77-1, Philedelphia, Pennsylvannia (1977).

17. M. Ottaviani, S. Panero, S. Morzilli, B. Scrosati, and M Lazzari, *Solid State Ionics*, **20**, 197 (1986).

18. W. Weppner and R.A. Huggins, *Ann. Rev. Mater. Sci.*, **8**, 269 (1978).

19. J. Crank, "The Mathematics of Diffusion", Oxford University Press, London, 1956, Chapt. 2.

20. J.S. Carslow and J.C. Jaeger, "Conduction of Heat in Solids", Oxford University Press, London, 1959, Chapt. 10.

21. R.M. Penner and C.R. Martin, submitted to J. Electrochem. Soc.

22. A.F. Diaz and J.I. Castillo, *J.C.S. Chem. Commun.*, 397 (1980).

23. F.G. Will, *J. Electrochem. Soc.*, **132**, 2093 (1985).

24. J.H. Kaufman, J.W. Kaufer, A.J. Heeger, R. Kaner, and A.G. MacDiarmid, *Phys. Rev. B.* **26**, 2327 (1982).

25. J.H. Kaufman, T. -C. Chung, A.J. Heeger, *Solid State Comm.*, **47**, 585 (1983).

26. J.H. Kaufman, T.-C. Chung, A.J. Heeger, *J. Electrochem. Soc.*, **131**, 2847 (1984).

27. A.F. Diaz, J.I. Castillo, J.A. Logan, and W.-Y. Lee, *J. Electroanal. Chem.*, **129**, 115 (1981).

28. P. Burgemayer and R.W. Murray, *J. Am. Chem. Soc.*, **104**, 6139 (1982).

29. C. Ho, I.D. Raistrick, and R.A. Huggins, *J. Electrochem. Soc.*, 127, 343 (1980).

30. G.B. Street, T.C. Clarke, M. Krounbi, K. Kanazawa, V. Lee, P. Pfluger, J.C. Scott, and G. Wieser, *Mol. Cryst. Liq. Cryst.*, 83, 253 (1982).

31. G.R. Kittlesen, H.S. White, and M.S. Wrighton, *J. Am. Chem. Soc.*, 106, 7389 (1984).

32. B.J. Feldman, P. Burgemayer, and R.W. Murray, J. Am. Chem. Soc., 107, 872 (1985).

33. I. Rubinstein, J. Rishpon, and S. Gottesfeld, *J. Electrochem. Soc.*, 133, 729 (1986).

34. E.M. Genies, G. Bidan, and A.F. Diaz, *J. Electroanal. Chem.*, 149, 101 (1983).

Table I. Measurement of the Electrolyte Concentration in Reduced Polypyrrole Thin Films

Experimental Method	Concentration Leaching Solution[a] (M)	Concentration Film[b] (M)
Unrinsed	$1.68 \times 10^{-4} \pm 8.9 \times 10^{-5}$	22.2 ± 13.1
Dip-rinsed	$4.06 \times 10^{-5} \pm 3.8 \times 10^{-6}$	5.40 ± 0.50
Long-rinsed[c]	$2.15 \times 10^{-5} \pm 6.0 \times 10^{-7}$	2.86 ± 0.08

[a]Leaching solution concentrations determined from the AC conductivity of solution obtained after a ca. 20 h extraction of reduced films.

[b]Film electrolyte concentrations were calculated assuming a film volume of 7.5×10^{-4} cm^3.

[c]Two films only were measured using this procedure.

Table II. Diffusion Coefficients For Polypyrrole Thin Films

Film Thickness μm	$D_{Et_4NBF_4}$ at x=0 $\times 10^{-10}$ cm^2 sec^{-1}	$D_{Et_4NBF_4}$ at x=1 $\times 10^{-10}$ cm^2 sec^{-1}	$D_{Et_4NB_4}$ gradient $\times 10^{-4}$ cm sec^{-1}
0.35[a]	83 ± 3	same	0
0.54[a]	62 ± 3	same	0
0.73[b]	42 ± 5	800 ± 90	2.0 ± 0.5
0.95[b]	3.0 ± 0.4	290 ± 40	2.0 ± 0.5

[a]Diffusion coefficients correspond to the best fit of the experimental ΔE_{oc} relaxation transient to that predicted from Eqs. 4 & 5. The values reported are averages obtained for eight trials; two different films and four current densities each (100 - 400 μA cm^{-2}).

[b]Diffusion coefficients were calculated as above except that a linear gradient of diffusion coefficents is assumed to obtain over the film thickness as described *vida infra*. The values reported are the averages obtained for eight trials as above.

Figure Captions

Figure 1 - ΔEoc vs. $t^{-1/2}$ plots at a series of current pulse amplitudes for a 0.5 μm polypyrrole film in 0.2 M Et_4NBF_4, MeCN.
Einitial = -0.4 V, Current pulse amplitudes are: A - 400 $\mu A\ cm^{-2}$, B - 300 $\mu A\ cm^{-2}$, C - 200 $\mu A\ cm^{-2}$, and D - 100 $\mu A\ cm^{-2}$.

Figure 2 - Polymerization charge vs. film thickness calibration curve for polypyrrole films prepared galvanostatically at ip = 1.0 $mA\ cm^{-2}$ in 0.5 M pyrrole, 0.2 M Et_4NBF_4, MeCN.

Figure 3 - Cyclic voltammogram for a typical 0.27 μm polypyrrole film at 20 $mV\ sec^{-1}$ in 0.2 M Et_4NBF_4, MeCN supporting electrolyte.

Figure 4 - (a) Polarization vs. time transients for a 0.27 μm polypyrrole film at four pulse current densities. $E_{initial}$ = -0.375 V, current pulse amplitudes for these transients were (from top): 1.17 $mA\ cm^{-2}$, 875 $\mu A\ cm^{-2}$, 585 $\mu A\ cm^{-2}$, and 290 $\mu A\ cm^{-2}$.
(b) Plots of dE/dt (closed circles) and iR (open circles) vs. current pulse amplitude for the data shown in figure 4a.

Figure 5 - C_{dl} (closed circles) and R_u (open circles) vs. open circuit potential obtained using the galvanostatic pulse method for 0.27 μm thick polypyrrole films.

Figure 6 - (a) $Q_{injected}$ and Q_{corr} vs. E_{oc} raw calibration curve data for 0.27 μm polypyrrole films in 0.2 M Et_4NBF_4, MeCN. Q_{corr} values were obtained by subtracting the capacitive contributions to the injected charge using capacitance values obtained from the galvanostatic pulse measurements.
(b) E_{oc} vs. C_{ppy+} calibration curve caluculated from the Q_{corr} vs. E_{oc} data in figure 6a.

Figure 7 - Simulated ΔE_{oc} vs. time transients for four diffusion coefficient values calculated for the following experimental parameters: $l = 0.5\ \mu m$, $\tau = 50$ msec, and diffusion coefficient values of: A - 2×10^{-9} cm^2 sec^{-1}, B - 2.5×10^{-9} cm^2 sec^{-1}, C - 3×10^{-9} cm^2 sec^{-1}, and, D - 4×10^{-9} cm^2 sec^{-1}.

Figure 8 - Simulated ΔE_{oc} vs. time transients for four values of the film thickness calculated for the following experimental parameters: t = 50 msec, $D = 1 \times 10^{-9}$ cm^2 sec^{-1}, and film thicknesses of: A - 0.20 μm, B - 0.25 μm, C - 0.30 μm, and D, 0.50 μm.

Figure 9 - Simulated ΔE_{oc} vs. time transients for four gradients of the diffusion coefficient, D_{grad}, calculated for the following experimental parameters: $\tau = 50$ msec, $D_{min} = 1 \times 10\text{-}9$ cm^2 sec^{-1}, $i_p = 100\ \mu A\ cm^{-2}$, and D_{grad} values of: A - 0 (no gradient), B - 2×10^{-5} cm sec^{-1}, C - 6×10^{-5} cm sec^{-1}, and D - 1×10^{-4} cm sec^{-1}.

Figure 10 - Simulated and experimental ΔE_{oc} vs. time transients for a typical 0.5 μm polypyrrole film in 0.2 M Et_4NBF_4, MeCN. $E_{initial} = -0.4$ V, $\tau = 50$ msec. Current pulse densities, i_p and diffusion coefficients for the calculated transients were as follows: (a) - $i_p = 100\ \mu A$ cm-2, $D_{Et4NBF4} = 6.0 \times 10^{-9}$ cm^2 sec^{-1}, (b) - ip = 200 $\mu A\ cm^{-2}$, $D_{Et4NBF4} = 6.0 \times 10^{-9}$ cm^2 sec^{-1}, (c) - ip = 300 $\mu A\ cm^{-2}$, $D_{Et4NBF4} = 6.0 \times 10^{-9}$ cm^2 sec^{-1}, and (d) - ip = 400 $\mu A\ cm^{-2}$, $D_{Et4NBF4} = 6.5 \times 10^{-9}$ cm^2 sec^{-1},

Figure 11 - Calculated and experiment ΔE_{oc} vs. time transients for 0.73 μm and 0.95 μm polypyrrole films. $\tau = 50$ msec, $i_p = 100\ \mu A\ cm^{-2}$. (a) - $l = 0.73\ \mu m$, simulated transients were calculated using the following $D_{Et4NBF4}$ values: A - 4.0×10^{-9} cm^2 sec^{-1},

B - 7.0×10^{-9} cm^2 sec^{-1}, C - $D_{Et_4NBF_4}$ gradient with $D_{min} = 4.2 \times 10^{-9}$ cm^2 sec^{-1} and $D_{grad} = 1.5 \times 10^{-4}$ cm sec^{-1}.

(b) - l = 0.95 μm, simulated transients were calculated using the following $D_{Et_4NBF_4}$ values: A - 5.0×10^{-10} cm^2 sec^{-1}, B - 1.0×10^{-9} cm^2 sec^{-1}, C - $D_{Et_4NBF_4}$ gradient with $D_{min} = 3.0 \times 10^{-10}$ cm^2 sec^{-1} and $D_{grad} = 2.0 \times 10^{-4}$ cm sec^{-1}.

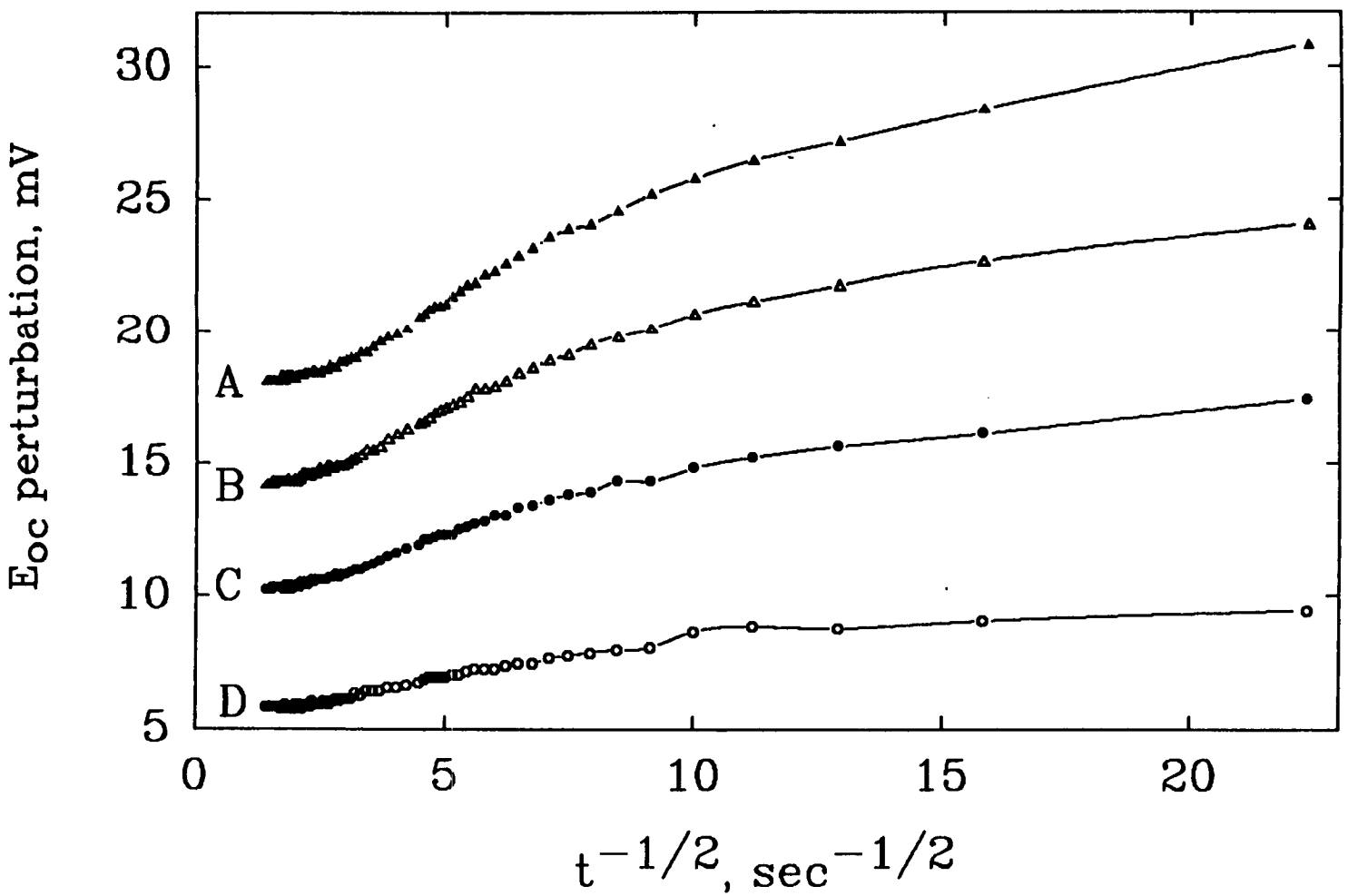

Figure 1

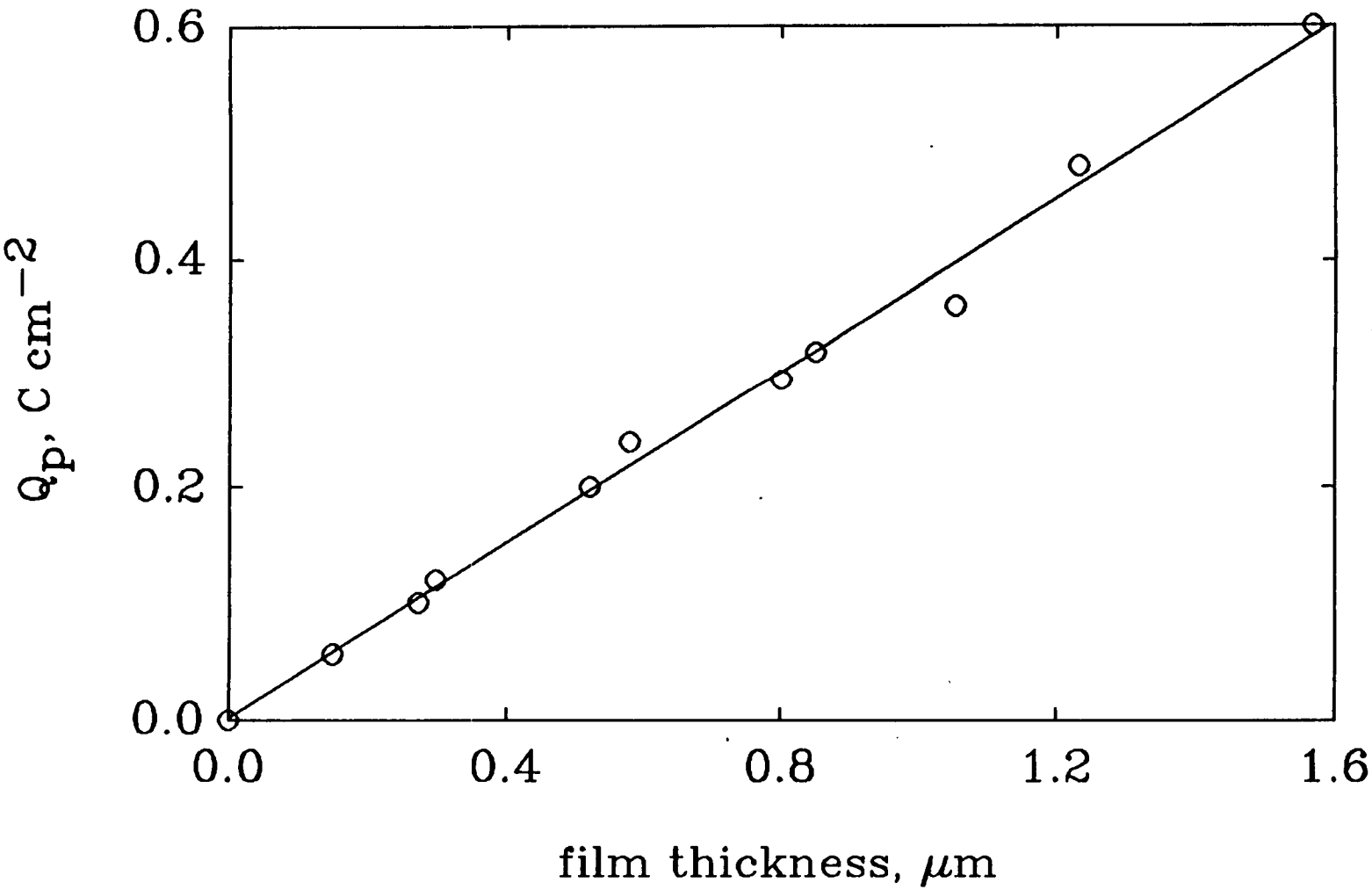

Figure 2

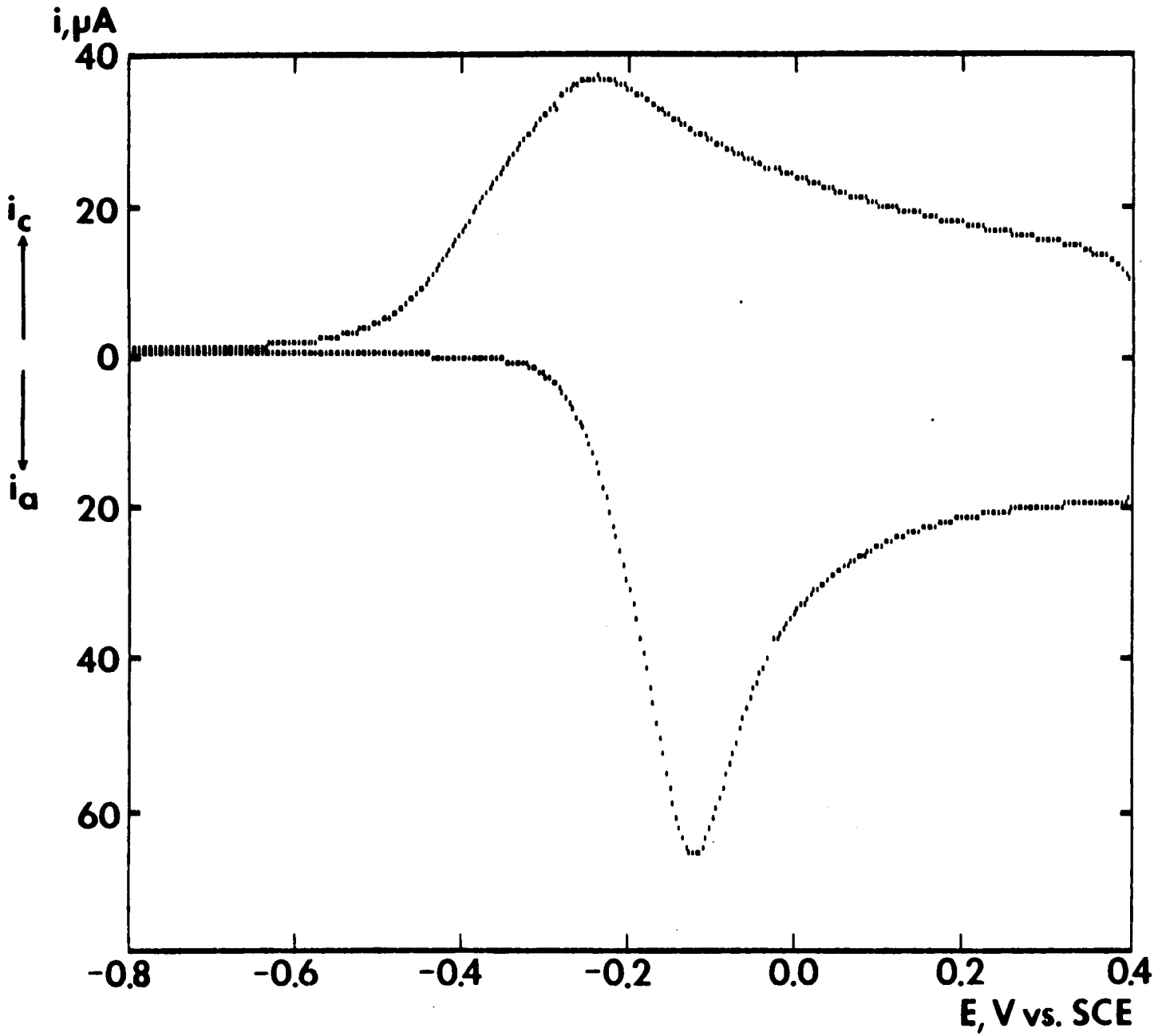

Figure 3

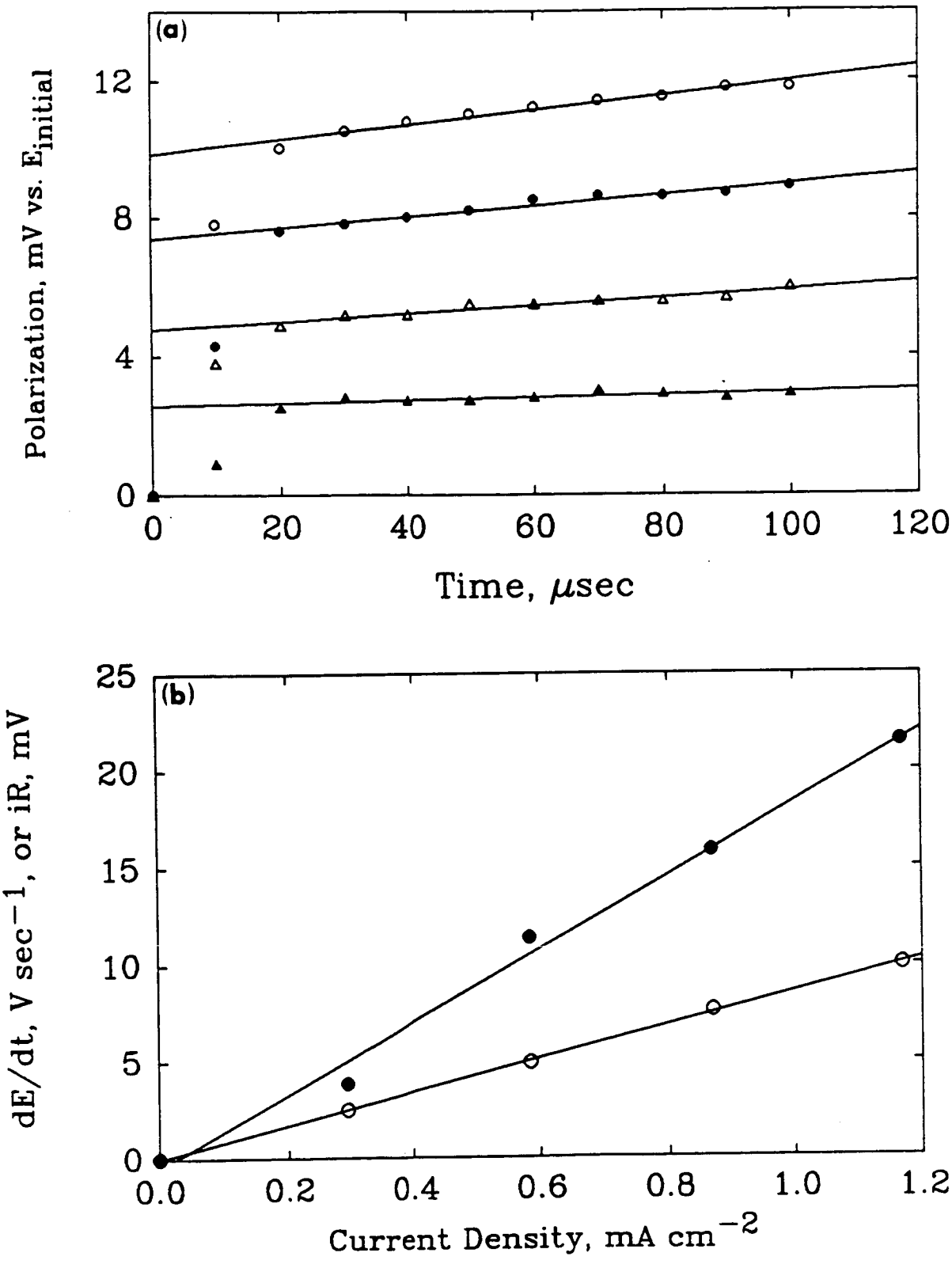
(a)
Polarization, mV vs. $E_{initial}$
12
8
4
0
0
20
40
60
80
100
120
Time, μsec
(b)
dE/dt, V sec^{-1}, or iR, mV
25
20
15
10
5
0
0.0
0.2
0.4
0.6
0.8
1.0
1.2
Current Density, mA cm^{-2}

Figure 4 (a), (b)

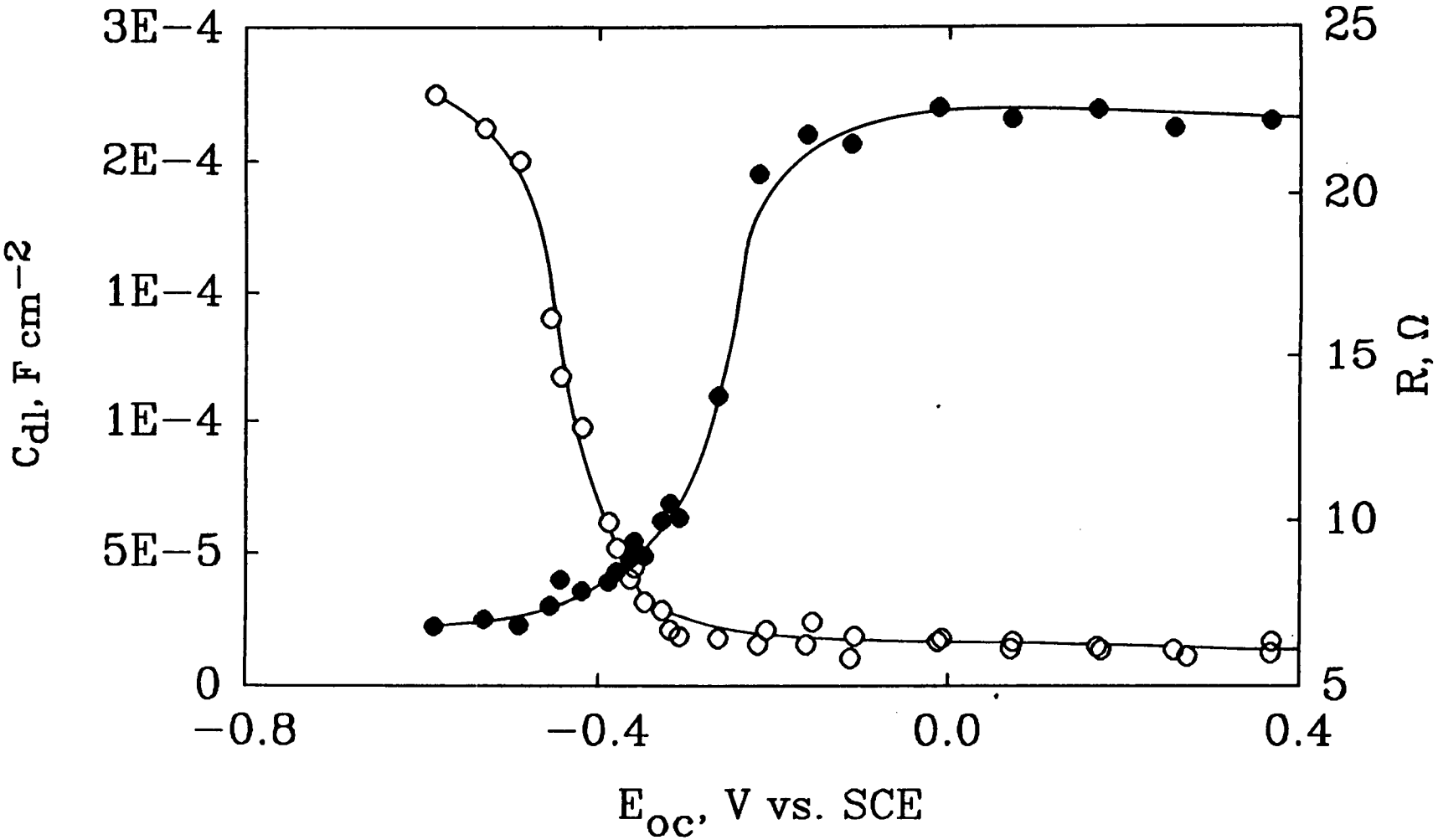
3E−4
2E−4
1E−4
1E−4
5E−5
0
25
20
15
10
5
−0.8
−0.4
0.0
0.4
C_{dl}, F cm^{-2}
R, Ω
E_{oc}, V vs. SCE

Figure 5

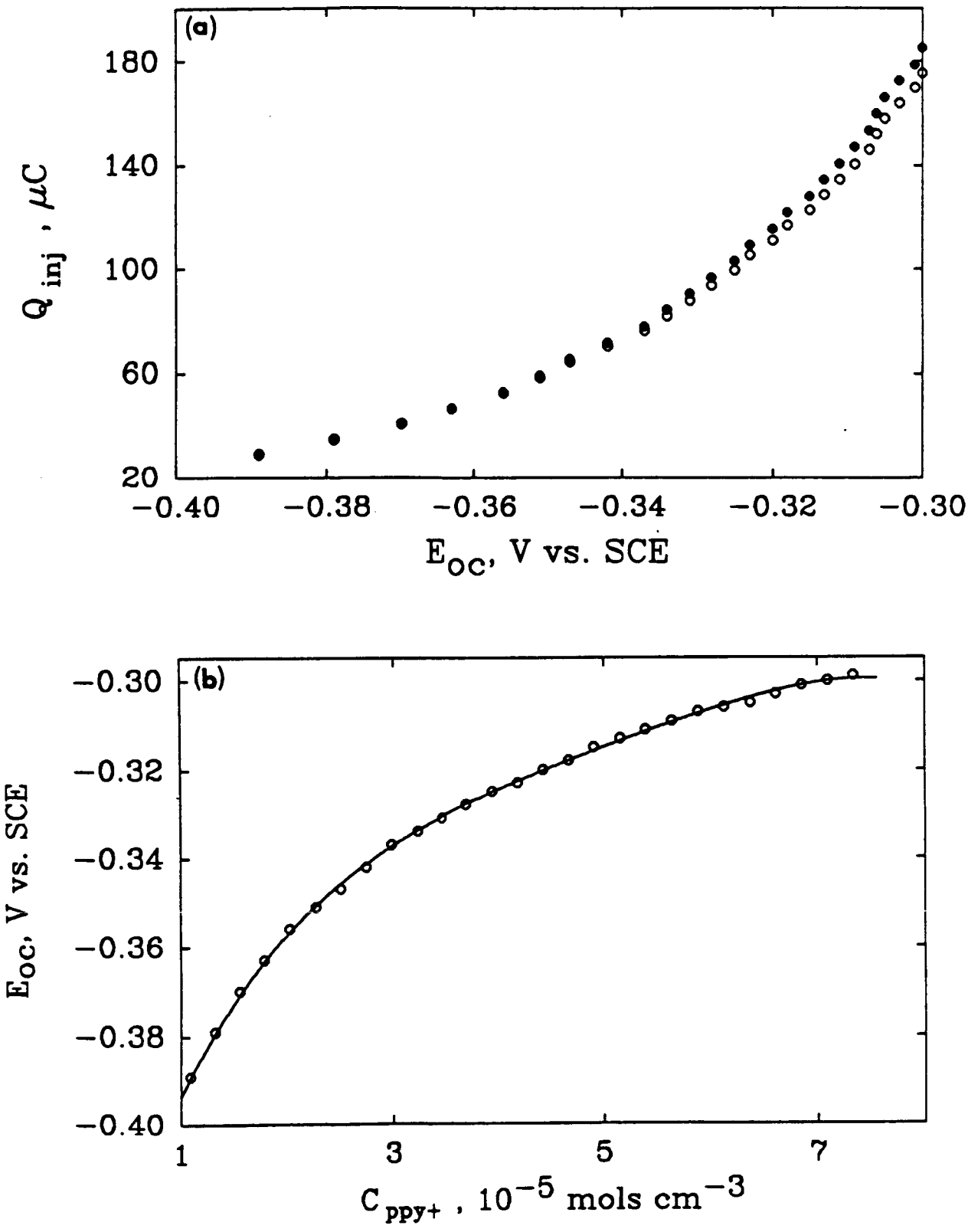
(a)
180
140
100
60
20
Q_{inj} , μC
−0.40
−0.38
−0.36
−0.34
−0.32
−0.30
E_{OC}, V vs. SCE
(b)
−0.30
−0.32
−0.34
−0.36
−0.38
−0.40
E_{OC}, V vs. SCE
1
3
5
7
C_{ppy+} , 10^{-5} mols cm^{-3}

Figure 6 (a), (b)

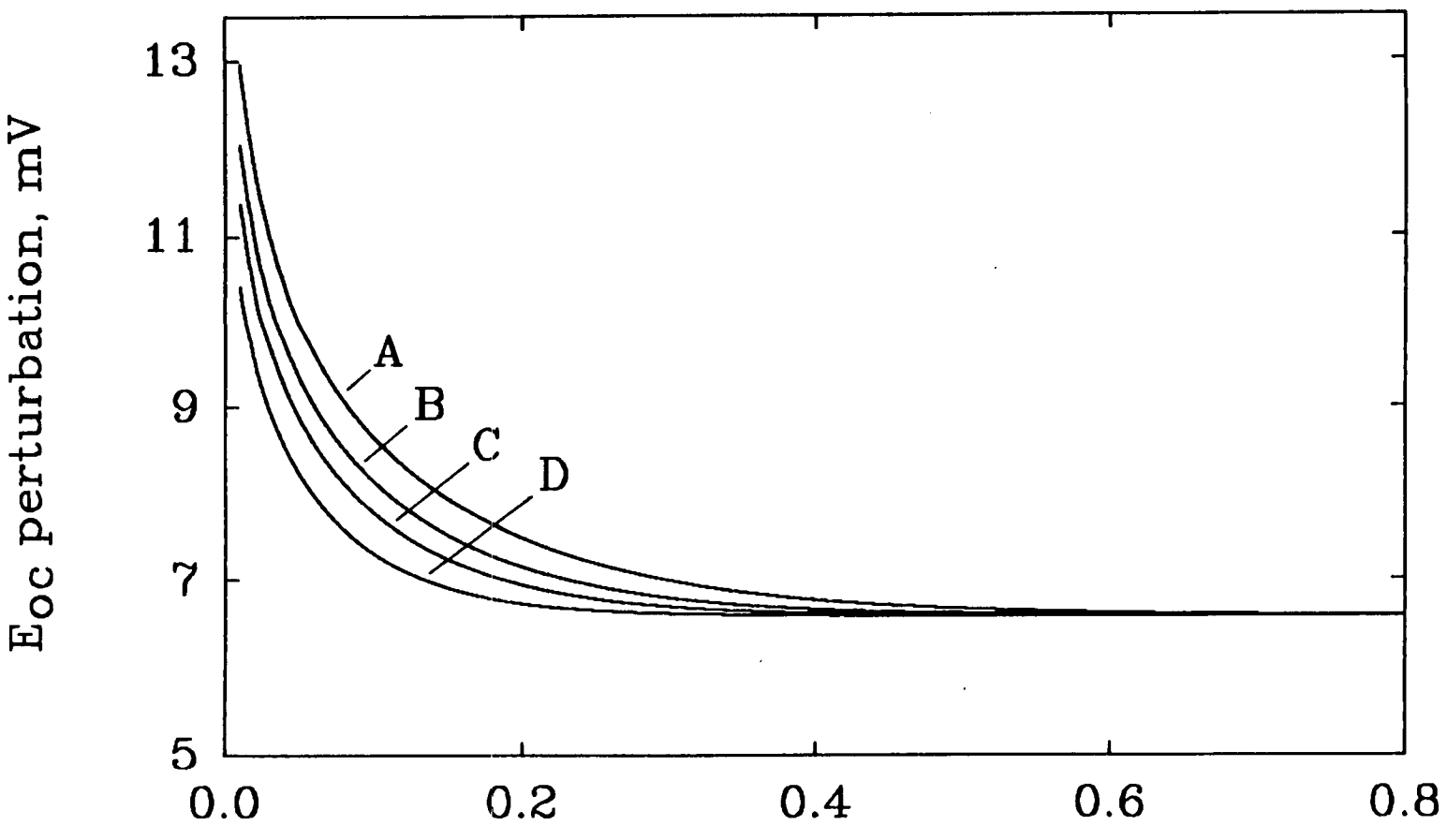

Figure 7

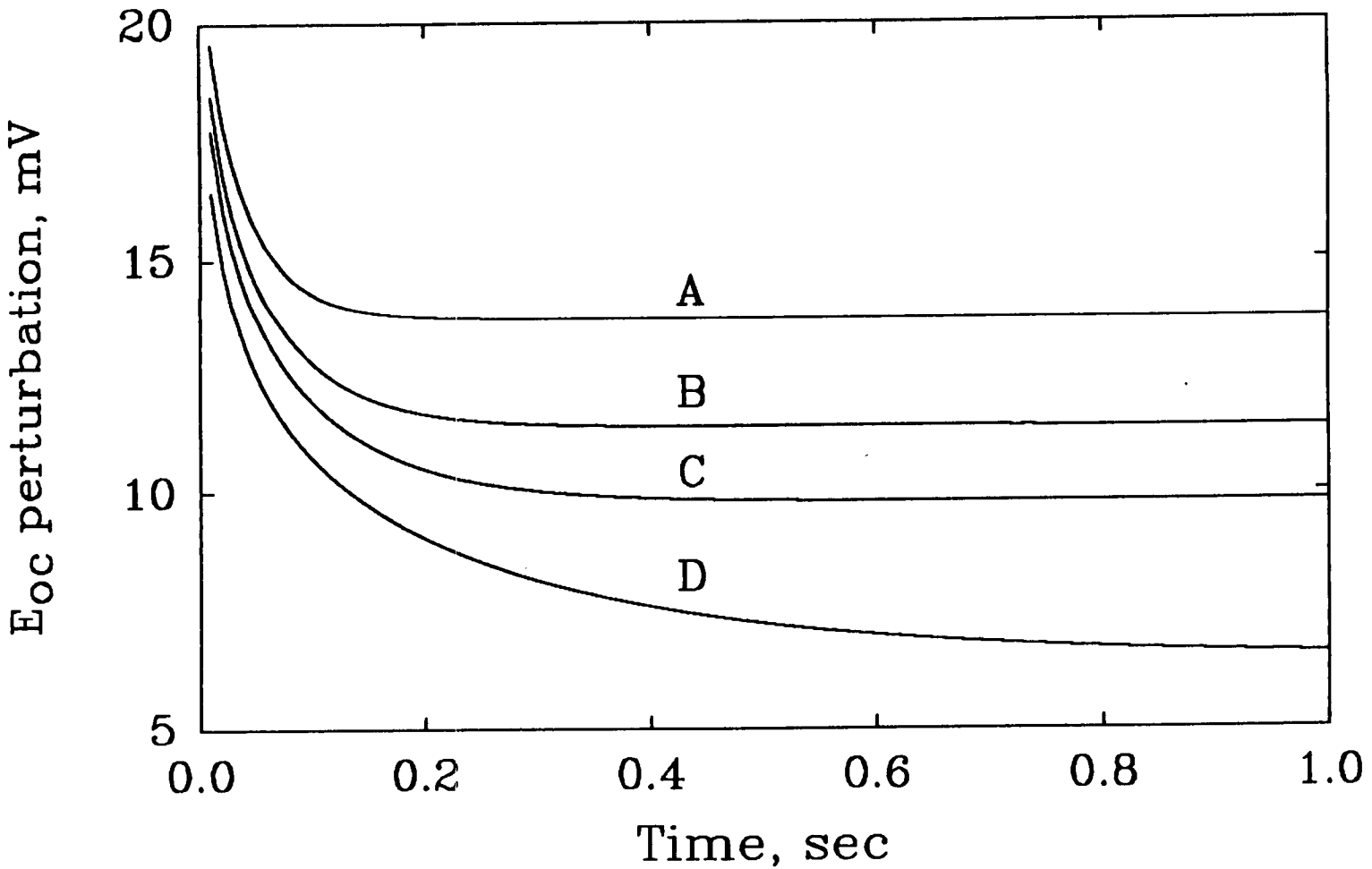

Figure 8

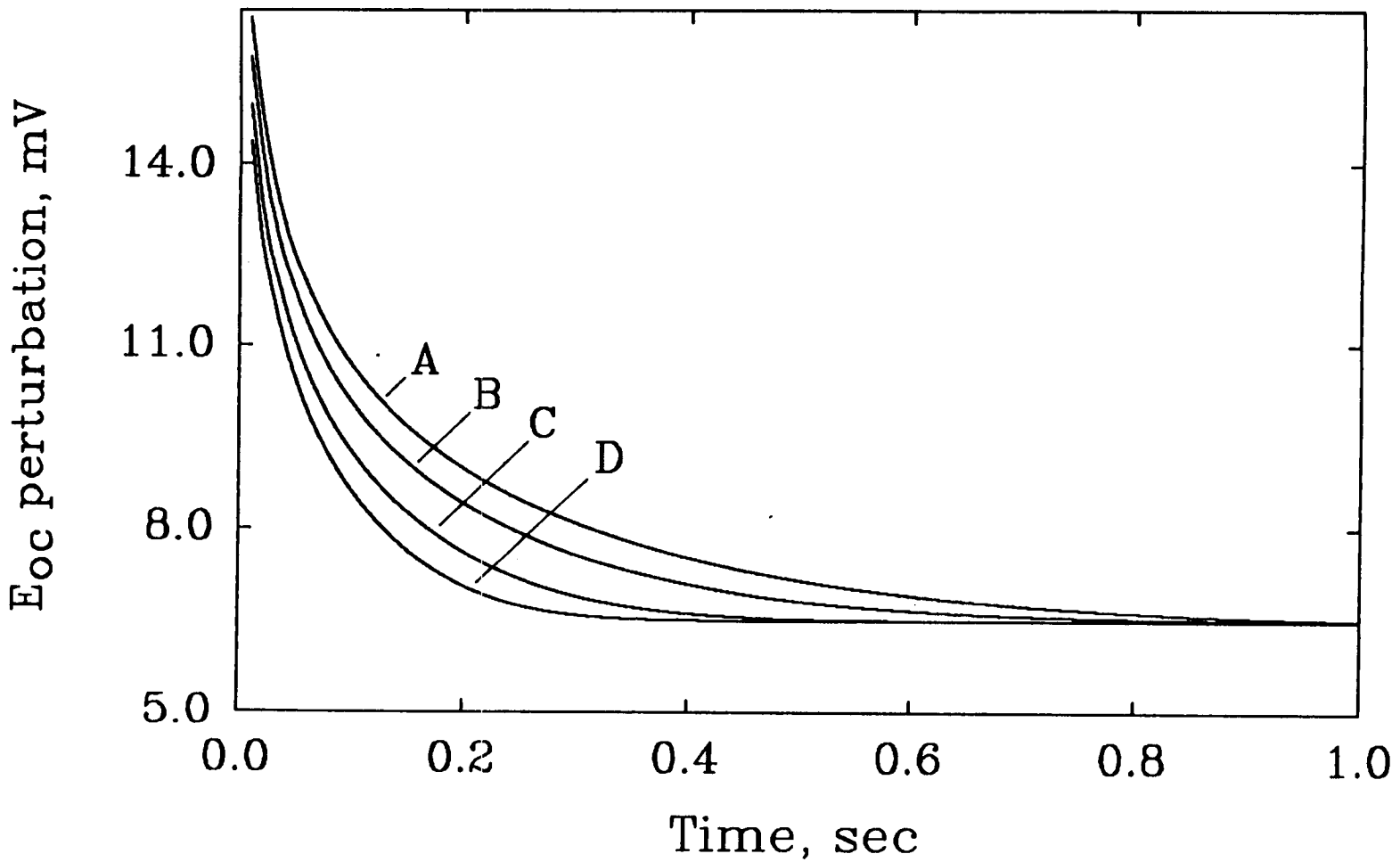
E_{oc} perturbation, mV
14.0
11.0
8.0
5.0
0.0
0.2
0.4
0.6
0.8
1.0
Time, sec
A
B
C
D

Figure 9

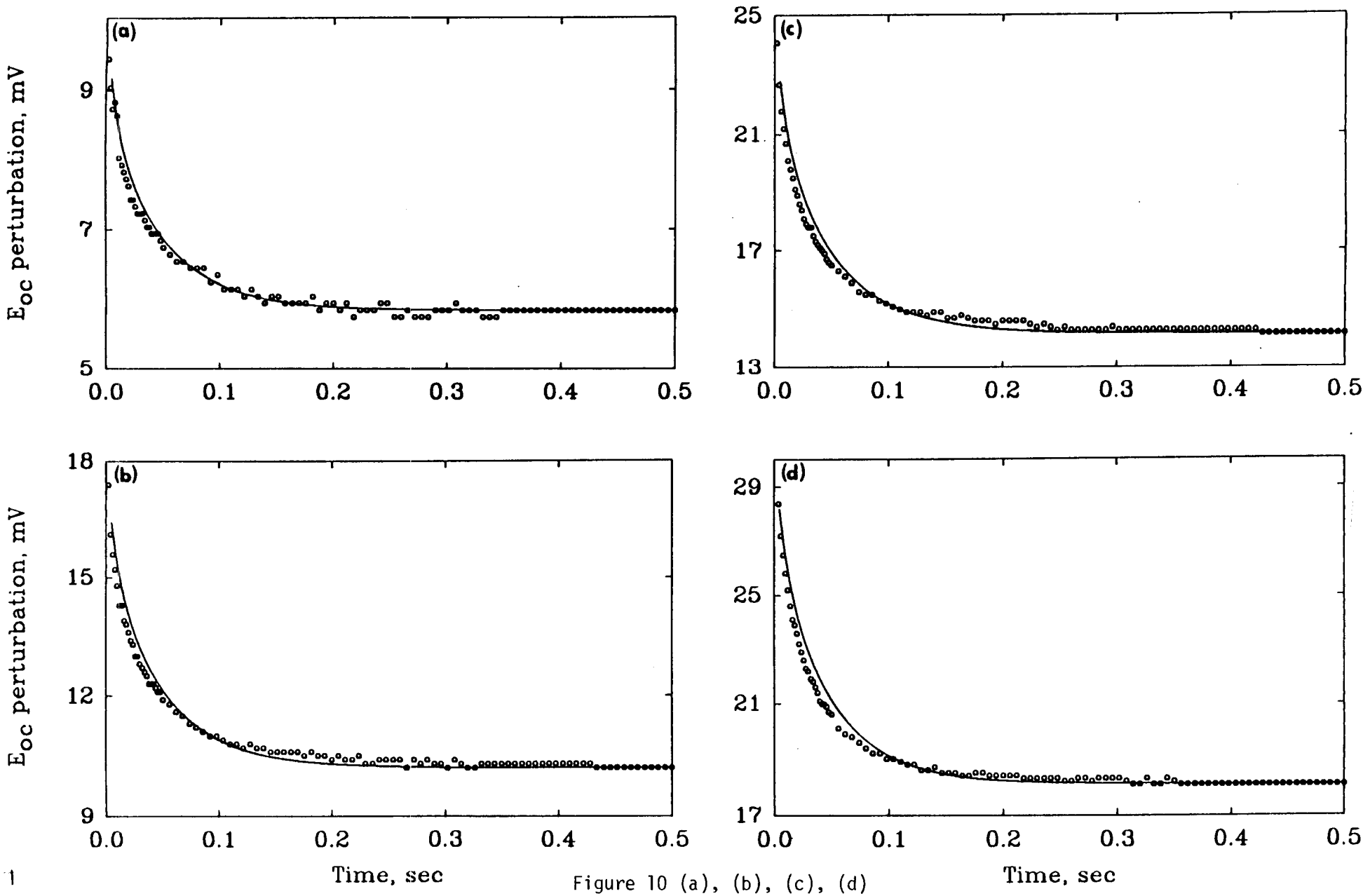

Figure 10 (a), (b), (c), (d)

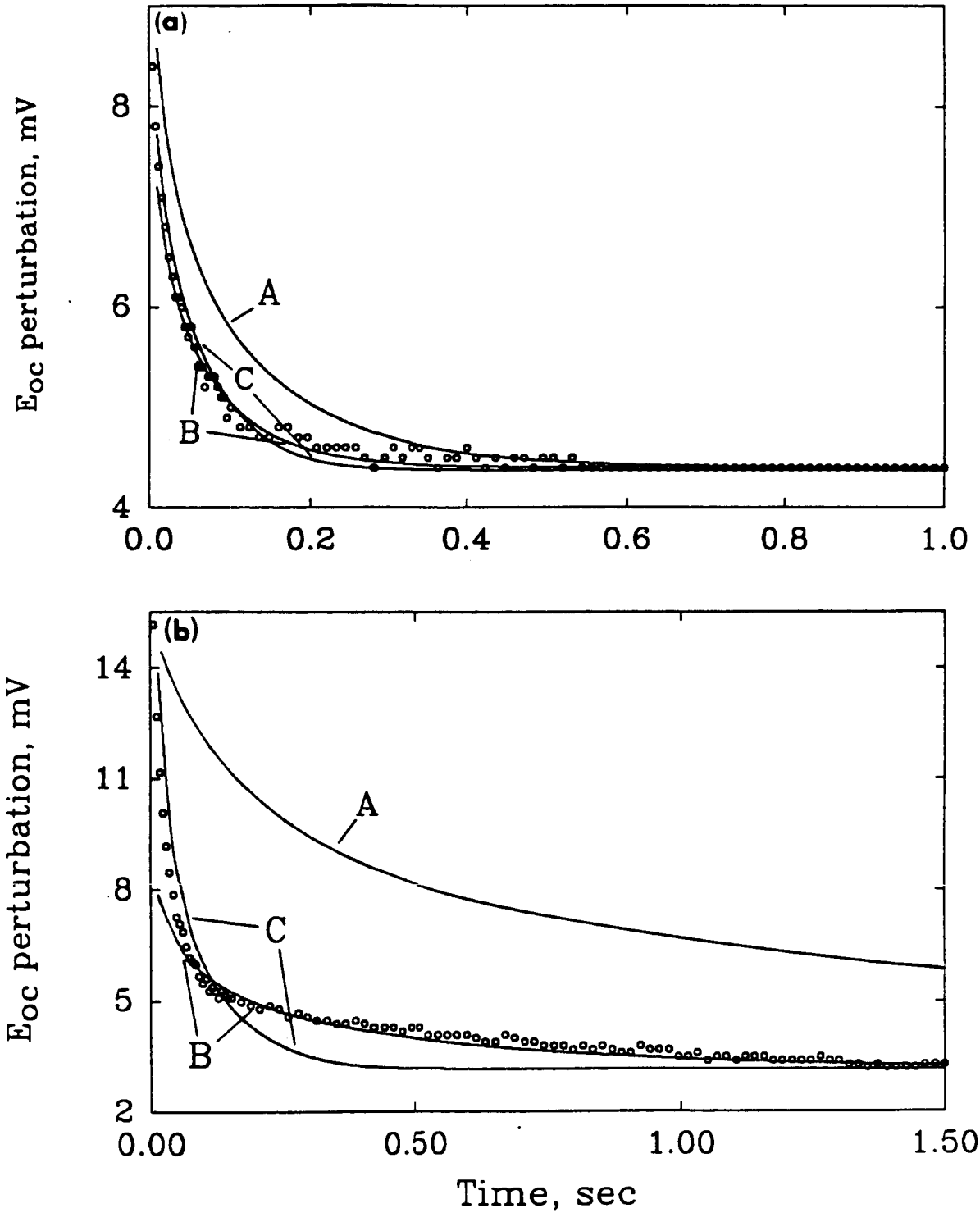
(a)
E_{oc} perturbation, mV
8
6
4
A
C
B
0.0
0.2
0.4
0.6
0.8
1.0
(b)
E_{oc} perturbation, mV
14
11
8
5
2
A
C
B
0.00
0.50
1.00
1.50
Time, sec

Figure 11 (a), (b)

APPENDIX C

A MATHEMATICAL MODEL FOR PREDICTING CYCLIC VOLTAMMOGRAMS OF ELECTRONICALLY CONDUCTIVE POLYPYRROLE

A MATHEMATICAL MODEL FOR PREDICTING CYCLIC VOLTAMMOGRAMS OF ELECTRONICALLY CONDUCTIVE POLYPYRROLE

submitted as a technical paper

to the

Editor

Journal of the Electrochemical Society

10 South Main Street

Pennington, New Jersey 08534-2896

prepared by

Taewhan Yeu*, Trung V. Nguyen*, and Ralph E. White**

Department of Chemical Engineering

Texas A&M University

College Station, Texas 77843-3122

August 1987

Key Words : Rotating Disk Electrode, Porous Electrode, Polymer Film

* Electrochemical Society Student Member

**Electrochemical Society Active Member

Abstract

Polypyrrole is an attractive polymer for use as a high-energy-density secondary battery because of its potential as an inexpensive, lightweight, and noncorrosive electrode material. A mathematical model to simulate cyclic voltammograms for polypyrrole is presented here. The model is for a conductive porous electrode film on a rotating disk electrode (RDE) and is used to predict the spatial and time dependence of concentration, overpotential, and stored charge profiles within a polypyrrole film. The model includes both faradaic and capacitive charge components in the total current density expression.

Introduction

Electrochemically synthesized conducting polypyrrole has received much attention as a secondary battery electrode because it has high conductivity, high specific charge capacity, and stable and reversible electrochemical redox behavior (1-4). Polypyrrole, in its conducting polycationic form (PPy^+), is readily obtained by a simple one-step electrochemical oxidation of the pyrrole monomer. This reaction is electronically irreversible and fairly complex. A detailed discussion of the mechanism of synthesis is beyond the scope of this study.

Electronically conductive polypyrrole has a number of potential technological applications. It is used 1) as a battery electrode, 2) in display devices, 3) in electronic devices, and 4) as a component of new high-energy-density secondary batteries. All of these applications rely on the ability of the polypyrrole to switch between the conductive and nonconductive states. Polypyrrole in its conducting polycationic form can be transformed by cathodic reduction into the neutral insulating state (PPy°) with conductivity less than 10^{-5} $ohm^{-1}cm^{-1}$. This film is extremely unstable and easily

reoxidized to yield PPy^+. In contrast, oxidized polypyrrole film is stable in a wide range of solvents.

An experimental cyclic voltammogram of polypyrrole approximates the behavior of a quasi-reversible couple with the distinct characteristic of a large capacitive background current (5). Some authors (6-8) have tried to analyze the capacitance effect in order to separate the faradaic current from the capacitive current. In spite of this, the capacitance effect is still not fully understood. Feldberg (6) suggested a mathematical model of the capacitive current with the electrochemical switching polymer films, but failed to include transport effects (diffusion and migration) of the counter-ions. Pickup and Osteryoung (7) developed a mathematical model for potential step chronoamperometry and concluded that a polymer film could be modeled as a porous electrode. The porous electrode model they used is not satisfactory because it is based on the assumption that faradaic reactions are negligible.

The model presented here is used to simulate potentiostatic cyclic voltammograms for a polypyrrole film on a RDE. The rotating disk electrode was chosen because of its well-defined hydrodynamics. The model consists of a combination of the models presented by Feldberg (6) for the capacitance effect on the current density and by Ryan *et al.* (9) for a conductive porous layer on a rotating disk electrode. The polypyrrole film is treated as a porous electrode with a high surface-to-volume ratio and a large double layer capacitance, which is proportional to the amount of oxidized polypyrrole film (4-7). These model conditions were chosen so that the simulated predictions could be compared to experimental results available in the literature. The faradaic and capacitive current components associated with the electrochemical switching of a film between the insulating and electronically conducting states are included in the model.

The transport equations of the model are based on the conservation of mass and charged species. The equations include migration of charged species in an electric field,

diffusion of charged and uncharged species, and the electrochemical reaction that occurs within the porous polypyrrole film. Since the surface of a solid electrode is composed of active (oxidized) and inactive (reduced) sites during charge and discharge processes, averaged values are used to describe local variables within a volume element throughout the porous layer to account for the effect of nonhomogeneity of the electrode surface (9).

The model is used to predict concentration, overpotential, and stored charge profiles within the polypyrrole film as a function of position and time. The model is also used to predict the dependence of the faradaic, capacitive, and total current density on applied overpotential.

Model Development

The model presented here is for predicting potentiostatically controlled cyclic voltammograms for a porous polypyrrole film on a RDE in a one-compartment cell. The one-compartment electrochemical cell contains a platinum RDE coated with polypyrrole film, a platinum counter electrode, and a saturated calomel reference electrode (SCE). A schematic diagram of a typical experimental system is shown in Fig. 1. The Luggin capillary tip of the reference electrode is placed as close as possible to the center of the disk. This enables one to use the reference electrode to detect the solution potential near the working electrode. The electrolyte consists of 0.1 M $LiClO_4$ in acetonitrile. In the solution, $LiClO_4$ dissociates into charged Li^+ and ClO_4^-.

During a potential sweep, a polypyrrole film can be cycled repetitively between its oxidized and reduced forms in the absence of oxygen with no evidence of polypyrrole decomposition (4). The reaction occurring during the potential sweep is assumed to

be described as follows:

$$PPy^{\circ} + ClO_4^- \rightleftharpoons PPy^+ClO_4^- + e^- \qquad [1]$$

The rate of this reaction is controlled primarily by the available electroactive area and the transport rate (diffusion and migration) of ClO_4^-.

Figure 2 is a schematic representation of the regions close to the RDE surface that are relevant to the development of the model equations. As shown in Fig. 2, there are two separate regions: the porous electrode region of width δ_{PE} and the solution diffusion region of width δ_{RE}.

The dependent variables in the diffusion layer are: the concentration of Li^+ (c_+), the concentration of ClO_4^- (c_-), and the potential of the solution phase (Φ_2). In the porous polypyrrole region, the dependent variables include the ones in the diffusion layer, the local faradaic charge per unit volume (Q_F), and the potential of the solid polymer phase (Φ_1). Values for these unknowns depend on the perpendicular distance from the electrode surface (y) and time (t), and they are obtained by solving the governing equations with associated boundary conditions.

Assumptions

The assumptions used in developing the governing equations for the model are as follows:

1) no homogeneous reactions occur in the bulk solution.
2) the solution is Newtonian and isothermal.
3) transport occurs only in the axial direction (i.e., y direction).
4) the platinum current collector is solid and inert.
5) the differential capacitance of the platinum is negligible.
6) the differential capacitance of the double layer is proportional to the amount of oxidized polypyrrole.

7) the differential capacitance of polypyrrole is independent of potential.

8) the electrochemical reaction occuring within the porous electrode is a pseudo-homogeneous reaction whose rate is based on the Butler-Volmer equation, as presented below.

Governing Equations – Solution Diffusion Layer

Mass transfer in the diffusion layer is governed by the following material balance equation for species i:

$$\frac{\partial c_i}{\partial t} = -\nabla \cdot \mathbf{N}_i \qquad \text{where} \quad i = +,- \qquad [2]$$

Eq. [2] depends on the flux, $\mathbf{N}_i$, of species i which is due to migration in the electric field, diffusion in the concentration gradient, and convection in the flow field

$$\mathbf{N}_i = -z_i u_i F c_i \nabla \Phi_2 - D_i \nabla c_i + c_i \mathbf{v} \qquad \text{where} \quad i = +,- \qquad [3]$$

The ionic mobility, u_i, is assumed to be described by the Nernst-Einstein equation (10)

$$u_i = \frac{D_i}{RT} \qquad \text{where} \quad i = +,- \qquad [4]$$

Only the axial component of Eq. [3] is considered in the model and the velocity component in that direction depends only on the normal distance from the electrode surface according to the no-slip condition (9)

$$v_y = -a'\Omega\sqrt{\frac{\Omega}{\nu}}(y - y_{PE})^2 \qquad [5]$$

Combining Eq. [2], [3], [4], and [5] yields the governing equation for species i within the solution diffusion layer on the RDE:

$$\frac{\partial c_i}{\partial t} = \frac{z_i D_i F}{RT}\left(c_i \frac{\partial^2 \Phi_2}{\partial y^2} + \frac{\partial c_i}{\partial y}\frac{\partial \Phi_2}{\partial y}\right) + D_i \frac{\partial^2 c_i}{\partial y^2} + a'\Omega\sqrt{\frac{\Omega}{\nu}}(y - y_{PE})^2 \qquad \text{where} \quad i = +,- \qquad [6]$$

The electroneutrality condition provides the additional governing equation needed to solve for Φ_2 within the diffusion layer

$$\sum_i z_i c_i = z_+ c_+ + z_- c_- = 0 \qquad [7]$$

Governing Equations – Porous Electrode Layer

To account for the nonhomogeneous structure of the polymer film, macroscopic properties are used to describe the porous electrode layer in terms of measurable parameters without regard for the actual geometric detail of the pore structure. Two of these properties are the porosity (ϵ) and the MacMullin number ($N_{M,PE}$). The porosity represents the void volume occupied by the electrolyte per unit volume of porous region. The MacMullin number (11) is defined as the ratio of the tortuosity to the porosity:

$$N_{M,PE} = \tau/\epsilon \qquad [8]$$

The porosity and MacMullin number are assumed to be constant.

Within the porous electrode layer, the material balance equation is formulated in terms of average quantities that include the reaction rate term for the electrochemical reaction

$$\frac{\partial \epsilon c_i}{\partial t} = -\nabla \cdot \mathbf{N}_i + R'_i \qquad \text{where} \quad i = +, - \qquad [9]$$

and R'_i is the production rate of species i due to a pseudo-homogeneous reaction (electrochemical reaction) within the porous electrode.

The flux expression, Eq. [3], is modified to account for the porous and tortuous structure of the polypyrrole film. This is accomplished by replacing the diffusion coefficient in Eq. [3] by an effective diffusion coefficient within the porous layer

$$D_{i,e} = \frac{D_i}{N_{M,PE}} \qquad \text{where} \quad i = +, - \qquad [10]$$

Thus, the flux of species i within the solution phase of the porous layer becomes

$$\mathbf{N}_i = -\frac{z_i D_i F}{N_{M,PE} RT} c_i \nabla \Phi_2 - \frac{D_i}{N_{M,PE}} \nabla c_i \qquad \text{where} \quad i = +, - \qquad [11]$$

and where it has been assumed that there is no convective flow within the porous layer. Combining Eq. [11] with the material balance expression, Eq. [9], subject to the

assumptions mentioned above, yields the governing equation for species i within the porous electrode layer:

$$\frac{\partial \epsilon c_i}{\partial t} = \frac{z_i D_i F}{N_{M,PE} RT}\left(c_i \frac{\partial^2 \Phi_2}{\partial y^2} + \frac{\partial c_i}{\partial y}\frac{\partial \Phi_2}{\partial y}\right) + \frac{D_i}{N_{M,PE}}\frac{\partial^2 c_i}{\partial y^2} + R_i' \qquad \text{where} \quad i = +,- \quad [12]$$

The production rate of species i due to an electrochemical reaction is given by (12):

$$R_i' = -\frac{s_i}{nF} j_F \qquad \text{where} \quad i = +,- \quad [13]$$

and j_F is the faradaic transfer current per unit volume (A/cm^3) of the porous region and is disscussed later.

It is a consequence of the assumption of electroneutrality that the charge which leaves the solid phase must enter the solution phase. This is expressed as (12)

$$\nabla \cdot i_1 + \nabla \cdot i_2 = 0 \quad [14]$$

where i_1 is the superficial current density (current per projected area of the electrode) in the solid electrode phase, and i_2 is the superficial current density in the solution phase. In the solid phase, the movement of electrons is governed by Ohm's law

$$i_1 = -\sigma(1-\epsilon)\frac{\partial \Phi_1}{\partial y} \quad [15]$$

where σ is the conductivity of polypyrrole, and $\sigma(1-\epsilon)$ is equivalent to the effective solid conductivity. It is assumed that the conductivity of polypyrrole is proportional to the degree of the oxidation of polypyrrole as follows:

$$\sigma = \frac{\sigma_{MIN} - \sigma_{MAX}}{Q_{F,MIN} - Q_{F,MAX}}\left(Q_F - Q_{F,MAX}\right) + \sigma_{MAX} \quad [16]$$

where σ_{MIN} represents the conductivity of the polypyrrole film at minimal charge state ($Q_{F,MIN}$), and σ_{MAX} represents the conductivity of the film at its maximal charge state ($Q_{F,MAX}$). The current density in the solution phase is given by

$$i_2 = -\frac{\kappa}{N_{M,PE}}\frac{\partial \Phi_2}{\partial y} \quad [17]$$

where κ is the specific conductivity of electrolyte and is assumed to be constant. The term $\kappa/N_{M,PE}$ is the effective solution conductivity. Substitution of Eq. [15] and [17] into the conservation of charge equation, Eq. [14], yields

$$\nabla \cdot \left(-\sigma(1-\epsilon)\frac{\partial \Phi_1}{\partial y}\right) + \nabla \cdot \left(-\frac{\kappa}{N_{M,PE}}\frac{\partial \Phi_2}{\partial y}\right) = 0 \qquad [18]$$

Electroneutrality, Eq. [7], is also used as the governing equation for Φ_2 in the porous region.

The rate of accumulation of the faradaic charge contained in the oxidized polypyrrole per unit volume, Q_F, is assumed to be related to the faradaic transfer current, j_F, as follows:

$$\frac{\partial Q_F}{\partial t} = j_F \qquad [19]$$

Current Density

The faradaic transfer current per unit volume, j_F, is assumed to be given by the Butler-Volmer equation (13):

$$j_F = a i_{O,REF}\left\{\left(\frac{Q_{F,MAX} - Q_F}{Q_{F,MAX}}\right)\left(\frac{c_-}{c_{-,REF}}\right)\exp\left(\frac{\alpha_a F}{RT}\eta\right) - \left(\frac{Q_F}{Q_{F,MAX}}\right)\exp\left(\frac{-\alpha_c F}{RT}\eta\right)\right\} \qquad [20]$$

where a is the electroactive surface area per unit volume, $i_{O,REF}$ is the exchange current density at a given reference concentration ($c_{i,REF}$), and η is the overpotential. The overpotential is defined as:

$$\eta = (\Phi_1 - \Phi_{RE}) - (\Phi_2 - \Phi_{RE}) - U_{REF} \qquad [21]$$

where Φ_{RE} is the solution potential at the Luggin tip, and U_{REF} is the open circuit potential at a given reference concentration ($c_{i,REF}$) and is relative to SCE. Anodic and cathodic current densities are taken to be positive and negative, respectively. Note

also that $\alpha_a + \alpha_c = n$. It can be seen that the local transfer current predicted by the Butler-Volmer kinetic expression, Eq. [20], depends upon the difference between the potential of the solid phase and that of the adjacent solution within the porous electrode.

The anodic faradaic current in the porous polymer film leads to charging of the double layer within the pores of the polymer film in a manner consistent with that proposed by Feldberg (6). That is, the amount of capacitive charge that goes to charging the double layers within the pores of the porous film, Q_C, is related to the amount of the faradaic charge added to the polymer film by the faradaic reaction:

$$Q_C = a^*(\eta - \eta_{PZC})Q_F \qquad [22]$$

where a^* is a proportional constant which is assumed to be independent of potential, and η_{PZC} is the total overpotential across the double layer at the point of zero charge (PZC) which is given by

$$\eta_{PZC} = \left\{(\Phi_1 - \Phi_{RE}) - (\Phi_2 - \Phi_{RE}) - U_{REF}\right\}_{PZC} \qquad [23]$$

The capacitive transfer current per unit volume, j_C, associated with charging of the double layer is defined as follows:

$$j_C = \frac{\partial Q_C}{\partial t} \qquad [24]$$

Substituting Eq. [19] and [22] into Eq. [24] shows that

$$j_C = a^*\left(Q_F \frac{\partial \eta}{\partial t} + (\eta - \eta_{PZC})j_F\right) \qquad [25]$$

with the assumption that $\Phi_{RE} = (\Phi_{RE})_{PZC}$. The total transfer current per unit volume, j_T, is defined as the sum of the faradaic and capacitive transfer currents per unit volume:

$$j_T = j_F + j_C \qquad [26]$$

Eq. [26] can be used to predict the total current density, i_T (current per projected area), by integrating j_T over the porous layer:

$$i_T = \int_{y=0}^{y=y_{PE}} j_T dy \qquad [27]$$

Note that the faradaic current density, i_F, and the capacitive current density, i_C, can be obtained in a similar manner from j_F and j_C, respectively.

Boundary Conditions

The boundary conditions at the polymer film/substrate interface ($y = 0$) are

$$-\frac{z_i D_i F}{RT} c_i \frac{\partial \Phi_2}{\partial y} - D_i \frac{\partial c_i}{\partial y} = 0 \qquad \text{where} \quad i = +, - \qquad [28]$$

$$\Phi_1 = E_{APP} + \Phi_{RE} \qquad [29]$$

$$\sum_i z_i c_i = z_+ c_+ + z_- c_- = 0 \qquad [30]$$

where E_{APP} and Φ_{RE} are constants. The boundary conditions at the polymer film/diffusion layer interface ($y = y_{PE}$) are

$$\mathbf{N}_{i,y}|_{\text{porous layer}} = \mathbf{N}_{i,y}|_{\text{diffusion layer}} \qquad \text{where} \quad i = +, - \qquad [31]$$

$$\frac{\partial \Phi_1}{\partial y} = 0 \qquad [32]$$

$$\sum_i z_i c_i = z_+ c_+ + z_- c_- = 0 \qquad [33]$$

The boundary conditions in the bulk solution ($y = y_{RE}$) are

$$c_i = c_{i,REF} \qquad \text{where} \quad i = +, - \qquad [34]$$

$$\Phi_2 = \Phi_{RE} \qquad [35]$$

Initial Conditions

The initial concentration of each species i is set equal to its bulk concentration:

$$c_i = c_{i,REF} \qquad \text{where} \quad i = +, - \qquad [36]$$

For convenience, it is assumed that the polypyrrole film is initially fully reduced and is ready to be oxidized. Consequently, the faradaic charge per unit volume in the porous region is initially equal to $Q_{F,MIN}$, a minimal charge state:

$$Q_F = Q_{F,MIN} \qquad [37]$$

Solution Method

The governing equations and boundary conditions can be written in finite difference form and solved by using Newman's pentadiagonal block matrix equation solver (14). Implicit stepping can be used for the time derivatives (15). In the diffusion layer, Q_F and Φ_2 are dummy variables treated as constants and are set arbitrarily equal to zero. During the potential sweep, the applied potential (E_{APP}), which is the difference between Φ_1 at y=0 and Φ_2 at y=y_{RE} (Φ_{RE}=0), is changed linearly between E_{INI} and E_{FIN} according to a specified scan rate (v_S).

Results and Discussion

Cyclic voltammograms of polypyrrole can be predicted using the model described above. The values used for the fixed parameter are given in Table I. Figure 3 shows predicted cyclic voltammograms for the polypyrrole film at various scan rates. Comparison of these predictions with those obtained experimentally for a similar system, as shown in Fig. 4, shows qualitative agreement.

Figure 5 shows the total current density and its components at a 100 mV/sec scan rate. Note that when the maximal quantity of oxidized polypyrrole is formed, no further oxidation of the film occurs and the current is entirely dominated by capacitive charge.

Figure 6 shows the dynamic profile of the concentration of ClO_4^- in the porous electrode region at an 100 mV/sec scan rate. For convenience, the concentration of ClO_4^- was made dimensionless relative to its reference concentrations ($c_{-,\mathrm{REF}}$). The position coordinate was made dimensionless by using the thickness of the film (δ_{PE}) so that $\xi = 1$ represents the interface between the diffusion layer and the polymer film. Time was made dimensionless by using the time required to scan the applied potential from E_{INI} to E_{FIN} (τ°) so that $\zeta = 1$ represents the intermediate point where the polypyrrole film is totally oxidized.

During the oxidation process, the reacting species (ClO_4^-) is transported from the bulk to the porous electrode layer where it diffuses and migrates to reactive sites within the porous layer. During reduction, the opposite is true. Since the effective diffusivities of Li^+ and ClO_4^- within the porous layer are smaller than the free stream diffusivity of these species, then concentration gradients within the porous region must be larger to make up for the slower movement of the ions. The concentration profiles of both species are the same because of the electroneutrality condition.

Figure 7 shows the faradaic charge per unit volume due to the electrochemical reaction within the film at a sweep rate of 100 mV/sec. The faradaic charge per unit volume was made dimensionless by using the maximum faradaic charge value ($Q_{\mathrm{F,MAX}}$) as the reference point. The rate of charge accumulation is faster in the outer layer of the film during oxidation because of diffusion and migration effects. Note that charge accumulates rapidly throughout the entire film.

Summary

Theoretical calculations were carried out that describe quantitatively the current responses of the quasi-reversible behavior of electronically conductive polypyrrole. Porous electrode theory was applied to the conductive polymer to provide the basis for understanding the transport behavior of the switching process within the polymer film. The effects of diffusion and migration were included because it is likely that counter-ion movement limits the oxidation and reduction rates. The net cyclic voltammetric current was decomposed into two components: a capacitive current due to the double layer charging and the faradaic current due to an electrochemical reaction. It may be possible to use this model together with experimental data and parameter estimation techniques to determine the transport and kinetic parameters of the model.

Acknowledgement

It is acknowledged gratefully that this work was supported by a National Aeronautics and Space Administration Grant (NAG-9-173). The authors wish to thank S. W. Feldberg, C. R. Martin, R. M. Penner, C. W. Walton, and J. L. Carbajal for their valuable, stimulating discussions.

NOTATION

a	specific surface area of the porous material, cm^{-1}
a'	0.51023
a^*	double layer constant, V^{-1}
c_+	concentration of Li^+, mol/cm^3
c_-	concentration of ClO_4^-, mol/cm^3
c_i	concentration of species i, mol/cm^3
c_i^*	dimensionless concentration of species i, $(c_i/c_{i,REF})$
$c_{i,REF}$	initial concentration of species i in the porous region, mol/cm^3
D_i	diffusion coefficient of species i, cm^2/sec
$D_{i,e}$	effective diffusion coefficient of species i in a porous layer, cm^2/sec
E_{APP}	applied potential (potential difference between the current collector and Φ_{RE}), V
E_{FIN}	final applied potential, V
E_{INI}	initial applied potential, V
F	Faraday's constant, 96487 C/mol
i_C	capacitive current density, A/cm^2
i_F	faradaic current density, A/cm^2
$i_{O,REF}$	exchange current density at reference concentrations, A/cm^2
i_T	total current density, A/cm^2
i_1	superficial current density in the porous electrode phase, A/cm^2
i_2	superficial current density in the solution phase, A/cm^2
j_C	capacitive transfer current per unit volume, A/cm^3
j_F	faradaic transfer current per unit volume, A/cm^3
j_T	total transfer current per unit volume, A/cm^3

NOTATION (Continued)

n	number of electrons transferred
$\mathbf{N}_i$	flux vector of species i, mol/cm^2-sec
$\mathbf{N}_{i,y}$	y component of flux vector of species i, mol/cm^2-sec
$N_{M,PE}$	MacMullin number for the porous electrode layer
Q_C	capacitive charge of double layer per unit volume, C/cm^3
Q_F	faradaic charge of polymer film per unit volume, C/cm^3
Q_F^*	dimensionless faradaic charge of polymer film, $(Q_F/Q_{F,MAX})$
$Q_{F,MAX}$	maximum faradaic charge of polymer film per unit volume, C/cm^3
$Q_{F,MIN}$	minimum faradaic charge of polymer film per unit volume, C/cm^3
R	universal gas constant, 8.3143 J/mol-K
R_i'	pseudohomogenous reaction rate of species i, mol/cm^3-sec
s_i	stoichiometric coefficient of species i
t	time, sec
T	absolute temperature, K
u_i	mobility of species i, mol-cm^2/J-sec
U_{REF}	theoretical open-circuit potential at reference concentration, V
v	electrolyte velocity vector, cm/sec
v_s	scan rate, V/sec
v_y	electrolyte velocity in the normal direction, cm/sec
y	perpendicular distance from a porous electrode/substrate interface, cm
y_{PE}	position of a porous region/diffusion layer interface in y coordinate, cm
y_{RE}	position of a bulk solution in y coordinate, cm
z_i	proton charge number of species i

NOTATION (Continued)

Greek Symbols

α_a	anodic transfer coefficient
α_c	cathodic transfer coefficient
δ_{PE}	thickness of polypyrrole film, cm
δ_{RE}	thickness of diffusion layer, cm
ϵ	porosity or void volume fraction
ζ	dimensionless time, (t/τ°)
η	overpotential, V
η_{PZC}	overpotential at point of zero charge, V
κ	solution conductivity, $\Omega^{-1}\text{cm}^{-1}$
ν	kinematic viscosity, cm^2/sec
ξ	dimensionless distance, $(1 - y/\delta_{PE})$
ρ_o	pure solvent density, kg/cm^3
σ	conductivity of polypyrrole film, $\Omega^{-1}\text{cm}^{-1}$
σ_{MAX}	conductivity of totally oxidized polypyrrole film, $\Omega^{-1}\text{cm}^{-1}$
σ_{MIN}	conductivity of totally reduced polypyrrole film, $\Omega^{-1}\text{cm}^{-1}$
τ	tortuosity of porous material
τ°	time required to scan the potential from E_{INI} to E_{FIN}, sec
Φ_1	potential in solid phase, V
Φ_2	potential in solution phase, V
Φ_{RE}	potential in the solution at $y = y_{RE}$, V
Ω	disk rotation velocity, rad/sec

REFERENCES

1. A. F. Diaz, K. K. Kanazawa, and G. P. Gardini, *J. Chem. Soc., Chem. Commun.*, 635 (1979).
2. K. K. Kanazawa, A. F. Diaz, W. D. Gill, P. M. Grant, G. B. Street, G. P. Gardini, and J. F. Kwak., *Synth. Met.*, **1**, 329 (1979/1980).
3. A. F. Diaz, *Chem. Scr.*, **17**, 145 (1981).
4. A. F. Diaz, J. I. Castillo, J. A. Logan, and W. Y. Lee, *J. Electroanal. Chem.*, **129**, 115 (1981).
5. R. A. Bull, F. F. Fan, and A. J. Bard, *J. Electrochem. Soc.*, **129**, 1009 (1982).
6. S. W. Feldberg, *J. Am. Chem. Soc.*, **106**, 4671 (1984).
7. P. G. Pickup and R. A. Osteryoung, *J. Electroanal. Chem.*, **195**, 271 (1985).
8. J. Tanguy, N. Mermilliod, and M. Hoclet, *J. Electrochem. Soc.*, **134**, 795 (1987).
9. W. E. Ryan, R. E. White, and S. L. Kelly, *J. Electrochem. Soc.*, **134**, 2154 (1987).
10. J. S. Newman, "Electrochemical Systems," Prentice-Hall, Englewood Cliffs, NJ (1973).
11. J. V. Zee, R. E. White, and A. T. Watson, *J. Electrochem. Soc.*, **133**, 501 (1986).
12. J. Newman and W. Tiedemann, *AIChE J.*, **21**, 25 (1975).
13. T. V. Nguyen, Ph. D. Dissertation, Texas A&M University, College Station, TX (1988).
14. J. V. Zee, G. Kleine, R. E. White, and J. S. Newman, in "Electrochemical Cell Design," R. E. White, Ed., pp 377-389, Plenum Press, New York (1984).
15. B. Carnahan, H. A. Luther, and J. O. Wilkes, "Applied Numerical Methods," John Wiley & Sons, New York (1969).
16. A. J. Bard and L. R. Faulkner, "Electrochemical Methods, Fundamentals and Applications," John Wiley & Sons, New York (1980).
17. J. M. Sullivan, D. C. Hanson, and K. Keller, *J. Electrochem. Soc.*, **117**, 779 (1970).

Table I. Fixed parameter values used for cyclic voltammograms.

Operating Variables	T	298.15 K
	Ω	377 rad/sec
	y_{RE}	0.01 cm [a]
	Φ_{RE}	0.0 V
	E_{INI}	-0.8 V (vs. SCE) [b]
	E_{FIN}	0.4 V (vs. SCE) [b]
Electrolyte Properties	D_+	1.03×10^{-5} cm^2/sec [c]
	D_-	1.81×10^{-5} cm^2/sec [c]
	$c_{+,\mathrm{REF}}$	1.547×10^{-4} mol/cm^3 [c]
	$c_{-,\mathrm{REF}}$	1.547×10^{-4} mol/cm^3 [c]
	κ	0.0165 Ω^{-1}cm^{-1} [c]
	ν	6.6×10^{-3} cm^2/sec [d]
	ρ	0.777×10^{-3} kg/cm^3 [d]
Electrode Properties	δ_{PE}	20 nm
	ϵ	0.1
	$N_{\mathrm{M,PE}}$	1.0×10^6
	$Q_{\mathrm{F,MAX}}$	344.65 C/cm^3 [b]
	$Q_{\mathrm{F,MIN}}$	1.0×10^{-14} C/cm^3
	σ_{MAX}	100.0 Ω^{-1}cm^{-1} [b]
	σ_{MIN}	1.0×10^{-14} Ω^{-1}cm^{-1}
Kinetic Parameters	$a \cdot i_{o,\mathrm{REF}}$	1.0×10^3 A/cm^3
	α_a	0.5
	α_c	0.5
	n	1
	U_{REF}	-0.2 V (vs. SCE) [b]
	a^*	1.076 V^{-1} [e]
	η_{PZC}	-0.1056 V (vs. SCE) [e]

[a] chosen arbitrarily
[b] obtained from Ref. (4)
[c] calculated from Ref. (16)
[d] obtained from Ref. (17)
[e] calculated from Ref. (6)

LIST OF FIGURE CAPTIONS

Fig. 1. Schematic of a one-compartment electrochemical cell with RDE.

Fig. 2. Schematic of the surface and associated diffusion layer of the RDE.

Fig. 3. Simulated current density profiles at various scan rates.

Fig. 4. Experimental cyclic voltammograms of a similar system (Ref. (4)).

Fig. 5. Simulated total current density and its components at $v_s = 100$ mV/sec.

Fig. 6. Dimensionless concentration profile of ClO_4^-.

Fig. 7. Dimensionless charge profile of polypyrrole film.

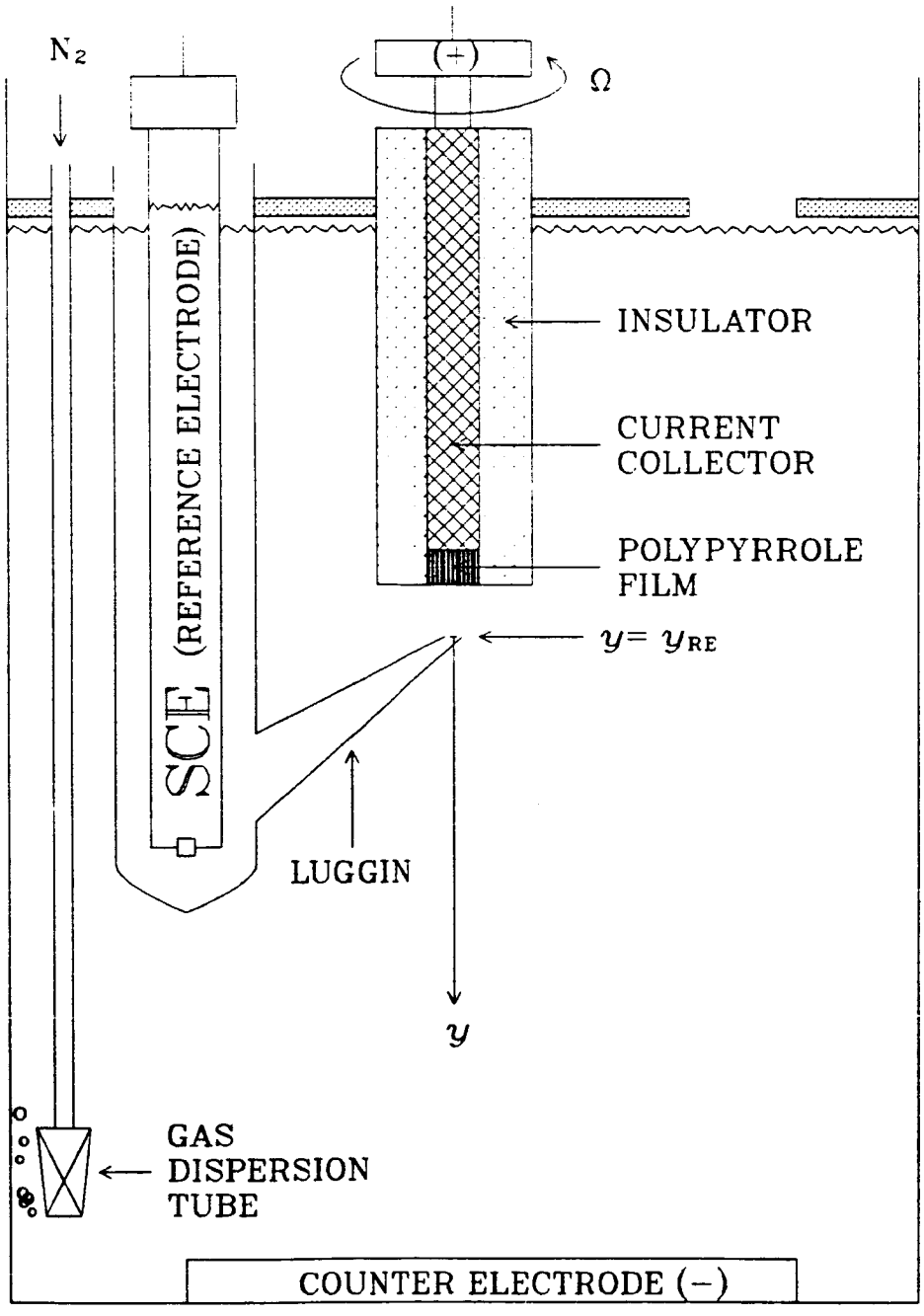

Fig. 1. T. Yeu *et al.*

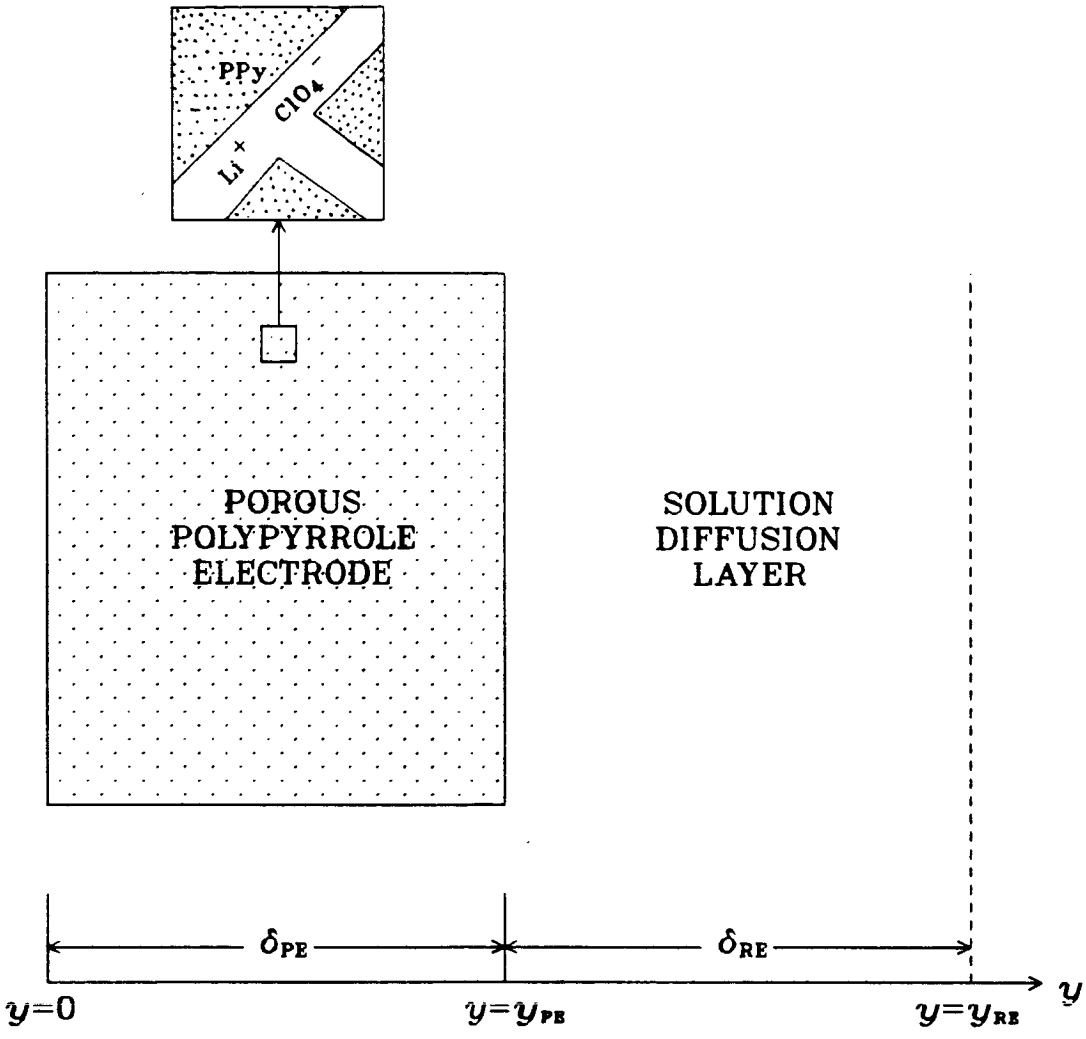

Fig. 2. T. Yeu *et al.*

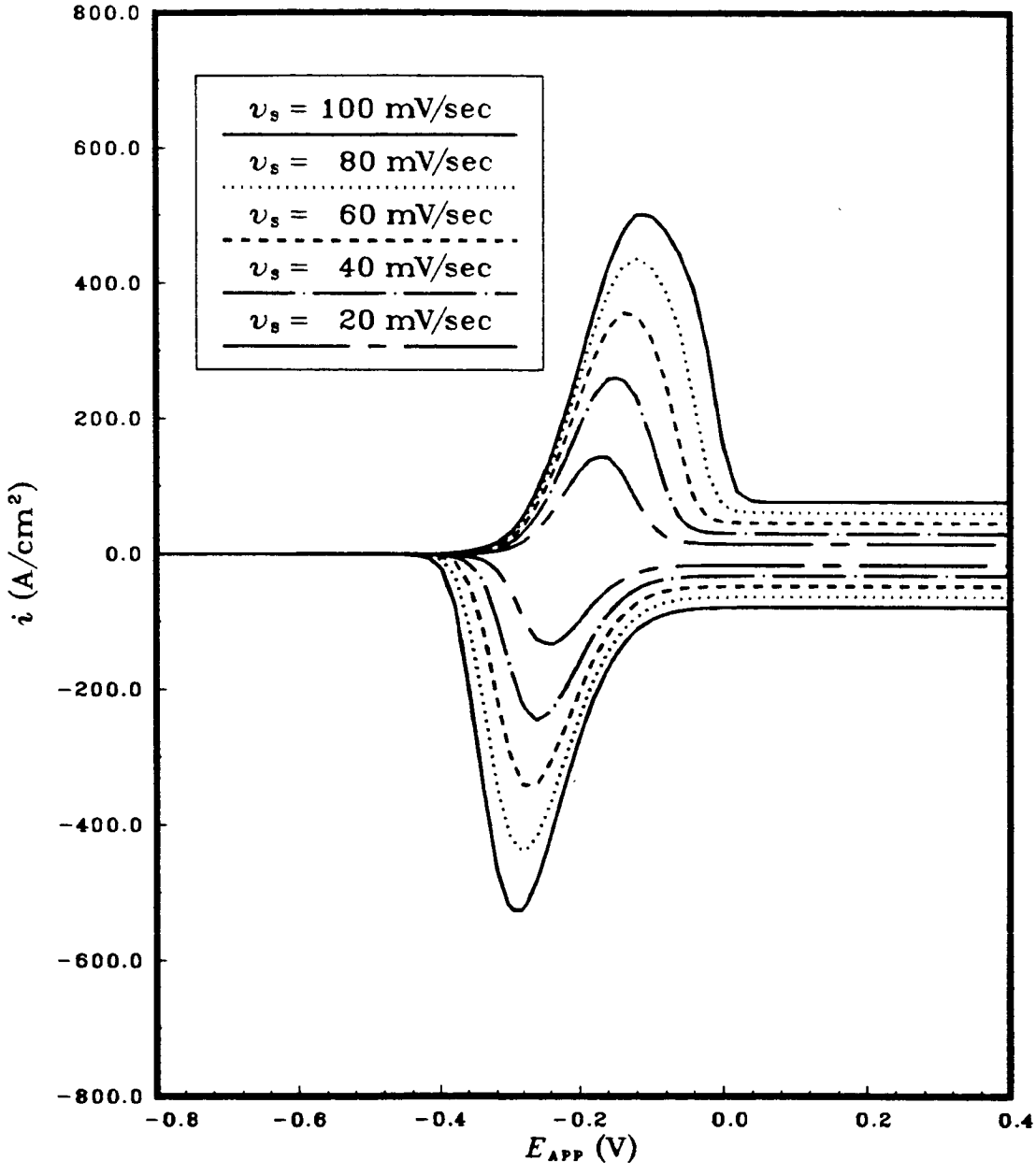

Fig. 3. T. Yeu *et al.*

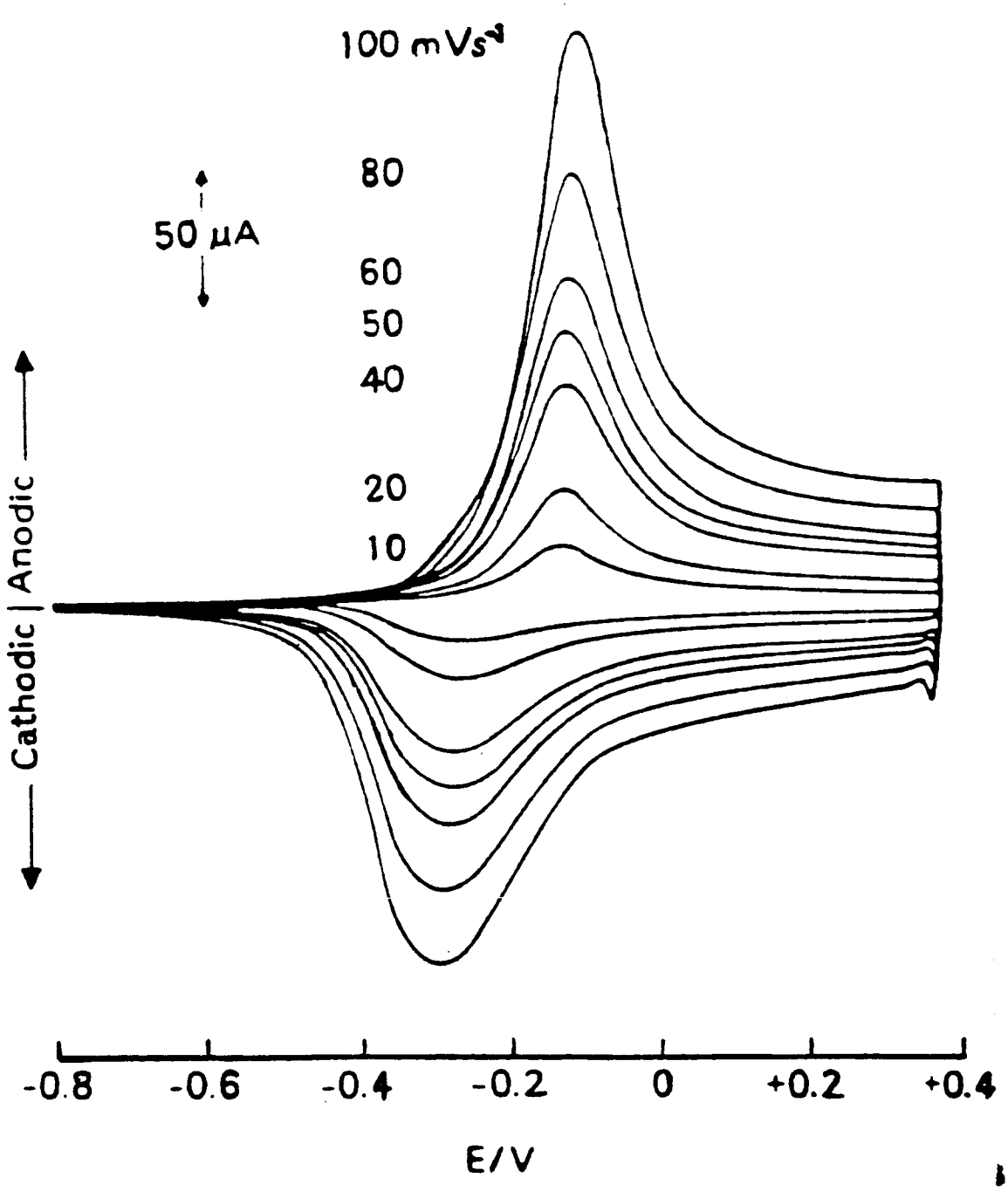

Fig.4. T. Yeu *et al.*

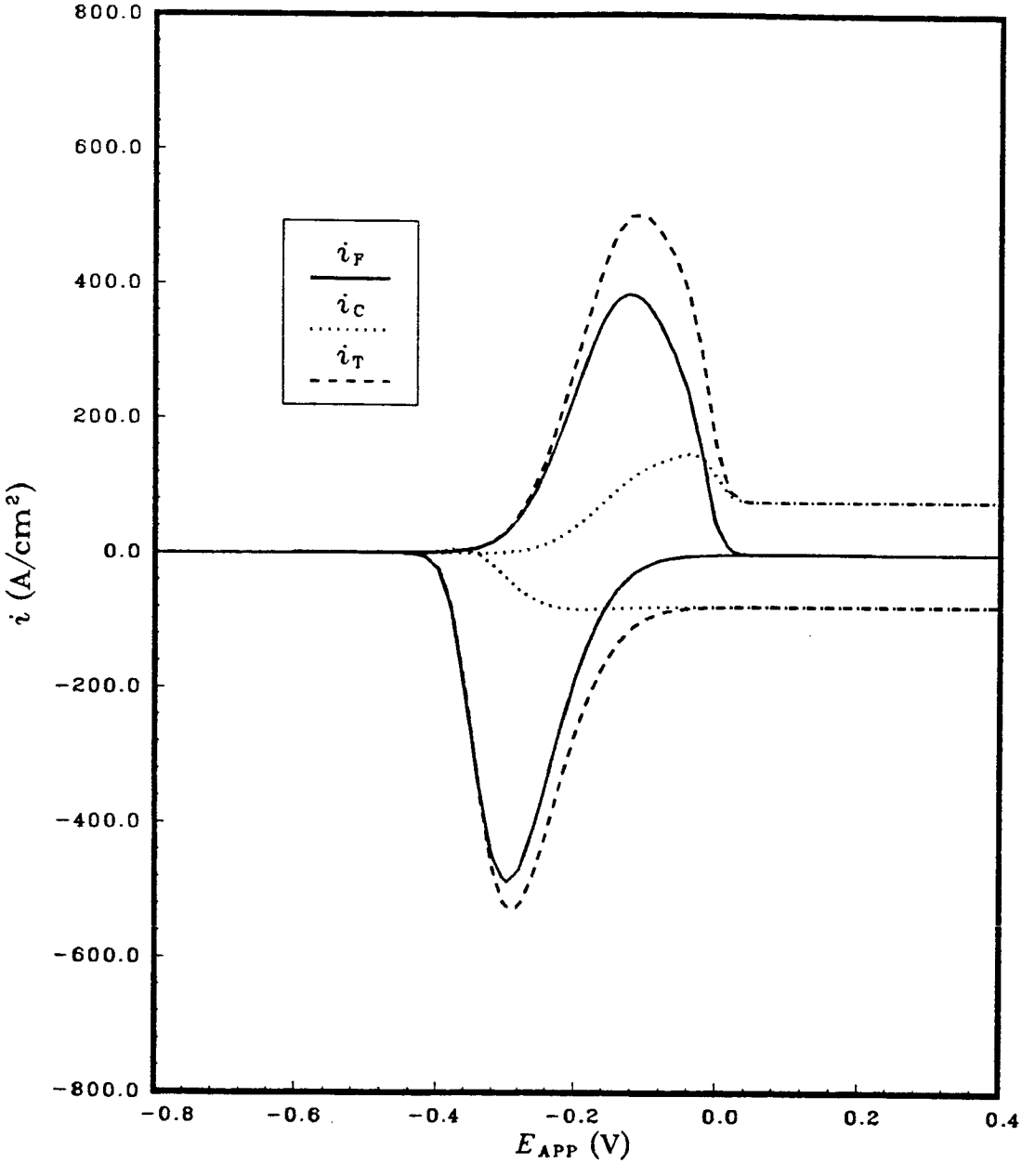

Fig. 5. T. Yeu *et al.*

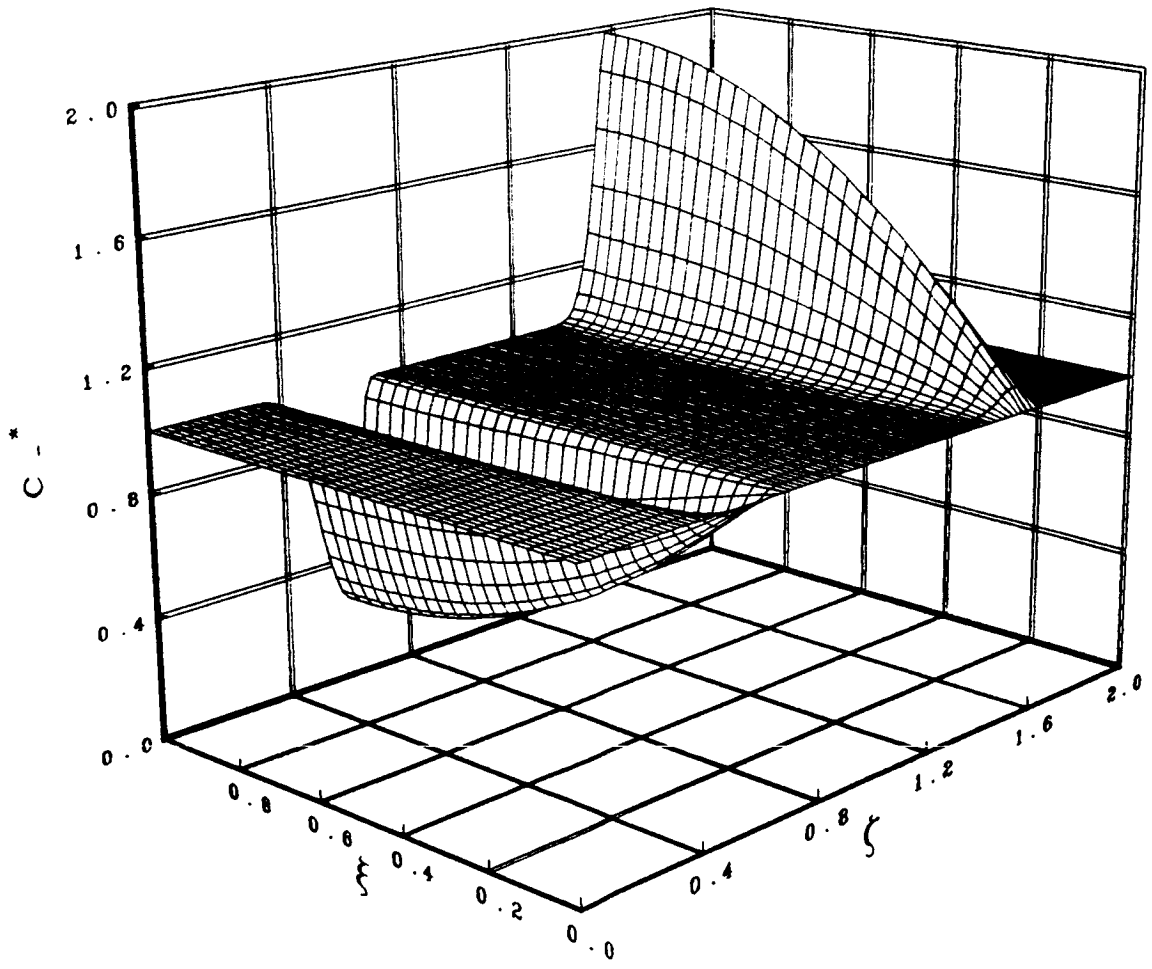

Fig. 6. T. Yeu *et al.*

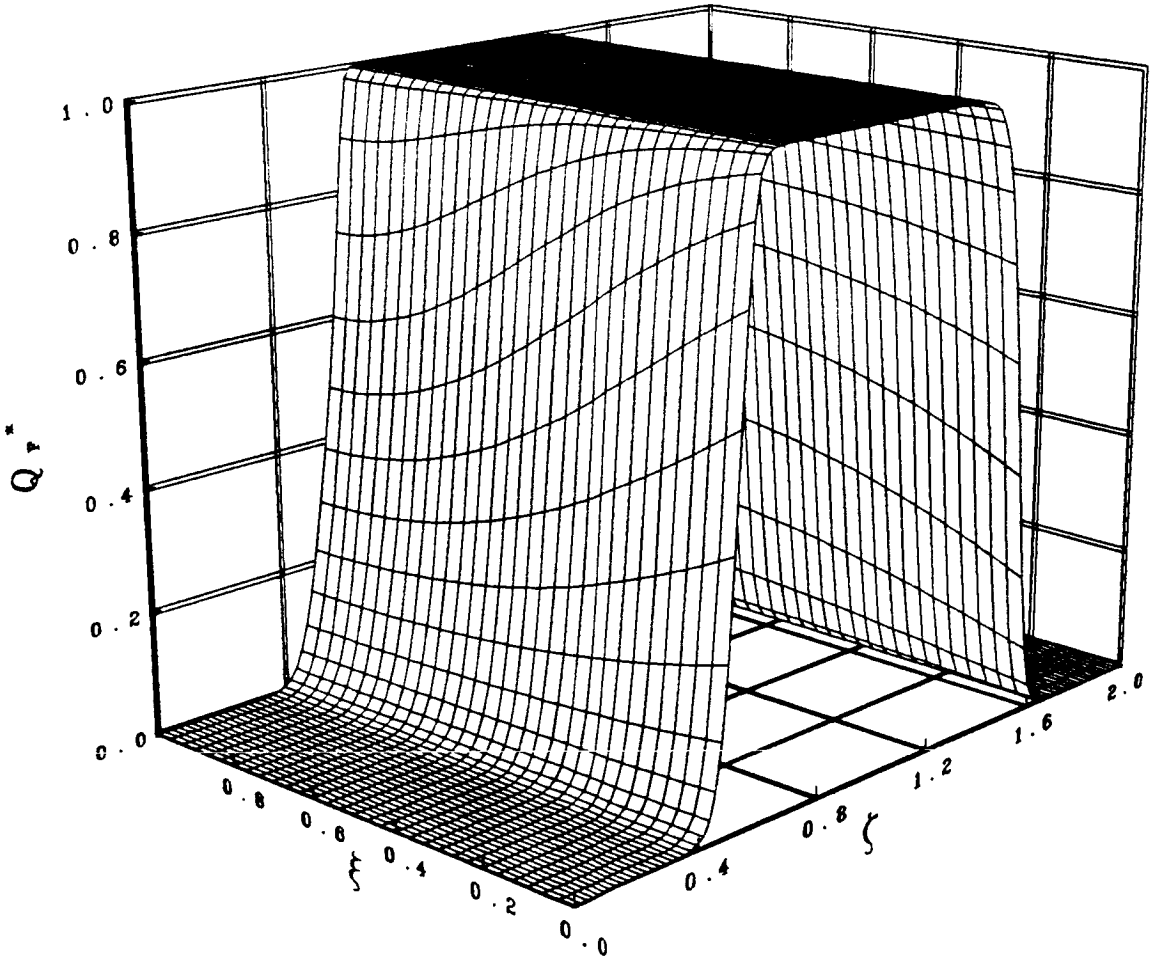

Fig. 7. T. Yeu *et al.*